



T.C.
İSTANBUL UNIVERSITY
INSTITUTE OF GRADUATE STUDIES
IN SCIENCE AND ENGINEERING



Ph.D. THESIS

STRUCTURAL AND VIBRATIONAL SPECTROSCOPIC ANALYSIS
OF RENAL STONES

Mustafa KOCADEMİR

Department of Physics

Physics Programme

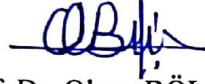
SUPERVISOR
Assoc. Prof. Dr. Olcay BÖLÜKBAŞI

November, 2017

İSTANBUL

This study was accepted on 8/11/2017 as a Ph. D. thesis in Department of Physics, Physics Programme by the following Committee.

Examining Committee Members



Assoc. Prof. Dr. Olcay BÖLÜKBAŞI (Supervisor)
İstanbul University
Faculty of Sciences



Prof. Dr. Sehban KARTAL
İstanbul University
Faculty of Sciences



Assoc. Prof. Dr. Gülce ÖĞRÜÇ İLDİZ
Kültür University
Faculty of Sciences



Prof. Dr. Deniz Değer ULUTAŞ
İstanbul University
Faculty of Science



Prof. Dr. Mehmet Özer
Kültür University
Faculty of Science



As required by the 9/2 and 22/2 articles of the Graduate Education Regulation which was published in the Official Gazette on 20.04.2016, this graduate thesis is reported as in accordance with criteria determined by the Institute of Graduate Studies in Science and Engineering by using the plagiarism software to which İstanbul University is a subscriber.

FOREWORD

I would like to express my gratitude to my several excellent advisors. First, I would like to thank my supervisor Assoc. Prof. Dr. Olcay Bölükbaşı Yalçınkaya for guidance with respect to my personal career development.

I would like to thank my committee members; Prof. Dr. Sehban Kartal and Assoc. Prof. Dr. Gülce Öğrüç Ildız for being a reliable source of suggestions. I also thank Assoc. Prof. Dr. Ayberk Yılmaz for his great advice and assistance. Besides, I express my thanks and appreciation to Prof. Dr. Mustafa Kumru, Prof. Dr. M. Lütfü Tahmaz, Prof. Dr. Abdülhadi Baykal and Assoc. Prof. Dr. Kurtuluş Gölcük for their support. Thanks to my dear friends, and thank you for all the sincere friendship Dr. Tayyibe Bardakçı, I am so glad to work with you.

And lastly, I want to thank my family for all the years of encouragement and support.

November 2017

Mustafa KOCADEMİR

TABLE OF CONTENTS

	Page
FOREWORD	iv
TABLE OF CONTENTS	v
LIST OF FIGURES	vii
LIST OF TABLES	xi
LIST OF SYMBOLS AND ABBREVIATIONS	xii
ÖZET	xiv
SUMMARY	xv
1. INTRODUCTION	1
2. MATERIALS AND METHODS	5
2.1. MATERIALS	5
2.1.1. Renal Stones.....	5
2.1.1.1. Occurrence of the Stone Types	6
2.1.1.2. Morphology of the Stones	10
2.1.1.3. Types of Renal Stones	11
2.1.2. Fluorescence Reduction Materials for Chemical Bleaching on Renal Stones	17
2.1.3. Urine Crystals.....	18
2.2. METHODS	20
2.2.1. Stone Analysis.....	20
2.2.2. Urine Crystal Analysis	21
2.2.3. Spectroscopy	23
2.2.3.1. Raman Spectroscopy.....	27
2.2.3.2. Fluorescence Reduction in Raman Spectroscopy.....	30
2.2.3.3. Infrared Spectroscopy	34
2.2.3.4. X-Ray Diffraction.....	38
2.2.3.5. Thermogravimetric Analysis	40
2.2.3.6. Scanning Electron Microscopy.....	41
3. RESULTS	45

3.1. CHARACTERIZATION OF RENAL STONES.....	45
3.1.1. X-Ray Analysis	45
3.1.2. FT-IR and FT-Raman Analysis.....	48
3.1.3. Thermogravimetric Analysis.....	52
3.2. FLUORESCENCE REDUCTION IN RAMAN SPECTROSCOPY WITH CHEMICAL BLEACHING ON RENAL STONES	61
3.2.1. FT-IR Spectra.....	64
3.2.2. Dispersive-Raman Spectra	65
3.2.3. FT-Raman Spectra.....	69
3.2.4. Comparison of the Raman Spectra.....	71
3.3. MICRO-RAMAN SPECTROSCOPIC INVESTIGATIONS ON URINE CRYSTALS	73
3.3.1. Micro-Raman Spectra	75
4. DISCUSSION.....	79
4.1. CHARACTERIZATION STUDOES ON RENAL STONES	79
4.1.1. X-Ray Analysis	79
4.1.2. FT-IR and FT-Raman Analysis.....	80
4.1.3. Thermogravimetric Analysis.....	81
4.1.4. SEM and EDX Analysis.....	81
4.2. FLUORESCENCE REDUCTION IN RAMAN SPECTROSCOPY WITH CHEMICAL BLEACHING ON RENAL STONES	82
4.2.1. FT-IR Spectra of Samples	82
4.2.2. Chemical Bleaching Process	83
4.2.3. Dispersive Raman Spectra	84
4.2.4. FT-Raman Spectra.....	85
4.2.5. Comparison of Raman Spectra.....	85
4.3. MICRO RAMAN SPECTROSCOPIC INVESTIGATIONS ON URINE CRYSTALS	85
4.3.1. Struvite	86
4.3.2. Uric Acid	87
4.3.3. Urea	87
5. CONCLUSION AND RECOMMENDATIONS	88
REFERENCES.....	92
CURRICULUM VITAE.....	109

LIST OF FIGURES

	Page
Figure 2.1: Stone formation mechanism diagram.	5
Figure 2.2: Core-shell differences of a renal stone, uric acid core and calcium oxalate monohydrate shell.	9
Figure 2.3: Urinary system and renal stones with their locations	10
Figure 2.4: Renal stones with various morphologies and types	11
Figure 2.5: Molecular structure of calcium oxalate monohydrate; a water molecule bind a calcium oxalate molecule in crystal form.	12
Figure 2.6: Molecular structure of calcium oxalate dihydrate; two water molecules bind a calcium oxalate molecule in crystal form	13
Figure 2.7: Molecular structure of Calcium phosphate	14
Figure 2.8: Molecular structure of calcium phosphate dihydrate	15
Figure 2.9: Molecular structure of Uric acid	15
Figure 2.10: Magnesium ammonium phosphate hexahydrate.	16
Figure 2.11: Molecular structure of cystine.	17
Figure 2.12: Structural formula of hydrogen peroxide molecule illustrated with bond angles.	18
Figure 2.13: Optical microscopic images of different urine crystals, a) cystine, b) struvite, c) calcium oxalate dihydrate, d) calcium oxalate monohydrate, e) uric acid, and f) irregular shaped uric acid.	19
Figure 2.14: Electromagnetic wave, black arrow shows the direction of propagation. Magnetic and electric fields are illustrated with blue and red lines, respectively. ...	24
Figure 2.15: Basic wave illustration.	25
Figure 2.16: Electromagnetic spectrum and its special regions.	26
Figure 2.17: Absorption and emission of photon at atomic level.	27
Figure 2.18: Energy level diagrams for Raman scattering. Both ground state and first excited state are given as an atomic level.	30

Figure 2.19: General types of light scattering from a specimen. Rayleigh, Raman and Fluorescence are illustrated.	31
Figure 2.20: Differences between Raman and fluorescence phenomena in atomic scale with a diagram.	32
Figure 2.21: The relation between laser wavelength and fluorescence emergence [136].	33
Figure 2.22: Internuclear distance vs Potential energy diagram for diatomic molecules, green and blue curves are shown harmonic and anharmonic oscillators, respectively.	35
Figure 2.23: Illustration for understanding Hooke's law on atoms, chemical bond behaves like as spring.	35
Figure 2.24: Fourier transform infrared spectrometer setup. Mirrors, light source, beam splitter, sample holder and detector are illustrated.	38
Figure 2.25: Coherent X-ray diffraction from crystal lattice. Red and green photons are reflected different layers of the crystal. But reflection angles are equal.	39
Figure 2.26: X-ray instrument diagram with source, sample holder, goniometer and detector parts.	40
Figure 2.27: Thermogravimetric analysis setup. A balance utilizes for understanding mass changes during the heating process.	41
Figure 2.28: Scanning electron microscopy instrument diagram. Sample holder, condensers, lens and coils are illustrated.	43
Figure 2.29: Emission of a characteristic X-rays from an atom after interaction with initial (external) and inner shell electron. Blue dot represents secondary electron and characteristic radiation emits after filling this orbital blank.	44
Figure 3.1: XRD powder patterns of sample A1 to A7. A1 and A2 have different XRD pattern then others.	47
Figure 3.2: FT-IR spectra of samples A1 to A7. A1 and A2 have different pattern then others.	48
Figure 3.3: FT-Raman spectra of samples A1 to A7. A1 and A2 have different pattern then others.	49
Figure 3.4: TGA thermograms of sample A1 to A7. A1 and A2 have different pattern then others.	53
Figure 3.5: The SEM micrographs and EDX spectra of A1 to A7.	54

Figure 3.6: Bleached and non-bleached (before and after of the chemical interaction process with hydrogen peroxide) parts of the Sample 1 and Sample 2, respectively.	63
Figure 3.7: FT-IR spectra of Sample 1 and Sample 2, for determining the composition of stone types (before the chemical bleaching process).	64
Figure 3.8: Changes of the Raman intensity which depends on the bleaching process time for Sample 1, Fluorescence background had been reduced for half-hour and two-hour bleached samples with same procedure, though it has not sufficient to obtain clear results.	66
Figure 3.9: Changes of the Raman intensity which depends on the bleaching process time for Sample 2, Fluorescence background had been reduced for half-hour and two-hour bleached samples with same procedure, though it has not sufficient to obtain clear results.	67
Figure 3.10: Dispersive Raman spectrum of the Sample 1, after the hydrogen peroxide based bleaching process (24 hour) for reduce fluorescence background.	68
Figure 3.11: Dispersive Raman spectrum of the Sample 2, after the hydrogen peroxide based bleaching process (24 hour) for reduce fluorescence background.	69
Figure 3.12: FT-Raman spectrum of Sample 1 with 1024 nm laser wavelength (before bleaching).	70
Figure 3.13: FT-Raman spectrum of Sample 2 with 1024 nm laser wavelength (before bleaching).	71
Figure 3.14: Sample 1 before (FT-Raman) and after (Dispersive Raman) bleaching spectra.	72
Figure 3.15: Sample 2 before (FT-Raman) and after (Dispersive Raman) bleaching spectra.	72
Figure 3.16: Confocal microscope images from urine sediment after centrifuge process for understanding the crystal existence.	73
Figure 3.17: Schematic diagram of the micro-Raman spectroscopy system, which utilized for the observation of both spectral data and microscopic images from urine samples simultaneously.	74
Figure 3.18: Images of Struvite (a), Uric acid (b), and Urea (c), crystals under the $\times 100$ objective Raman Microscope.	75
Figure 3.19: micro-Raman spectrum of Struvite crystal, it is observed with $\times 100$ Raman microscope.	77

Figure 3.20: micro-Raman spectrum of Uric acid crystal, it is observed with $\times 100$ Raman microscope.77

Figure 3.21: micro-Raman spectrum of Urea crystal, it is observed with $\times 100$ Raman microscope.78



LIST OF TABLES

	Page
Table 2.1: Most common renal stone components, their well-known names and chemical formulas.	7
Table 2.2: Different types of urinary stones and their occurrence rates	8
Table 3.1: Composition, formulas, international card numbers and average crystallite size of each sample.	46
Table 3.2: FT-IR frequencies (cm^{-1}), tentative assignments and compound names of the samples.	50
Table 3.3: FT-Raman frequencies (cm^{-1}), tentative assignments and compound names of the samples.	51
Table 3.4: The total weight losses (parts of inorganic and organic content) for the samples.	52
Table 3.5: FT-IR frequencies (cm^{-1}), tentative assignments and compound names of the Sample 1 and Sample 2 (before the bleaching process).	65
Table 3.6: Raman frequencies and compound names of the Sample 1 and Sample 2 before and after bleaching.	71
Table 3.7: The most intense Raman frequencies and assignments of investigated urine crystals with $\times 100$ Raman microscope.	76

LIST OF SYMBOLS AND ABBREVIATIONS

Symbol	Explanation
s	: Second
h	: Hour
°	: Degree
Å	: Angstrom
θ	: Angle
n	: Integer
λ	: Wavelength
d	: Distance
(hkl)	: Directions
D	: Crystallite size
β	: Full width at half maximum
t	: Time
m	: Mass
T	: Temperature
E	: Electric field
H	: Magnetic field
F	: Force
k	: Spring constant
\emptyset	: Phase
α	: Polarizability

Abbreviation	Explanation
XRD	: X-Ray Diffraction
FT-IR	: Fourier Transform Infrared
FT-Raman	: Fourier Transform Raman
Disp-Raman	: Dispersive Raman
SEM	: Scanning Electron Microscopy
EDX	: Energy-Dispersive X-ray Analysis

TGA	: Thermogravimetric Analysis
COM	: Calcium Oxalate Monohydrate
COD	: Calcium Oxalate Dihydrate
CP	: Calcium Phosphate
CPD	: Calcium Phosphate Dihydrate
UA	: Uric Acid
MAP	: Magnesium Ammonium Phosphate Hexahydrate
UV	: Ultra-Violet
HP	: Hydrogen Peroxide
ATR	: Attenuated Total Reflectance
3-D	: Three Dimension
ICDD	: International Centre for Diffraction Data

ÖZET

DOKTORA TEZİ

BÖBREK TAŞLARININ YAPISAL VE TİTREŞİMSSEL SPEKTROSKOPİK ANALİZİ

Mustafa KOCADEMİR

İstanbul Üniversitesi

Fen Bilimleri Enstitüsü

Fizik Anabilim Dalı

Danışman : Doç. Dr. Olcay BÖLÜKBAŞI

Bu tezde, atom ve molekül fiziğinin temel uygulamalarından olan spektroskopik teknikler ile böbrek taşları ve idrarda bulunan böbrek taşı kristalleri incelendi. X-Işını Kırınımı (XRD), Furier Dönüşümlü Kırmızı altı (FT-IR) ve Furier dönüşümlü Raman (FT-Raman) spektroskopik teknikleri numunelerin kristal yapıları ve bileşenlerinin tespiti, Taramalı Elektron Mikroskobu (SEM) görüntüleri ve Enerji Dağılımı X-ışını analizi (EDX) sonuçları ise morfolojik yapısının ve elementel özelliklerinin araştırılmasında kullanıldı. Termogravimetrik Analiz (TGA) yöntemiyle de böbrek taşı numunelerinin organik ve inorganik özellikleri belirlendi. Sonuç olarak kalsiyum oksalat monohidrat ve kalsiyum fosfat yapıları belirlendi. Ardından, Raman spektroskopisi ölçümlerinde sıklıkla karşılaşılan çok önemli bir sorun olan floresan oluşumunun azaltılması için, numunelere kimyasal ağartma uygulaması yapıldı. Bu sayede ölçüm yapılmasını engelleyen floresan arka plan sorununa etkin bir çözüm sunuldu. Son olarak ise Mikro-Raman spektroskopisi tekniğiyle idrarda bulunan çok küçük boyutlu böbrek taşı kristalleri görüntülendi ve bu kristaller karakterize edilerek, sütrivit, ürik asit ve üre kristalleri tespit edildi.

Kasım 2017, 126 sayfa.

Anahtar kelimeler: Böbrek taşları; İdrar kristalleri; X-ışını kırınımı; Kırmızı altı-Raman spektroskopisi; Termogravimetrik analiz; Elektron mikroskobu

SUMMARY

Ph.D. THESIS

STRUCTURAL AND VIBRATIONAL SPECTROSCOPIC ANALYSIS OF RENAL STONES

Mustafa KOCADEMİR

İstanbul University

Institute of Graduate Studies in Science and Engineering

Department of Physics

Supervisor : Assoc. Prof. Dr. Olcay BÖLÜKBAŞI

In this thesis, renal stones and urine crystals are investigated with variety of efficient spectroscopic techniques. X-ray Diffraction (XRD), Fourier Transform Infrared (FT-IR) and Raman (FT-Raman) spectroscopic techniques are carried out for determining crystal structures and compositions of the samples. Scanning Electron Microscopy (SEM) images and Energy-Dispersive X-ray Analysis (EDX) spectra are recorded to investigate morphological and elemental characteristics. Thermogravimetric Analysis (TGA) is also used for the identification of organic and inorganic properties. As a result, calcium oxalate monohydrate and calcium phosphate are found. Furthermore, chemical bleaching procedure was performed in order to reduce the fluorescence which is frequently encountered in urinary stones analysis with Raman spectroscopy. In this way, a novel solution for the eliminating of fluorescence in Raman spectroscopic analysis of urinary stones is suggested. Finally, sub-visible sized urine crystals are monitored with Micro-Raman spectroscopy, and characterization studies are performed. So, struvite, uric acid and urea crystals are determined.

November 2017, 126 pages.

Keywords: Renal stones; Urine crystals; X-ray diffraction; Raman-Infrared spectroscopy; Thermogravimetric analysis; Electron microscopy

1. INTRODUCTION

Urolithiasis is one of the oldest and a common urological sickness and causes serious health problems. It appears between 1 % - 20 % of the general population of the world [1- 6]. Frequency of the occurrence is increasing with each passing day [7]. This disease arises as stone formation at the urinary system. These formations are known as kidney stones, which are also named as renal stones, urinary calculus or urinary calculi in the literature. Urinary calculi are described as crystalline deposits that have aggregated together to form a hard solid structure in the kidneys. Structures which greater than 1 mm are usually considered as urinary stone.

Kidneys play a significant role in the urinary system, because they filter the blood and remove metabolic debris from the body. A number of people experience kidney stones in their life one or more times. Also, some animals, especially cats and dogs form kidney stones like humans. Presence of a renal stone can cause severe pain and infections for the patient, or sometimes they may induce damage of whole kidneys [8, 9]. Additionally, the disease costs millions of dollars for its diagnosis and treatment throughout the world. Lifestyle, ethnicity, and family history (genetic factors) also play important role for the urinary stone formation.

Despite the stone analysis is very important and influences correct diagnosis and treatment, mechanism of the stone formation is not fully understood yet [10-13]. Generally, treatment can be a painful experience and especially large kidney stones are traditionally removed by invasive surgery. Fortunately, modern treatment techniques provide an opportunity for less painful applications. However after these kind of modern treatment techniques, residual stone fragments become smaller. Hence the collection and characterization becomes more difficult.

Researchers have indicated that treatment and prevention of urinary stones can't be achieved without knowledge of the stone formation process. Because the treatment of disease is specified according to the stone types. And unfortunately some misdiagnosis

facts have been reported for urinary stone analysis [14]. Reliable and efficient treatment of urolithiasis depends on the information of the chemical composition and size of the stone, which in turn enables classification of the disease. The structure and composition of renal stones are very complex and depends on many factors such as environment, food habits, age, sex, and metabolism [15, 16].

Several approaches have been utilized in order to collect information of urinary stones which include complicated techniques such as spectroscopy, crystallography, and microscopy. Within these methods, vibrational spectroscopy, thermogravimetry, X-ray diffraction, electron microscopy with energy dispersion, and polarized microscopy are the most popular ones for the composition analysis. Since they ensure fast, sensitive, and exact information about the major chemical components of the stone without any destruction, these techniques are very ideal for renal stone analysis.

Therefore, this study aims to give general information about the renal stones and the analysis methods used in this field. The first part of the study involves detailed human urinary stone investigation which were collected from urolithiasis patients from Istanbul, Turkey. Concordantly X-ray diffraction (XRD), Fourier-Transform Infrared (FT-IR) and Fourier-Transform Raman (FT-Raman) spectroscopic investigations have been carried out in order to determine crystal structure and chemical compositions of that stones. By using the XRD powder diffraction patterns, FT-IR and FT-Raman spectra techniques the chemical constituents of urinary stones have identified. The crystallite size of the different stone types have been calculated from X-ray spectral data. Scanning Electron Microscopy (SEM) images and Energy-Dispersive X-ray Analysis (EDX) spectra have been recorded in order to investigate the morphological and elemental characteristics. Also Thermogravimetric Analysis (TGA) has been studied in order to indicate that the organic and inorganic properties of stones. Hence by using all of these techniques, this study shows the reliability and accuracy of the methods. Moreover, there is no such a comprehensive study in Turkey which uses and compares these methods on the analysis of renal stones.

In the second part of the study, the use of Raman spectroscopy on renal stones is examined in detail. Raman spectroscopy is a vibrational spectroscopic technique and it has excellent applications on material science. Since most matters have a unique Raman spectra,

generally it can be used to evaluate molecular structure of compounds. Especially, Raman spectroscopy is very prevalent for biological sample analysis, because water molecules can't effect the Raman measurements. Furthermore, rapid, inexpensive, noninvasive, and wet sample analysis is also possible with this method.

Raman spectroscopy is widely used in urinary calculi investigations and characterizations [17-22]. Besides, some minerals which include hydroxyapatite (bone, teeth and renal stones) have been studied in several researches [23, 24]. However fluorescence signals can overlap Raman spectrum completely. That problem acts critical role in Raman spectroscopic studies. Fluorescence phenomenon acts a catastrophic effect for Raman spectroscopic measurements. Because it can overlap entire spectrum.

In this context, this part aims to reduce fluorescence background intensity from Raman spectra of the renal stones which have lower excitation laser wavelengths. So, the hypothesis of this section is that fluorescence background can be eliminated with hydrogen peroxide based chemical bleaching procedure and renal stones can be characterized exactly with 532 nm excitation laser.

A large number of Raman investigators try to develop methods in order to prevent fluorescence. Although lots of papers have investigated bone or dental tissues, there is not any study associated with the fluorescence reduction in the conditions of chemical bleaching for the urinary stones in the literature. Hence, in this study, hydrogen peroxide solution was used for the first time with chemical bleach-based fluorescence reduction application in Raman spectroscopic measurements on calcium oxalate and calcium phosphate types renal stones.

A comparative measurement using Dispersive Raman spectroscopy with 532 nm laser excitation wavelength has been performed. The main aim is to reduce fluorescence background from Raman spectra by applying 30 % hydrogen peroxide and acetone process. In addition, optimum bleaching time for eliminating the fluorescence background have been identified. Also, for determining ideal conditions for this type of specimens with different laser powers have been tried. Thus that study had introduced the bleaching procedure of urinary stones for Raman spectroscopy and it is shown that

chemical bleaching can be used in place of photo-bleaching or other fluorescence reduction methods.

Finally, in the last part of the study our aim is to identify urine crystals (sub-visible renal stone particles) from directly urine by using micro-Raman spectroscopy. Although there are some of the studies for urine crystals done by Raman spectroscopy, urea crystal had been measured for the first time with micro-Raman spectroscopy. Micro-Raman spectroscopic approaches may provide quick and widespread approximations for renal stone characterization and prediction in clinics [25]. Also, urine microcrystalline analysis can provide opportunities for personalized treatments [26, 27]. Concordantly, Raman spectroscopy may be utilized as an alternative detection method for urine crystal analysis. Because, micro-Raman spectrometer works with Raman spectrometer and an optical microscope simultaneously, it means the technique allows research on different micro areas on sample surface, so especially is very useful tool for biological sample analysis. Consequently, It is evidenced that micro-Raman spectroscopy is especially favorable for identification of micro crystals from directly urine.

Thus, this part indicates that Raman spectroscopy is a powerful tool in identifying different urine crystals. In this research, dispersive micro-Raman spectrometer have been used for the characterization of urinary crystallites, in which urine sample have been collected from a urolithiasis patient. This quick and convenient method can be used in the prediction of urinary stone types by providing early diagnostic possibility for the stone growth.

2. MATERIALS AND METHODS

2.1 MATERIALS

2.1.1 Renal Stones

Urinary calculi has solid structure, components of the stones consisted both crystalline and organic materials with the ratio of 95 % and 5 %, respectively [28]. There are many different chemical groups, and the most common components are; calcium oxalate monohydrate, calcium oxalate dihydrate, calcium phosphate also known as apatite, calcium hydrogen phosphate dehydrate known as brushite, magnesium ammonium phosphate hexahydrate known as struvite, uric acid, cystine, drug induced stones and organic substances [29].

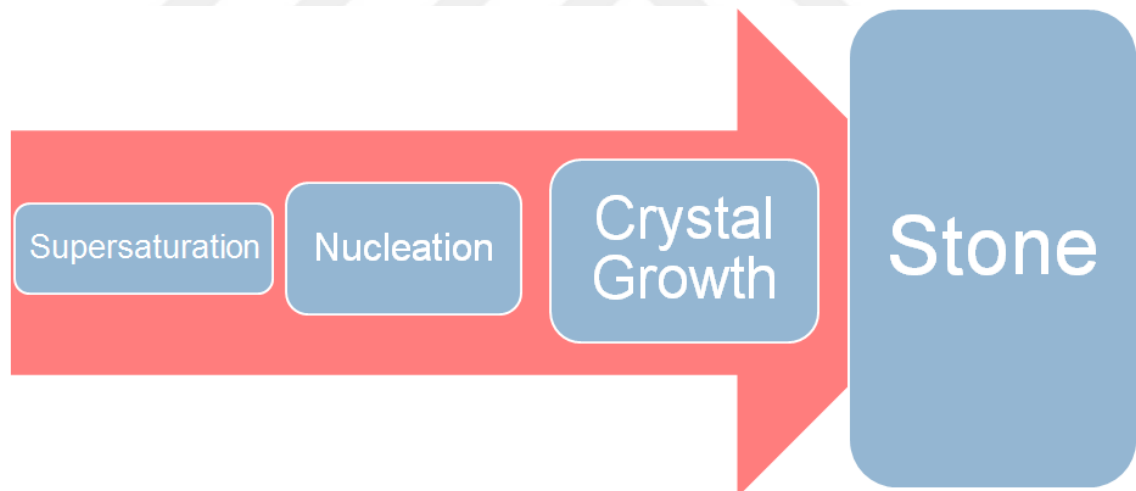


Figure 2.1: Stone formation mechanism diagram.

Unfortunately the prevalence of urinary calculi increases day by day, but its formation process is not completely understood [30, 31]. Lots of reasons can be considered for the beginning of the renal stone disease. Main factors have listed by scientists and also these factors are strongly related with the renal stone types [32].

Several biochemical disorders can trigger precipitation of urinary constituents and depends of this situation, kidney stone formation may begin [33]. As well, some other factors affect stone nucleation and growth such as pH, supersaturation, temperature, ionic ratios of urine [34]. Stone formation mechanism is illustrated as a diagram with three steps in Figure 2.1. If the concentration of substance in a solution is above the saturation point, the solution describes as supersaturated and that can support the crystal formation. In addition, when urine supersaturation is excessive, crystals begin to nucleate and these nucleated crystals are grow. Finally multiple crystals can be aggregate to form a renal stone.

2.1.1.1 Occurrence of the Stone Types

Some prevalent renal stone components are listed in Table 2.1 with the chemical formulas and their well-known mineralogical names. Up to now, 82 different components are recorded from various renal stones, however only seven of them have a frequency of occurrence of higher than 1 % [29, 35]. Further the distribution of components are very different.

Calcium oxalate (CaOx) and calcium phosphate (CaP) structures are the most common kidney stone components, which appear approximately 80 % of all types of stones [36-40]. In addition calcium oxalate stones are reported as the most frequent renal stone type [41-43]. Calcium oxalate monohydrate (COM) stones are thermodynamically stable than other calcium oxalate derivate and occurrence frequency higher than Calcium oxalate dihydrate [44-46].

Calcium phosphate stones which called as (Apatite) are very common and they have 33 % frequency [28]. Calcium hydrogen phosphate dehydrate (Brushite) has low rate around 1-2 %, and tricalcium phosphate (Whitlockite) is very rare [28]. Magnesium ammonium phosphate hexahydrate (Struvite) stones are also frequent, and its rate around 6 %. Uric acid (UA) stones are common and rate is 8-10 % [48, 49]. Cystine is a rare stone and its occurrence rate is only 1-2 % [50-52].

Table 2.1: Most common renal stone components, their well-known names and chemical formulas.

Chemical Name	Formula
Calcium oxalate monohydrate (Whewellite)	(CaC ₂ O ₄ .H ₂ O)
Calcium oxalate dihydrate (Weddellite)	(CaC ₂ O ₄ .2H ₂ O)
Calcium phosphate (Apatite)	(Ca ₅ (PO ₄) ₃ .OH)
Calcium hydrogen phosphate dehydrate (Brushite)	(CaHPO ₄ .2H ₂ O)
Magnesium ammonium phosphate hexahydrate (Struvite)	(MgNH ₄ .PO ₄ .6H ₂ O)
Uric acid	(C ₅ H ₄ N ₄ O ₃)
Uric acid monohydrate	(C ₅ H ₄ N ₄ O ₃ . H ₂ O)
Uric acid dihydrate	(C ₅ H ₄ N ₄ O ₃ .2H ₂ O)
Xanthine	(C ₅ H ₄ N ₄ O ₂)
Tricalcium phosphate (Whitlockite)	(Ca ₃ (PO) ₄)
Magnesium hydrogen phosphate trihydrate (Newberyite)	(MgHPO ₄ .3H ₂ O)
Cystine	(C ₆ H ₁₂ N ₂ O ₄ S ₂)
Drug induced stones	-
Organic substances	-

Moreover Table 2.2 gives mix type stone and their occurrence rates. 34 % of renal stones form as only mono-mineral structure, however 44 % of the stones grow up with two

different kinds of minerals (mix type). That ratio is an evidence that mixed stone analysis has an important role for the urinary calculi characterization [47].

Table 2.2: Different types of urinary stones and their occurrence rates [47].

Urinary Stone type	Rate (%)
Whewellite	28
Whewellite - Weddellite	24,6
Whewellite – Weddellite - Apatite	17,8
Whewellite – Apatite	4,8
Struvite – Apatite	4,6
Uric acid - Uric acid dihydrate	4,1
Artifacts	2,5
Uric acid	2,1
Whewellite - Uric acid	1,9
Weddellite - Apatite	1,3
Apatite	1,1

Different types of urinary stones and their occurrence rates are listed in Table 2.2. Also, core-shell relation is important too, because usually different components can be separated homogenously between nucleus and the outer shell of the stone [53]. A mixed stone is given in Figure 2.2. Several components can be separately located in different shell layers and core of the stone.

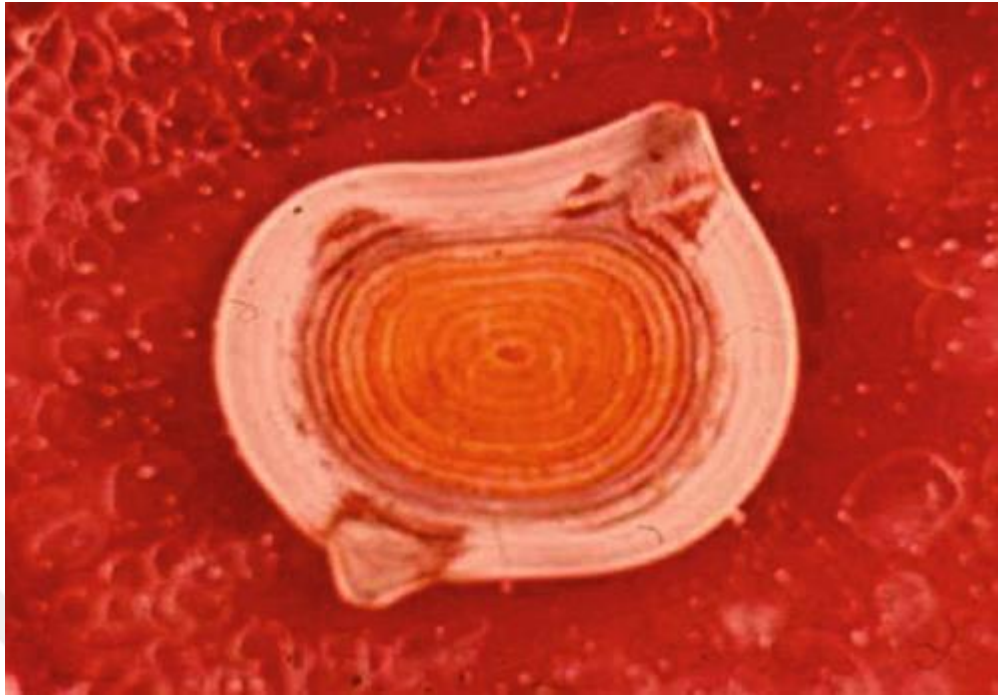


Figure 2.2: Core-shell differences of a renal stone, uric acid core and calcium oxalate monohydrate shell [29].

According to this, collecting information about composition and structure of renal stones is quite important for determining etiological factors and understanding preventing ways for recurrence [54]. Besides, renal stones can grow up different locations in the urinary system, such as, urinary bladder, ureters or kidneys. Also, there is a relation between appearance of the stone and locations. Figure 2.3 illustrates stones and their forming locations.

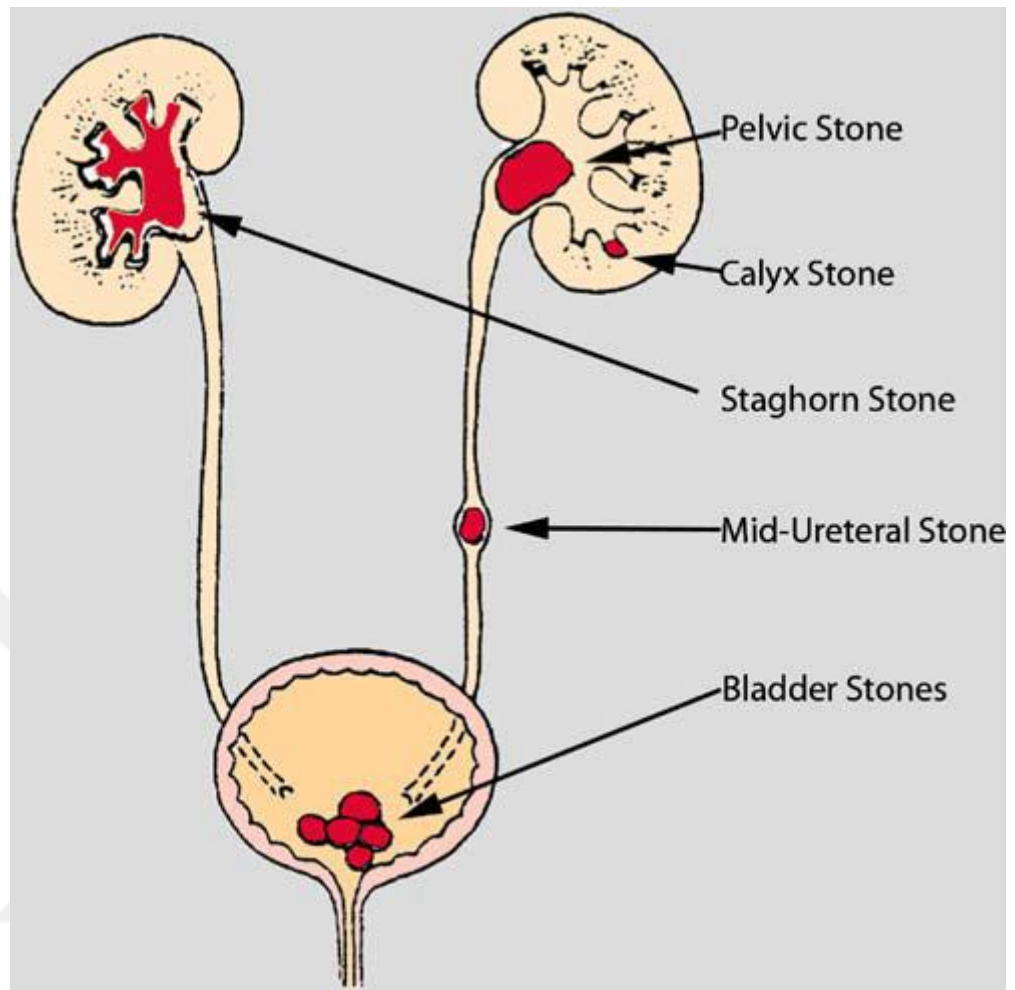


Figure 2.3: Urinary system and renal stones with their locations [55].

2.1.1.2 Morphology of the Stones

Renal stones can be formed into various sizes, morphologies and shapes. These particles can be as small as a sand or as great as an egg. Further, components and morphology of stones involve important knowledge about supersaturation [56]. These morphological and physical difference depend on the formation location and chemical structure (type) of the stone.

In addition, the majority of the renal stones examined are smooth and ovular shapes, but infrequently some stones have sharp structures and edges. Also, drug metabolites have been found in the nucleus (core) of some stones [57]. Figure 2.4 illustrates various morphologies and physical shapes of many types of renal stone [58].



Figure 2.4: Renal stones with various morphologies and types [59].

2.1.1.3 Types of Renal Stones

Calcium oxalate monohydrate COM and Calcium oxalate dehydrate COD are different forms of calcium oxalate mineral with one water molecule. Its chemical formula is $(\text{CaC}_2\text{O}_4 \cdot \text{H}_2\text{O})$. The occurrence rate of COM is generally rare in nature however that compound appears with high frequency in urinary stones. COM mineral exhibits brown or yellow-green color and often disintegration of these crystals are very difficult [60]. Molecular structure of COM is shown in Figure 2.5. One water molecule and one calcium ion bind with oxalate molecule. The crystal system of COM is monoclinic structure [61].

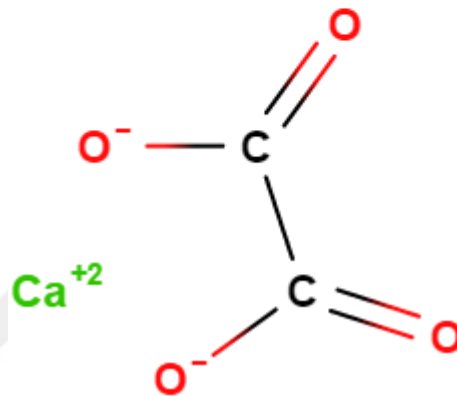
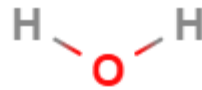


Figure 2.5: Molecular structure of calcium oxalate monohydrate; a water molecule binds a calcium oxalate molecule in crystal form [62].

COD was discovered in the sea of Antarctica at 1930s. COD mineral is also called weddellite ($\text{CaC}_2\text{O}_4 \cdot 2\text{H}_2\text{O}$). Most frequently, COD and COM minerals appear together and they can be found in kidney stones very frequently. Many studies prove that crystal structures of these crystals are very similar [61, 63 and 64]. COD mineral has a tetragonal crystal system [65]. Figure 2.6 shows molecular structure of COD.

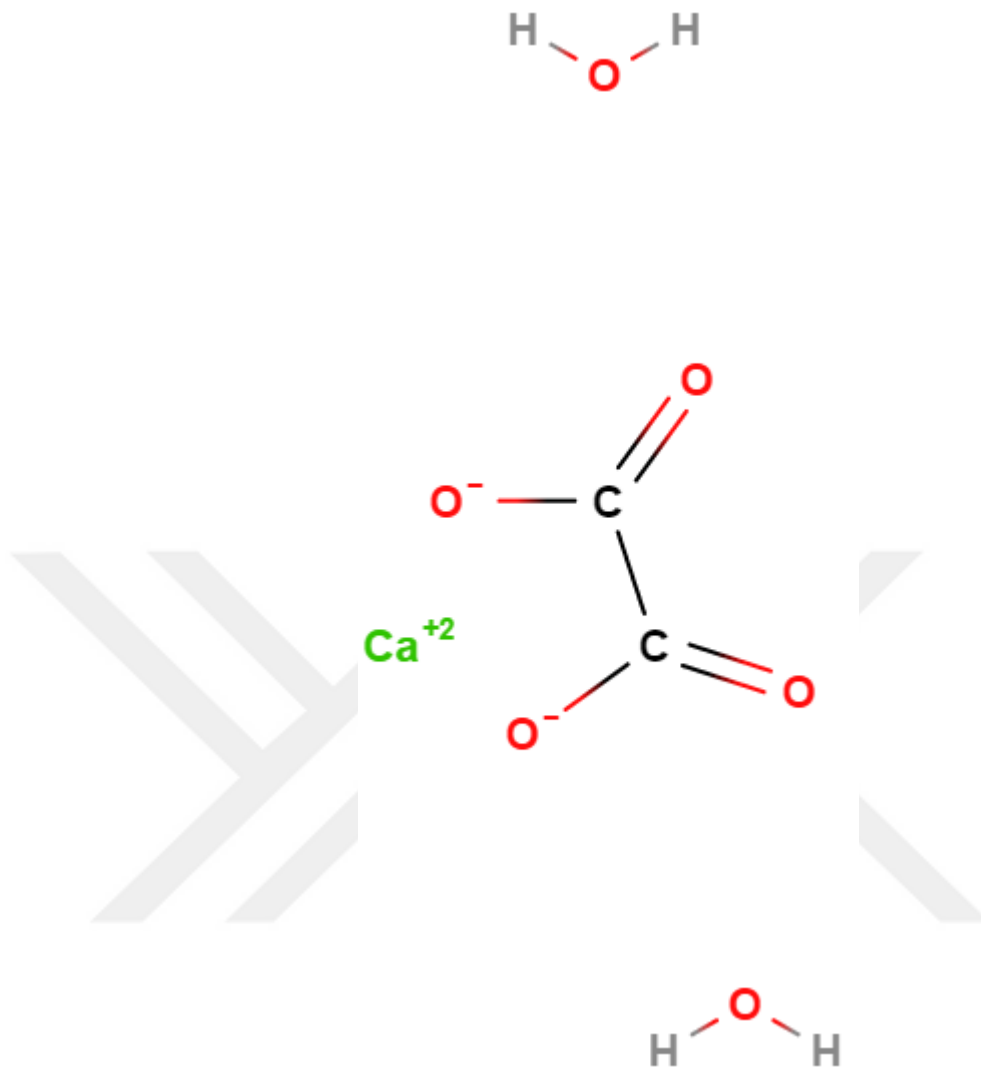


Figure 2.6: Molecular structure of calcium oxalate dihydrate; two water molecules bind a calcium oxalate molecule in crystal form [62].

CP or a well-known name apatite is a very common mineral in nature and also it has great importance for bones and teeth. Apatite, generally is used to define similar minerals such as, hydroxyapatite, chlorapatite and fluorapatite. Their chemical formula can be written as $\text{Ca}_5(\text{PO}_4)_3(\text{OH},\text{F},\text{Cl})$, $\text{Ca}_{10}(\text{PO}_4)_6(\text{OH})_2$, $\text{Ca}_{10}(\text{PO}_4)_6(\text{Cl})_2$ and $\text{Ca}_{10}(\text{PO}_4)_6(\text{F})_2$. The apatite mineral belongs to hexagonal dipyramidal crystal system [66]. It appears in urinary stones, and often it can exist in the nucleus. Besides, generally occurs together with other kidney stone minerals [67]. Molecular structure of calcium phosphate is shown in Figure 2.7 with five calcium ions, three phosphate molecules and one hydroxide.

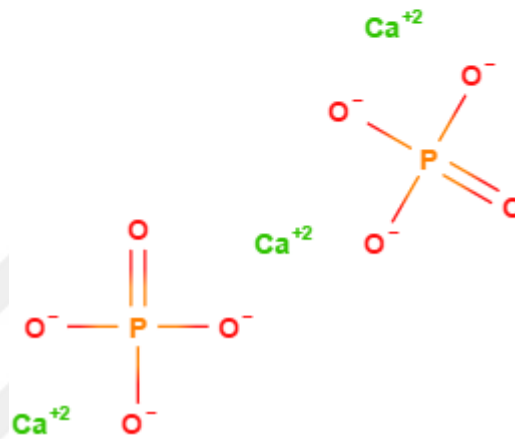
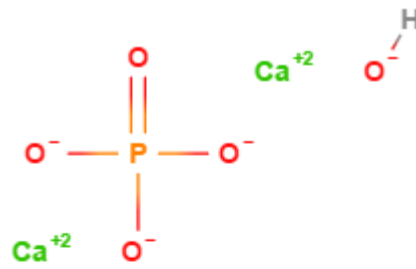


Figure 2.7: Molecular structure of Calcium phosphate [62].

The chemical formula of Calcium Phosphate Dihydrate (CPD) is $(\text{CaHPO}_4 \cdot 2\text{H}_2\text{O})$. Its mineralogical name is Brushite. Figure 2.8 presents a calcium phosphate ion and two water molecules. The CPD mineral is indeed another type of calcium phosphate structure. However, brushite is found rare when compared to apatite in urinary stone formation [68]. Additionally, CPD is a soft mineral, its color is usually pale-yellow, and CPD can be found with monoclinic prismatic crystals systems [69].

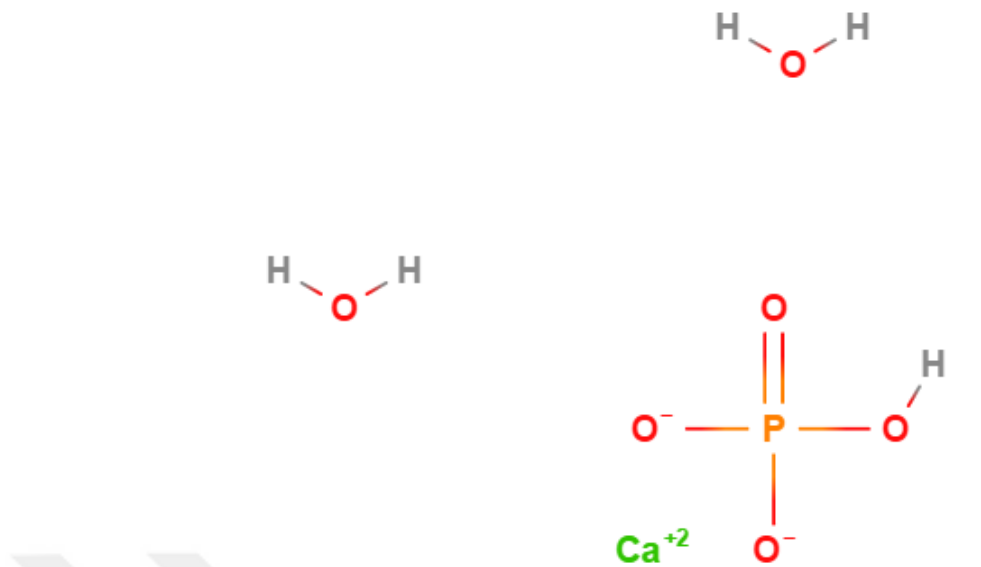


Figure 2.8: Molecular structure of calcium phosphate dihydrate [62].

Uric acid (UA) is also another well-known kidney stone component. It may occur in urinary system after break down of purine molecules. $C_5H_4N_4O_3$ is the chemical formula. Uric acid existence is attributed to with urine's low pH levels. Structure has monoclinic crystal system with four molecules in a unit cell [70]. Molecular structure of Uric acid is illustrated in Figure 2.9.

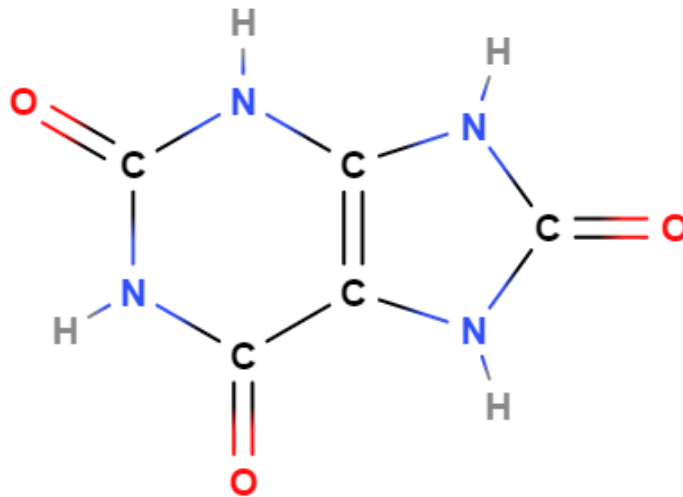


Figure 2.9: Molecular structure of Uric acid [62].

($MgNH_4PO_4 \cdot 6H_2O$) is the chemical formula of Struvite (MAP). It appears with infections, which caused by a bacterium in the urinary system. That bacterium lives in the kidneys of struvite stone patients. Also, alkaline urine (pH is greater than 7) is responsible for the formation of these crystals. Struvite treatment process is quite difficult. Mineral

grows quickly and spreads central structures of kidney, therefore it often takes place as staghorn stone. [60, 71].

Besides, the texture of the stone may be quite large and if it is untreated, disease can lead to kidney damages. Molecular structure has orthorhombic pyramidal crystal system [72]. Figure 2.10 shows struvite structure; six water molecules bind with a magnesium and ammonium ion.

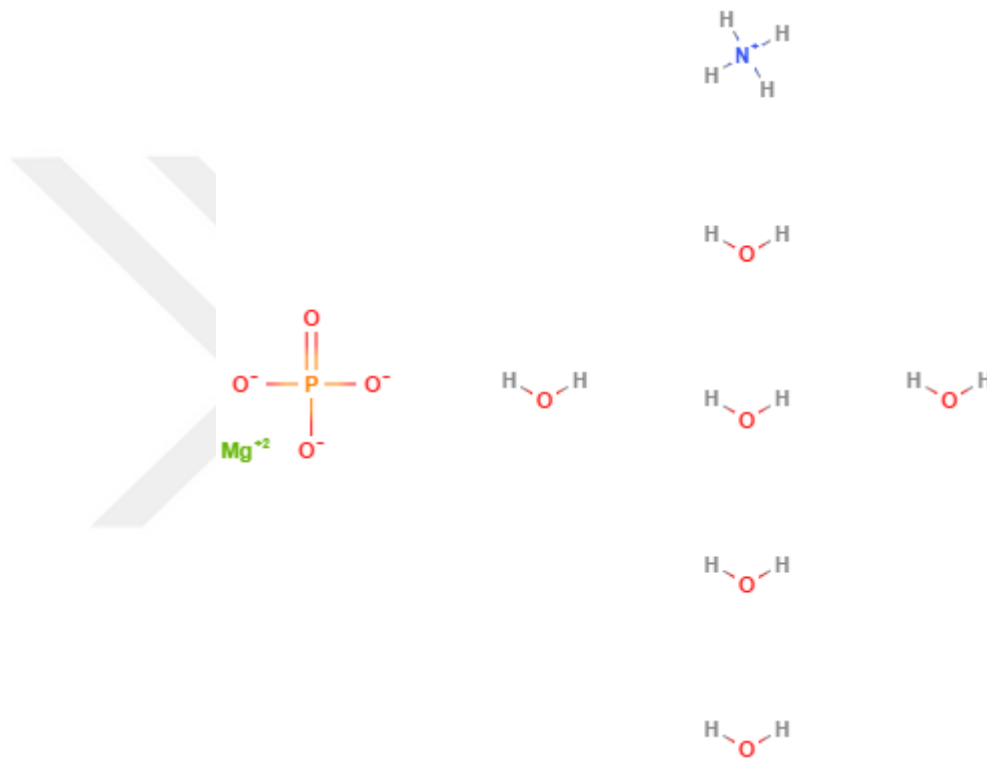


Figure 2.10: Magnesium ammonium phosphate hexahydrate [62].

Cystine molecule is a kind of amino acid. The formation of cystine stones depend on the high concentrations of the cysteine molecules in the urine, and it can appear in the bladder, ureters or kidneys. Cystine occurrence rate is very rare but the frequency of recurrence is high if we take into account other rare urinary stones types [60]. Cystine molecules form as hexagonal-shaped crystal system. Figure 2.11 presents cystine molecular structure.

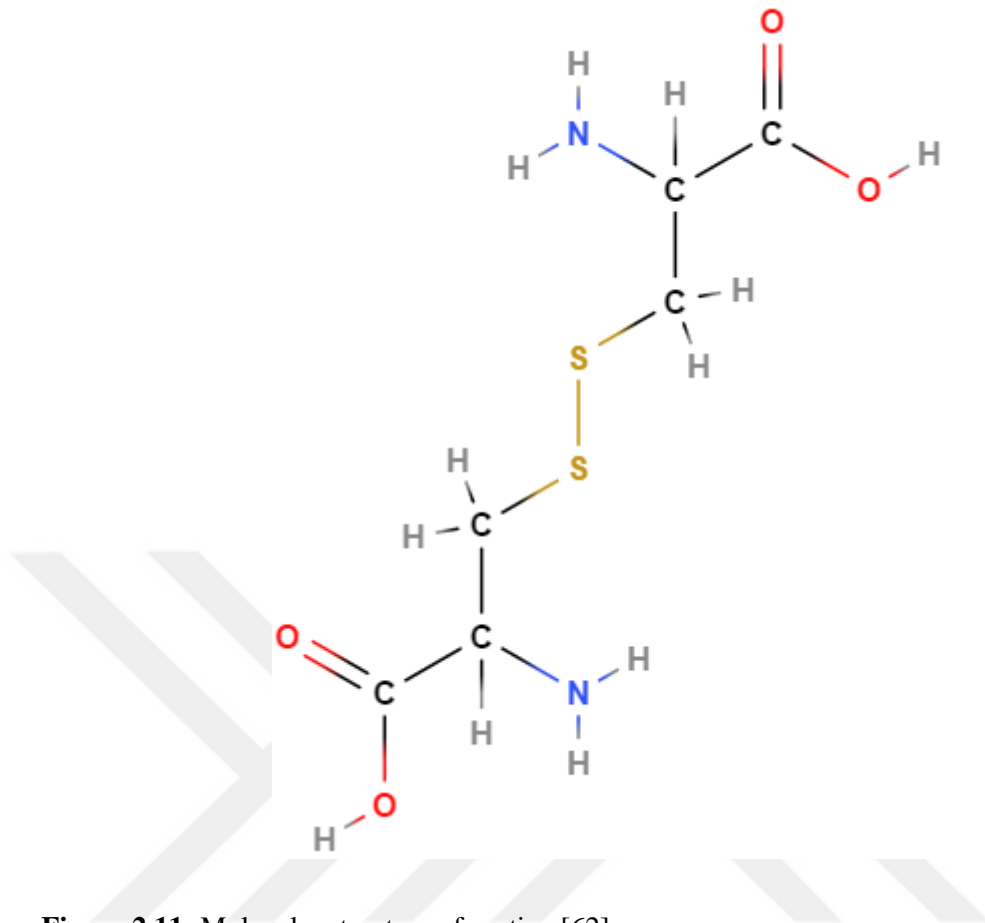


Figure 2.11: Molecular structure of cystine [62].

2.1.2 Fluorescence Reduction Materials for Chemical Bleaching on Renal Stones

Hydrogen peroxide and acetone have used as chemical agents for the bleaching process of the renal stones. Hydrogen peroxide is a strong oxidizer. Its chemical formula is (H₂O₂) and structural formula is H-O-O-H, it contains an oxygen–oxygen single bond. Figure 2.12 shows differences between hydrogen peroxide molecule and water. H-O radicals are appear easily after broken bond of oxygen atoms. HP is usually used for bleaching processes. Also, reacts for large number of organic forms such as fungi, spores, bacteria and viruses.

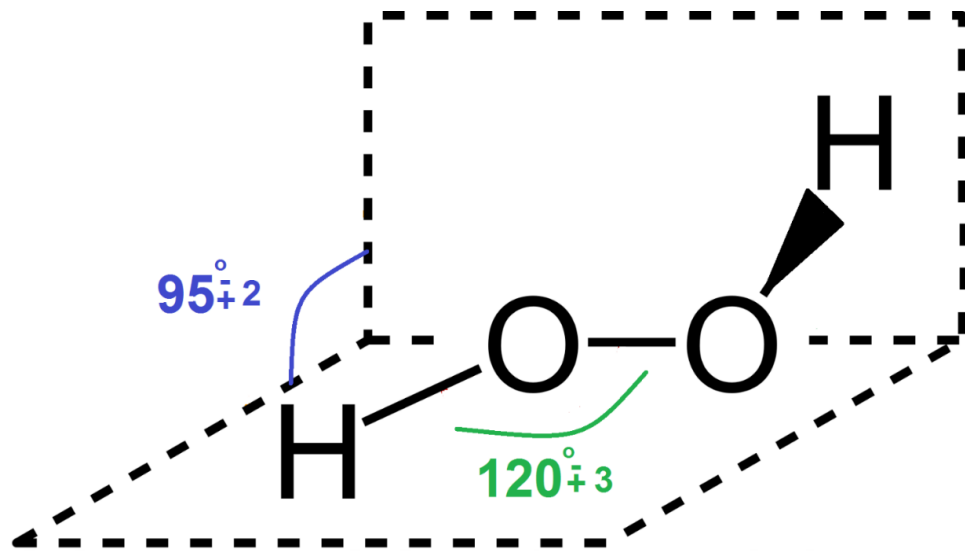


Figure 2.12: Structural formula of hydrogen peroxide molecule illustrated with bond angles.

2.1.3 Urine Crystals

Urine sediment includes some crystal particles, which crystals named as urine crystals or urinary crystallites. Urine crystals were identified after urine examined for the first time with classical optical microscope by Fabricius Nicolaus in early 1600s [73]. Most of the urine crystals were characterized in the 19th century, and urine examination was utilized for clinically. Also urine crystals were described as main particles of urine [74]. First book which related with urinary deposits were released in 1844 [75]. Around end of the 1800s, there was not any difference about the knowledge of urinary crystals with modern days [76]. Light microscopic images of most prevalent crystals such as; cysteine, struvite, calcium oxalate dihydrate, calcium oxalate monohydrate and regular-irregular shaped uric acid crystals are shown in Figure 2.13, respectively.

Additionally, researchers remark that urinary crystals are significance for urinary stone diseases [77-81]. Crystal growth is the start point for urinary stone disease, and these crystals are like as building blocks of renal stones. Likewise, the adhesion interaction between surfaces of kidney cells and urinary crystallites has importance for the urinary calculi formation [82]. Because in normal conditions, micrometer sized crystals are not attached to the kidney cells and they can be easily excreted with the urine. Crystal growth and aggregation process are main steps of stone formation [83].

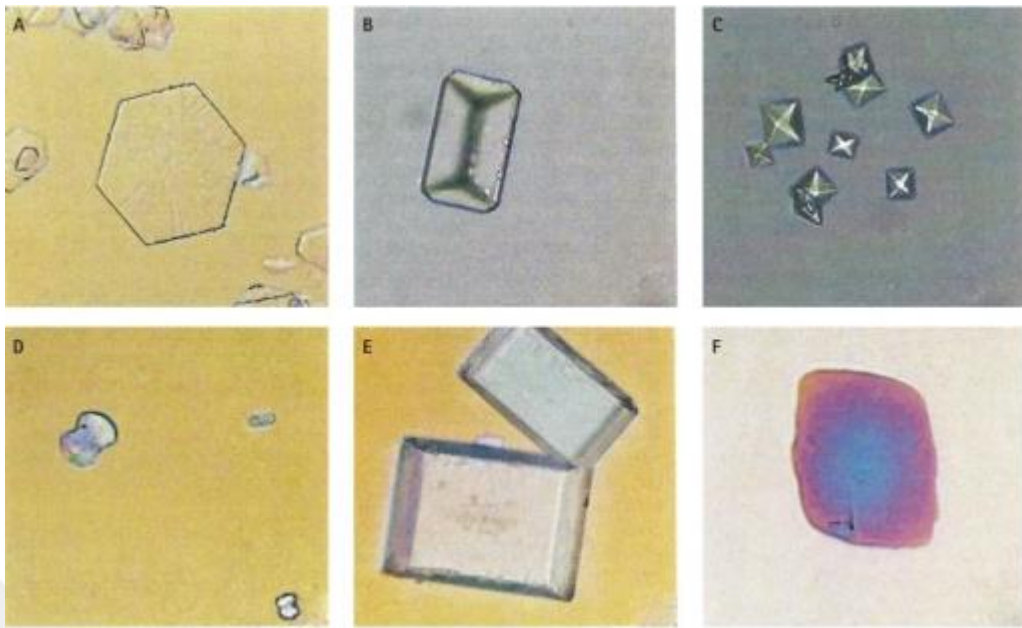


Figure 2.13: Optical microscopic images of different urine crystals, a) cystine, b) struvite, c) calcium oxalate dihydrate, d) calcium oxalate monohydrate, e) uric acid, and f) irregular shaped uric acid.

Besides, urine crystals can exist both in healthy persons and urinary stone patients [84, 85]. However, there are some important differences between two kinds of urine (healthy and lithogenic). Some studies indicated that urinary crystals mark variations in particle size, morphology, aggregation, and crystal phase between healthy humans and urinary stone patients [86, 87]. Healthy urine subjects are dispersed and rounded rather than lithogenic samples, also their size are smaller [88]. Crystals which exist in patient urine, have same sharp edges and tips [82]. Particles sizes which under the 20 μm can be easily excreted directly with the urine [89]. The number of crystals which size higher than 12 μm may found around 16 - 65 % in the urine of stone formers, however in healthy persons, this ratio is approximately 13 % [90]. Morphological differences between the healthy and lithogenic types of urinary crystallites are generally related with variations of the inhibitors in kidneys because they can balance crystal sizes [91, 92], inhibitor concentrations and activities are dissimilar [90, 93-96].

However there is not directly relation between particle size (crystal) and disease, for example sometimes particle sizes of the lithogenic urine are smaller than healthy subjects, additionally properties may vary for male and female patients. Also, food metabolism is

often impress the size of crystals [97, 98]. But generally urinary crystallites of healthy subjects are stable than patients [99].

2.2 METHODS

This section also gives an overview of main characterization techniques for utilizing on renal stone and urine crystal characterizations and investigations.

2.2.1 Stone Analysis

Stone analysis is recommended for investigation of urinary stone patients (lithogenic) all over the world. Reliable and efficient treatment of the renal stone disease depends on the information of the chemical composition of the calculi, which in return enables classification of the disease. A large number of techniques are used for renal stone analysis. But in recent years some methods such as X-ray diffraction and IR spectroscopy have overtaken the others. These methods ensure fast, sensitive, and extract information about the major chemical components of the stones without any destruction [33].

Additionally, vibrational spectroscopy has been effectively connected to the examination of the urinary stones in recent years. Different characterization techniques like as; SEM, EDX and TGA are also used to determine the organic and inorganic constituents of “human stones”. Analysis from minimum two different methods have been recommended for comparison of the results. Accurate and complete analyses of these samples are presented in next sections.

In this thesis, several experimental methods have been applied on kidney stones. The purpose of calculi analysis may be qualitative or quantitative. Since, stones have usually small size, fragile and heterogeneous structures. Especially after the modern treatment techniques, it is difficult to analyze them related with their sizes [100].

However, collecting information on chemical components provides correct diagnosis and treatment. Various numbers of analysis techniques were used for the characterization of the components of the renal stones. Generally combination of two methods which given below is advised for determining exact stone compositions. Fourier Transform Infrared (FT-IR), Fourier Transform Raman (FT-Raman), Dispersive Raman (Disp-Raman), X-

Ray Diffraction (XRD), Thermogravimetric Analysis (TGA) and lastly Scanning Electron Microscopy (SEM) with Energy dispersive X-ray spectroscopy (EDX) are given in different articles as most popular and effective methods.

2.2.2 Urine Crystal Analysis

A large number of studies are performed on kidney stone analysis with several approximations [101-104]. Each characterization method have different benefits. For this reason any two of the above mentioned techniques can be used as complementary in order to understand the structure and composition of the calculi. Also, sufficient amounts of stones can easily be characterized with commonly used techniques; however characterization would be difficult when stones formed as sand like (powder) particles or sub-visible crystals. However, usually in clinical applications, urinary stone formation can't be predicted before their appearance. If stones could be detected before their formation, prevention or treatment process would performed more effectively and easily. Since it has great economical value and the recurrence rate of the disease is very high, early diagnosis and prevention of stone recurrence is crucial [105].

Eventually, renal stone formation is a deviant bio-mineralization activity and several studies show that there is a remarkable relation between urinary stones and the types of urinary crystallites. Especially, this similarity increases when we consider the urinary stone patients [24, 106-109]. Urine salt components such as oxalate ion, can grow and turn to be a large stone piece in a short span of time in stone former patients. However calculi mineral components can only grow up unimportant small sized urine crystals in healthy people, so they can be transferred easily with daily urine [88].

On the other hand, urine examination is very extensive method for understanding urological sickness and crystal formation in hospitals [99]. The crystal precipitation starts in the urinary system and it can continue after the end of the excretion from body with urine, since temperature and pH conditions may affect this process directly [74]. For example 4 C° conservation conditions can lead to precipitation of phosphate and urate crystals [74]. Since the storage time and these mentioned conditions have a great importance for urinary crystal investigations, examination of the stones must be finished as soon as possible in addition to keeping the body conditions carefully [110].

In this sense, generally classical light microscopy or polarized light microscopes are prevalently used for the identification of that urine crystals [111]. These classical methods can ensure good results in order to observe small urine crystals. However, in these techniques, the definitions are based on only their crystal shape (physical appearance). But, since the urine crystals are frequently irregular shaped and colorless, they can't be easily defined. Besides, determining and imaging of urine crystals with classical microscopes involve some different problems like having small sizes and low densities [112, 113]. These kinds of particles (urine crystals) usually have a size under 100 μm and they are defined as sub-visible [114]. Also, probing the solubility properties of crystals is an alternative way for characterization. Some chemicals can be used as a marker for different crystals; for instance calcium phosphate and triple phosphate are soluble in acetic acid and hydrochloric acid or calcium oxalate is soluble in hydrochloric acid and sodium hydroxide [115]. However this kind of biochemical analysis procedures has some limitations [74]. In this context more complicated techniques must be required for obvious crystal analysis.

In recent years, modern treatment techniques have developed, such as extracorporeal shock wave lithotripsy (ESWL) and ureteroscopic lithotripsy (URSL). They can provide effective stone management and less painful treatment than previous techniques. However, after applying these modern techniques, residual stone fragments are generally too small for considering collection and analysis. Mainly, great deals of researches are carried out studies on the samples which have enough size for classical analysis methods and these samples are acquired via surgery or natural ways. In this sense, micro-spectroscopic techniques can be utilized for collecting information from these small stone particles. Current urinary calculi analysis techniques need at least visible size of samples in practice, but only a few investigations have tried to identify invisible stone fragments or urine crystals from directly urine.

Micro spectroscopic techniques include both qualitative and quantitative measurements. They have many advantages over traditional biochemical methods, especially micro-Raman spectroscopy has several features, which can be used for medical and biological analysis. The technique enables high chemical specificity, faster data analysis, nonspecific sample preparation and molecular characterization [116].

Several investigations are interested with this topic. For example; Xin-yuan et al., studied various sizes of calcium oxalate monohydrate and dihydrate crystals [117]. Kreshnik Angonil et al., were reported spectroscopic investigations of urinary sands, and they were used Raman spectroscopy for illustrates the presence of struvite and apatite in their study [118]. Yi-Chun Chiu et al, reported the use of micro-Raman spectroscopy for determining the composition of the renal stone sediments directly from the urine after the treatment procedure.

2.2.3 Spectroscopy

Spectroscopy is an important branch of modern physics. It utilizes several analysis methods [119], instruments which are used in this field are called as spectrometers. The discipline (spectroscopy) is concerned with absorption, emission, scattering and diffraction of electromagnetic radiation with mater [120].

Emission and absorption of the electromagnetic waves are a consequence of the energy transfer between radiation and matter. However scattering is terms of electromagnetic wave deflection from matter (atom or molecule), scattering can occur each direction and elastic and inelastic types are exists. Additionally, diffraction emerges from the nature of the electromagnetic waves [121].

Spectral results can give information about the atomic and molecular structure of any system, such as; molecular geometries and symmetries (bond angles, bond lengths, and torsion angles), electric and magnetic properties, electron densities or energy level distributions [122, 123]. In recent years, molecular spectroscopic techniques are commonly used in both quantitative or qualitative analysis and characterization of materials, eventually, spectroscopy plays an essential role for several sub-branch of physics [124, 125].

The physical properties of light were determined by James Clerk Maxwell in 1870s. Accordingly, electromagnetic radiation can be defined as; a wave produced by both of electric “E” and magnetic “H” fields, which fluctuate perpendicular to each other and perpendicular to the propagation direction [126]. Likewise, the direction of propagation of both electric and magnetic fields can be located in any axis. Also the electric and

magnetic fields of the electromagnetic radiation can be calculated by equations (2.1) and (2.2), respectively. These formulas arise from Maxwell equation.

$$E = E_0 \cos \left[2\pi \left(\frac{x}{\lambda} - vt \right) \right] = E_0 \cos(kx - \omega t) \quad (2.1)$$

$$H = E_0 \cos \left[2\pi \left(\frac{x}{\lambda} - vt \right) \right] = E_0 \cos(kx - \omega t) \quad (2.2)$$

Here; “k” is the angular wavenumber and “ ω ” is angular frequency.

$$k = \frac{2\pi}{\lambda} \quad (2.3)$$

$$\omega = kv \quad (2.4)$$

An electromagnetic wave shows in Figure 2.14. Where; E_0 and H_0 are the maximum values of the electric and magnetic fields of the electromagnetic waves, respectively. In addition, “v” is equal to “c” in free space.

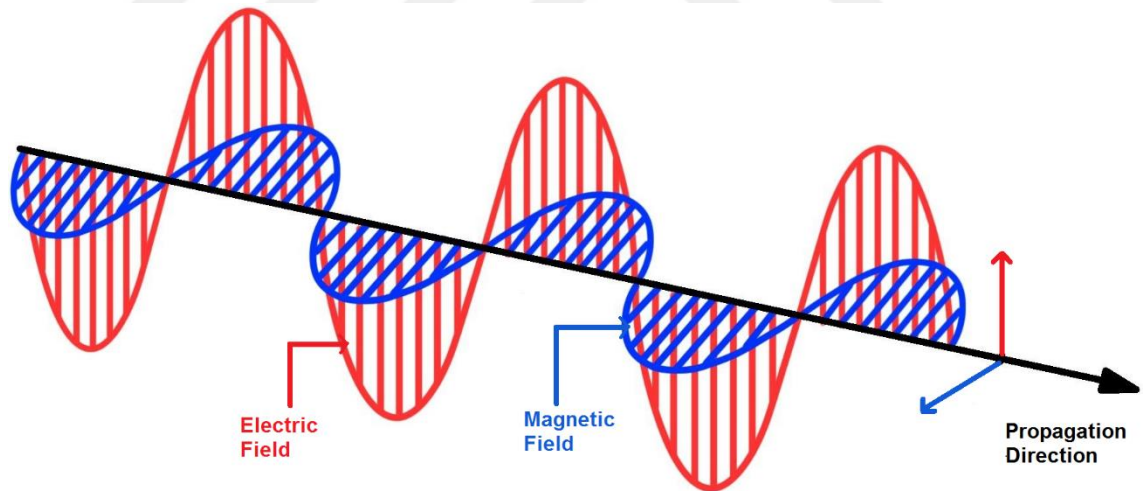


Figure 2.14: Electromagnetic wave, black arrow shows the direction of propagation. Magnetic and electric fields are illustrated with blue and red lines, respectively.

$$\tilde{\nu} = \frac{1}{\lambda} \quad (2.5)$$

“ λ ” is the radiation wavelength and it describes as the distance between two neighbor peak points of electromagnetic wave. Also “ ν ” is the frequency, and it can be define as number of fluctuate at one point in a second, the unit of the frequency is *Hertz*.

Another approximation came up with Planck and Einstein, which was based on quantum mechanics, this approximation states that, electromagnetic radiation is comprised physical properties of a particle. In this approach, energy packets which defined as *photons* are generate the electromagnetic radiation, in this place, the energy of any photon can be calculated by Planck's equation (2.6). Where; "v" is the frequency of the photon and "h" is Planck's constant.

$$E = h\nu \quad (2.6)$$

After that, in 1924 particle-wave dualism was postulated by L. de Broglie. He was stated that if electromagnetic waves present particle properties, the moving matter can also exhibit properties like as waves [127]. According to the de Broglie's approximation; moving particles behave as wave properties, and also they have a linear momentum "p", related to its wavelength "λ". Basic wave illustration gives in Figure 2.15. Equation (2.7). Where; m is the mass of the moving particle, and v is the velocity. As a consequence, several spectroscopic characterization techniques are available, such as, electron and neutron diffraction in which the de Broglie's approximation is used to determine matter-wave properties [128].

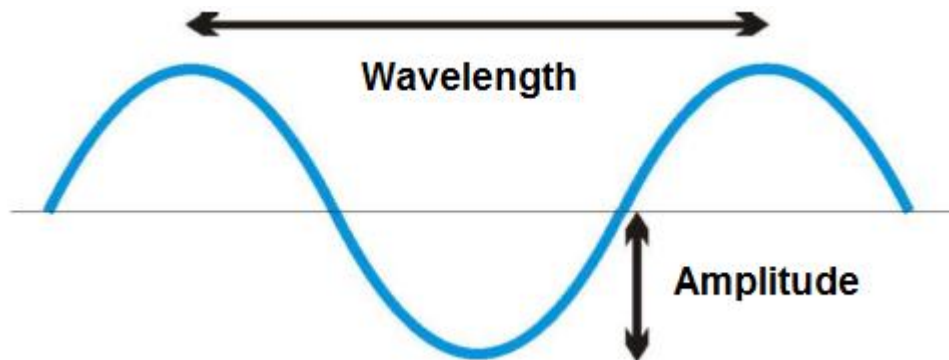


Figure 2.15: Basic wave illustration.

$$\lambda = \frac{h}{p} = \frac{h}{mv} \quad (2.7)$$

The electromagnetic spectrum divided different regions which related with its energy or in other words depend on its wavelength or frequency [128]. Figure 2.16 shows the electromagnetic spectrum and its special parts. Generally, wavelength parameters are utilized in the characterization of the regions.

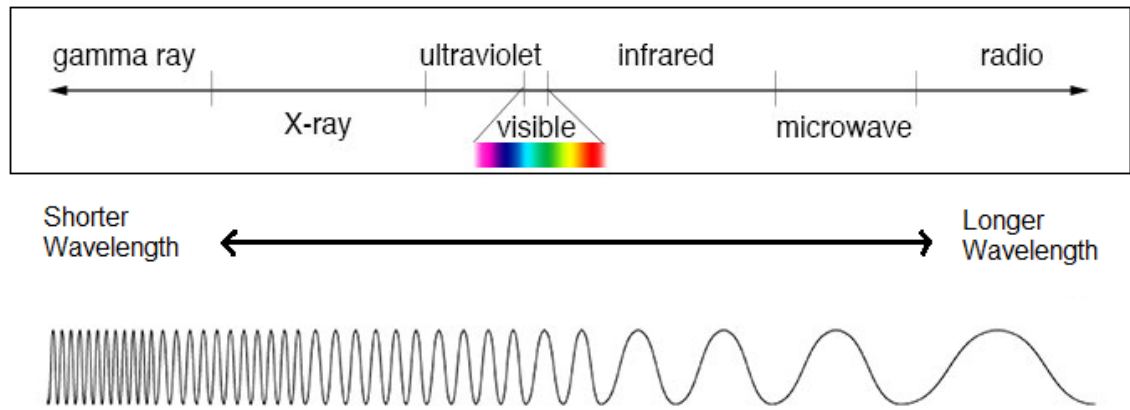


Figure 2.16: Electromagnetic spectrum and its special regions.

In here, the well-known visible radiation (400-700 nm) is only a part of the electromagnetic spectrum. Besides that, different regions can be described such as; gamma rays (0,003-0,3 Å), X-rays (0,3-100 Å), ultraviolet (10-400 nm), infrared (1 μm-0,1 mm), microwave (0,1 mm- 10 cm) and radio waves (10 cm-30 m). Actually these parts of the electromagnetic spectrum are only postulated conceptions, because all of the electromagnetic waves have same physical properties. However, each parts can be utilized depends on its interaction capacities with matter. For example (from TV-radio communications, x-ray imaging or microwave applications).

Quantum mechanical approximations are widely used in spectroscopic methods [129, 130]. Because energy transfer mechanism between radiation and matter is easily explained by quantum mechanical theory. Emission or absorption of the electromagnetic radiation is only allowed with quantized energy levels. According to the Bohr's theory; electromagnetic radiation can be only absorbed, if its energy is equal to the energy differences between quantized levels (E_1 and E_2), such as equation (2.8).

$$\Delta E_{1 \rightarrow 2} = E_2 - E_1 = h\nu \quad (2.8)$$

Otherwise, after absorption of the electromagnetic radiation, excited atomic system could turn back to ground energy level with emitting an electromagnetic radiation, also the frequency of that radiation is equal to energy differences of states (E_1 and E_2). Figure 2.17 shows absorption and emission process at atomic level respectively.

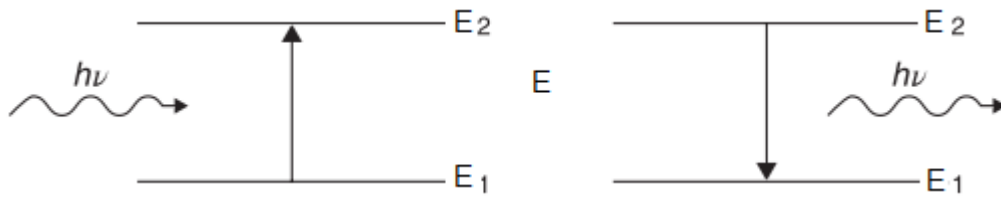


Figure 2.17: Absorption and emission of photon at atomic level.

2.2.3.1 Raman Spectroscopy

Raman spectroscopy is a kind of vibrational spectroscopic technique which exist after inelastic light scattering from matter. It conventionally works with, monochromatic laser light which located in the range of UV, visible or near-Infrared radiation. If photons do not pass-through directly from matter, they may be absorbed from the specimen, in this point molecules are excited to an excited electronic state from the ground state [131]. But this absorption can only take place when the molecular energy gap is equal to the energy of the photon. However photons can be scattered if these energy levels (molecular energy gap and photon) are different. Thus, Raman Effect is observed during this scattering phenomena. Scattering can be described as two different types which are Rayleigh and Raman [132].

Although molecules which have net dipole moment are measurable in infrared spectroscopy, Raman interaction indicates for only polarizable molecules, and also it depends on molecular vibrational motions. However Raman scattering is very rare process than other scattering types, because most of the photons are expose to Rayleigh scattering. But, this difficulty can be eliminated with efficient filters and very sensitive detectors.

In Rayleigh scattering, process between photon and molecule is elastic which means, molecules return back its own ground state energy level after interaction with light (photon) without any energy transfer. However, Raman scattering process is inelastic, and different from Rayleigh scattering, a portion of energy can be transferred between the photon and the molecule. Since molecules absorb photon's energy and go up to a virtual energy state, after that molecule returns back to its own ground state energy level as soon as possible by emitting a new photon, and that new photons energy must be different from the initial frequency [131].

The Raman Effect can be defined easily with classic theoretical approach. First we consider a photon (light) with its frequency (ν_0), and electric field (E);

$$E = E_0 \cos \omega t \quad (2.9)$$

Where ω is angular frequency;

$$\omega = 2\pi\nu_0 \quad (2.10)$$

Also, E_0 is the amplitude and t is the time.

If this photon (light) illustrates a diatomic molecule, the dipole moment μ can be given by the equation (2.11);

$$\mu = \alpha E = \alpha E_0 \cos 2\pi\nu_0 t \quad (2.11)$$

If that diatomic molecule is vibrating another frequency (ν_1), we can write the nuclear displacement (Q) with equation (2.12);

$$Q = Q_0 \cos 2\pi\nu_1 t \quad (2.12)$$

In here Q_0 is the amplitude of the vibration.

For small values of vibrations “ α ” is;

$$\alpha = \alpha_0 \left(\frac{d\alpha}{dQ} \right)_0 Q \quad (2.13)$$

In here, “ α_0 ” is the polarizability at the equilibrium position. So, the change of the polarizability can be written as equation (2.14);

$$\left(\frac{d\alpha}{dQ} \right)_0 \quad (2.14)$$

Finally, dipole moment can be defined as combination of equations (2.11), (2.12), (2.13);

$$\mu = \alpha E_0 \cos 2\pi\nu_0 t \quad (2.15)$$

$$\mu = \alpha_0 E_0 \cos 2\pi\nu_0 t + \left(\frac{d\alpha}{dQ} \right)_0 Q_0 E_0 \cos 2\pi\nu_0 t \cdot \cos 2\pi\nu_1 t \quad (2.16)$$

$$\mu = \alpha_0 E_0 \cos 2\pi\nu_0 t + \frac{1}{2} \left(\frac{d\alpha}{dQ} \right)_0 Q_0 E_0 [\cos\{2\pi(\nu_0 + \nu_1)t\} + \cos\{2\pi(\nu_0 - \nu_1)t\}]$$
(2.17)

First term in equation (2.9) express oscillating dipole of the incident photon radiation, in other words it means that Rayleigh scattering, and second part describes that Raman scattering frequencies; $(\nu_0 + \nu_1)$, is anti-stokes scattering and $(\nu_0 - \nu_1)$ is stokes term of the Raman spectral shifts.

Raman scattering appears two different types, they are called as, Stokes scattering and Anti-Stokes scattering. Stokes scattering occurs when photons scattered with lower frequency than the initial source excitation energy. However, Anti-stokes scattering consists when energies of scattered photons are greater than initial excitation frequency [133]. Besides, the Stokes and anti-stokes Raman intensities are directly proportional to the number of molecules in the lowest and highest vibrational levels.

So, that energy transfer emerges as frequency shifts for the initial monochromatic light. Hence, different frequency shift patterns appear a fingerprint (unique), for any compound. Raman Effect can be described using the energy level diagram which shown in Figure 2.18, Stokes and Anti-Stokes Raman scattering are illustrated by red and green transition at atomic level, respectively.

Usually, Stokes scattering Raman intensities are greater than the Anti-Stokes Raman intensities. Because, in normal conditions, the number of molecules which located at the higher vibrational energy level is less than the number of molecules at the lower vibrational energy levels. Raman spectra are plotted with both the scattered intensities and Raman shift values. Raman shift is described as, the energy differences between scattered and incident photon frequencies. Also “ cm^{-1} ” generally utilizes for the unit of Raman shift. Consequently, these shifted frequencies are characteristic fingerprints for the each individual molecule [134].

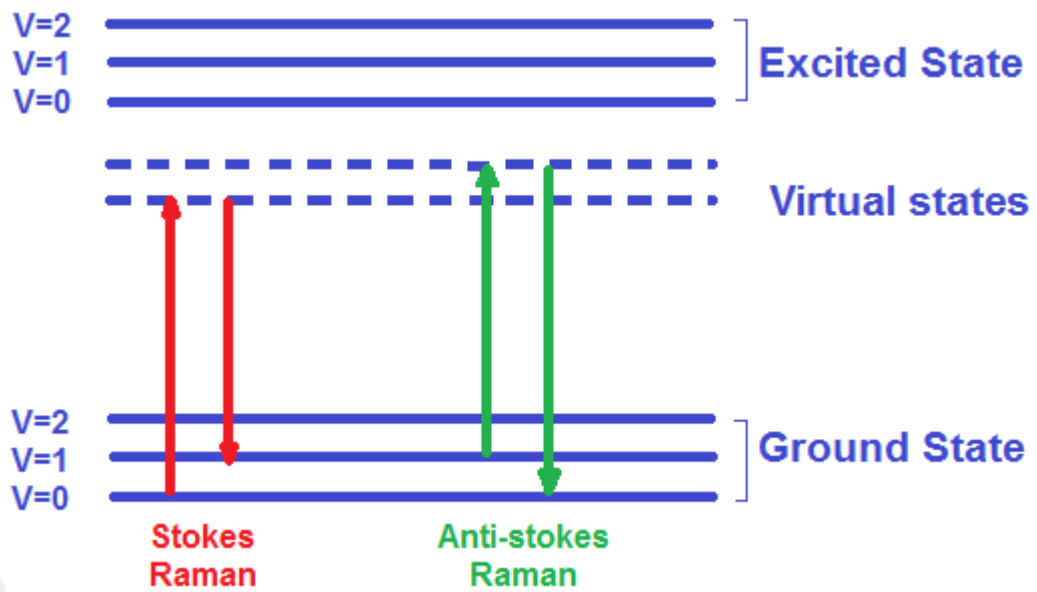


Figure 2.18: Energy level diagrams for Raman scattering. Both ground state and first excited state are given as an atomic level.

Besides, Raman spectroscopy has several advantages. Raman spectrometers can work with lasers which located in the visible part of the electromagnetic spectrum. Also, required optical technology are simple and inexpensive. Further, monochromatic laser beam is utilize which may be focused precisely and selectively over any part of a solid sample. Also, the analysis of wet samples are also possible in this technique. The main disadvantage of Raman spectroscopy is the inherent interference from the fluorescence. However there are several methods which can use for eliminating that fluorescence background.

2.2.3.2 Fluorescence Reduction in Raman Spectroscopy

There are some significant restrictions to the Raman spectroscopy. The most important limitation is background fluorescence problem. That problem acts critical role in Raman spectroscopic studies. Fluorescence phenomenon acts a catastrophic effect for Raman spectroscopic measurements. Because it can overlap entire spectrum. If fluorescence occurs, the background is usually dominated by fluorescence signals and Raman bands become indistinguishable [135]. Fluorescence and Raman scattering are two very similar process but, which have different mechanism. Figure 2.19 shows general types of light scattering from a specimen.

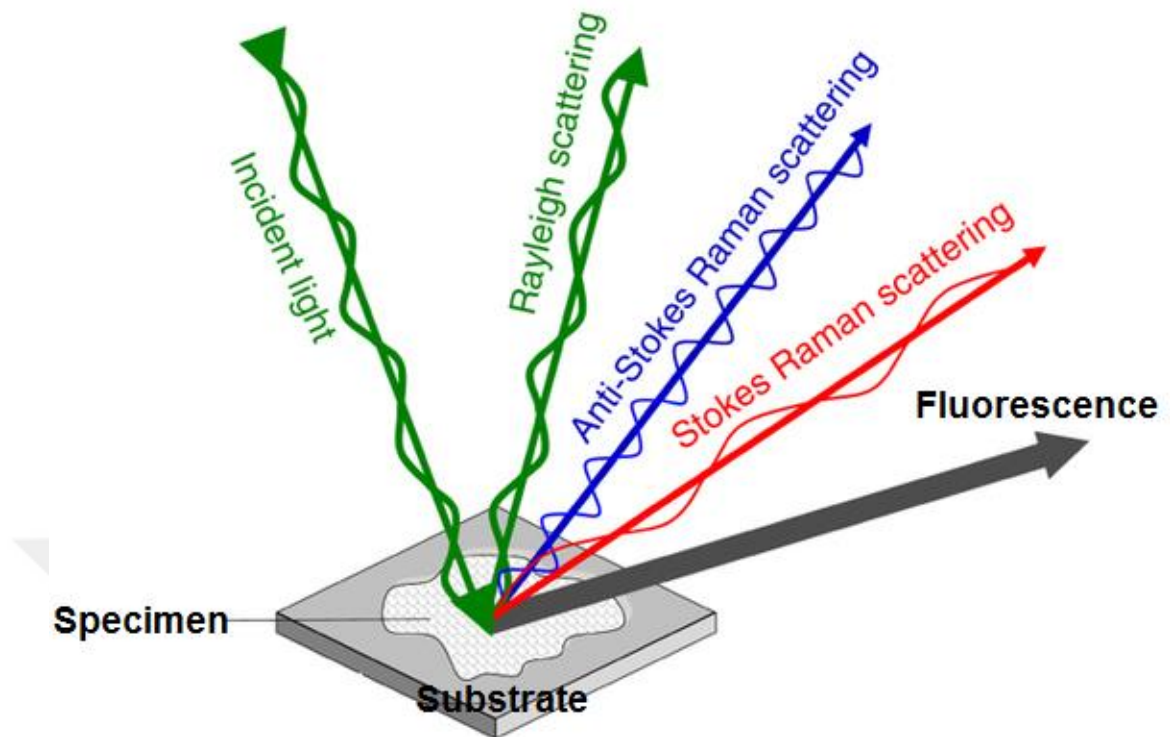


Figure 2.19: General types of light scattering from a specimen. Rayleigh, Raman and Fluorescence are illustrated [136].

Normally, most of the molecules can exist in the ground electronic state (especially lowest vibrational levels) at the room temperature, and after interaction with electromagnetic radiation, some molecules gain energy and occupy higher vibrational levels of the excited the electronic states. After this level, molecules are lose their energy by collisions immediately, and go to the lowest vibrational level of the excited state. Finally, molecules may fall to any of the vibrational levels of the ground state, so the energy differences between both electronic states arise as form of fluorescence radiation. Fluorescence is the most important disadvantage of Raman spectroscopy, especially for biological sample investigations [137-139].

After the interaction between specimen and laser beam, Raman signals are almost instantly exist (approximately $\leq 10^{-15}$ s), because there is not any excited state transition [140]. However fluorescence is a slow process and needs more time than the Raman phenomena, it occurs occurring at time scales of 10^{-9} to 10^{-7} s [141]. Figure 2.20 shows differences between Raman and fluorescence in atomic scale with a diagram. Usually the most important reason for fluorescence is impurities and pollutes of samples, such as hemoglobin, collagen, lipids and proteins particles inside of biological samples [142].

Moreover fluorescence intensity could be as great as 10^4 than Raman signals [143, 144]. It means that Raman peaks can be covered up by a strong and broad fluorescence spectrum at same frequency band.

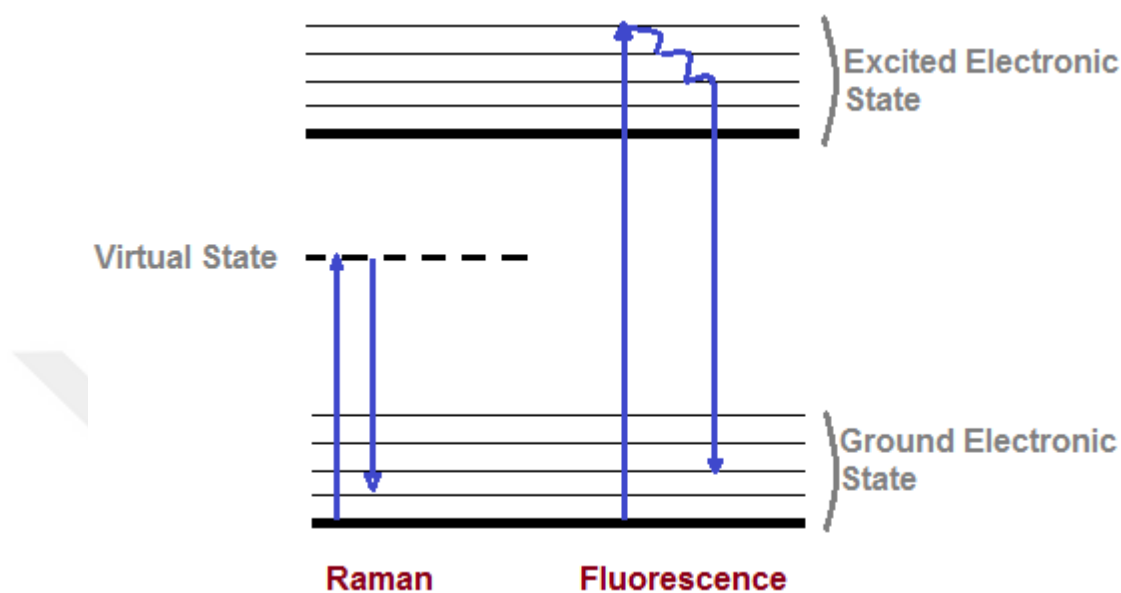


Figure 2.20: Differences between Raman and fluorescence phenomena in atomic scale with a diagram.

Therefore Raman spectroscopy utilization is limited to blockade of the fluorescence. The occurrence of that situation is very prevalent and also depends on excitation laser wavelength. The relation between laser wavelength and fluorescence emergence is shown in Figure 2.21.

Raman spectrum involves more knowledge about such molecules rather than the fluorescence signals. Therefore, several techniques such as; experimental, computational, photo bleaching or chemical bleaching can be used in order to avoid fluorescence background from Raman spectra [142, 145, and 146]. Additionally, in order to keep away from the fluorescence, choosing correct excitation laser wavelength is also fundamental method. The probability of fluorescence emitting could decrease with low laser frequencies [147]. For this reason most of the applications are not useable in visible wavelengths. For example, using higher wavelengths at near infrared region is helpful for reducing fluorescence effect or, laser frequencies can be chosen lower than electronic transition levels.

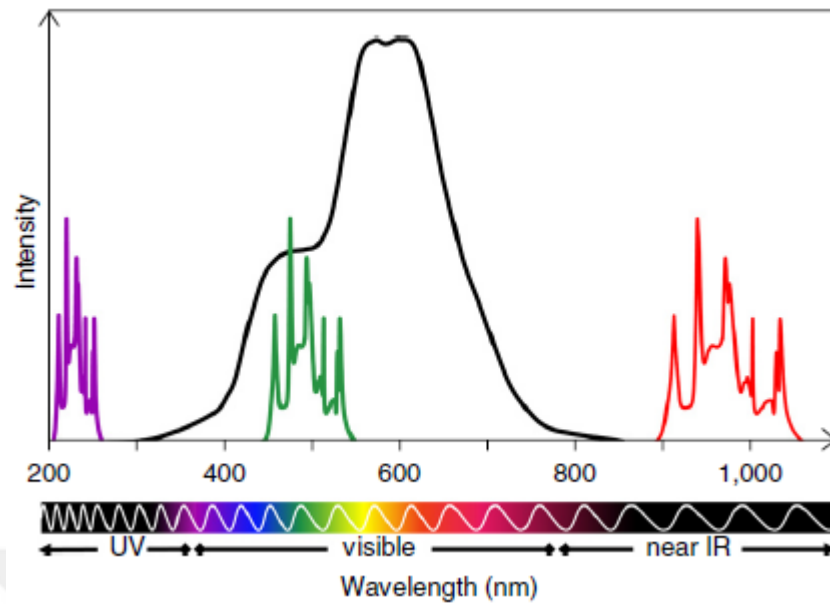


Figure 2.21: The relation between laser wavelength and fluorescence emergence [136].

In this context, various studies have been performed in order to reduce fluorescence from biological tissues. For example, Gölcük K. et al. investigated photo-bleaching effect on fluorescence background and they used bone tissue as specimen [148]. Also some researchers utilized hydrogen peroxide for bleaching, because this chemical can be decrease background fluorescence ratio from Raman spectrum with the effect of the chemical-bleaching. In this approximation, fluorescence could be reduced from the photo-induced reaction of the used chemicals with fluorophores [149].

There are different types of papers concerning with this phenomenon such as “Effect of Hydrogen Peroxide Bleaching on Bone Mineral/Matrix Ratio” written by Chen T. et al. Fluorescence reduction in the bone by Raman spectra with hydrogen peroxide chemical reduction protocol had been explained in this article. Additionally in a different paper, bone tissue and 30 % hydrogen peroxide interaction has been studied from Penel et al., and noticed that characteristic Raman frequencies of the sample had not changed after this application [150].

On the other hand, some studies express that the intensity of phosphates bands of the samples are decreases after chemical bleaching application. However, according to study of the ref. [151], a group of teeth has divided by three parts, for determining the chemical activation of bleaching agents which include different concentration of hydrogen

peroxide. The results of the mentioned investigation show that, there was not any significant differences for the phosphate concentration of the teeth group of 9.5 % hydrogen peroxide, but the phosphate concentration is dramatically decreased for the teeth group of 38 % hydrogen peroxide bleaching agent.

As a result, such studies have shown that chemical bleaching for fluorescence reduction is not appropriate for quantitative Raman spectroscopic studies. In recent years, studies which are based on Raman spectroscopy for the investigation of bio-mineralized tissues such as bones and teeth are very prevalent [136, 152-155]. Several bio-apatite such as, bone, teeth or renal stones give similar Raman frequencies [156-158].

2.2.3.3 Infrared Spectroscopy

When infrared region of the electromagnetic spectrum interacts with matter, the radiation will be transmitted or absorbed consistent with vibrational modes of the molecules [159, 160]. That means, when photons of the infrared radiation interact with matter, vibrationally excited molecules will appear [161]. Furthermore, molecules have different vibrational modes, and the number of the modes depends on structure of the molecule. Hence, infrared radiation can be utilize for characterization of several types of matter.

A Beginning for the introduction of the harmonic vibration, at first, we have to consider molecules as; point masses which are connected to each other with mass-less springs (Wilson et al. 1955). Figure 2.22 shows a diagram for understanding the differences of the harmonic and anharmonic oscillators.

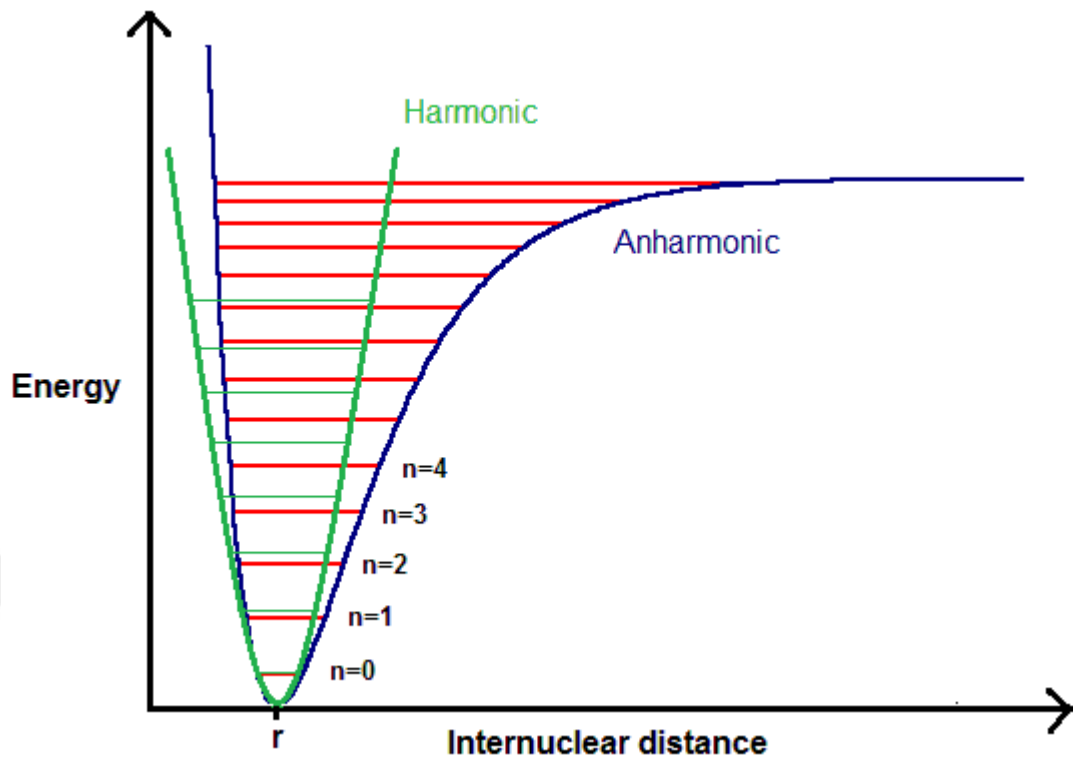


Figure 2.22: Internuclear distance vs Potential energy diagram for diatomic molecules, green and blue curves are shown harmonic and anharmonic oscillators, respectively.

In equation (2.18); “ F_x ” is the force (Hooke’s law), “ k ” is the spring constant, and expresses the rigidity of the spring. Figure 2.23 illustrates double atomic system with their spring like chemical bond for understanding Hooke’s law at atomic level. In this case; M_1 and M_2 denotes the mass of two different atom, also Δx is the distance from the equilibrium position from x-axis.

$$F_x = -k\Delta x \quad (2.18)$$

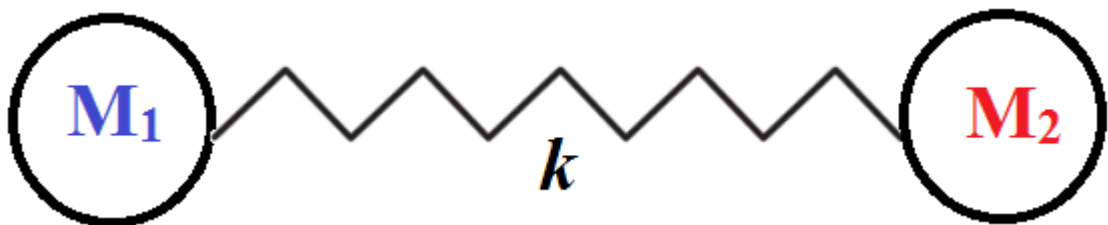


Figure 2.23: Illustration for understanding Hooke’s law on atoms, chemical bond behaves like as spring.

Also; potential energy;

$$E_p = \frac{1}{2} k \Delta x^2 \quad (2.19)$$

And kinetic energy;

$$E_K = \frac{1}{2} \mu (\Delta \dot{x})^2 \quad (2.20)$$

Here;

$$\mu = \frac{M_1 \cdot M_2}{M_1 + M_2} \quad (2.21)$$

This equation must be in good agreement with conservation of energy. The total energy ($E_p + E_K$) must be constant,

So;

$$0 = \frac{dE_p}{dt} + \frac{dE_K}{dt} = \frac{1}{2} \frac{d(\Delta \dot{x}^2)}{dt} + \frac{1}{2} k \frac{d(\Delta x^2)}{dt} \quad (2.22)$$

From Newton's equation of motion;

$$\frac{d^2 \Delta x}{dt^2} + \frac{k}{\mu} \Delta x = 0 \quad (2.23)$$

Where;

$$\Delta x = A \cos(\omega t + \emptyset) \quad (2.24)$$

In here; A is amplitude, ω is angular frequency and \emptyset is the phase.

Combination of equation (2.23) and (2.24);

$$\frac{d^2 \Delta x}{dt^2} + \omega^2 \Delta x = 0 \quad (2.25)$$

Finally, as a result;

$$\omega = \sqrt{\frac{k}{\mu}} \quad (2.26)$$

Equation (2.26) expresses that frequency of harmonic motion increases when the rigidity of the spring increases, however decreasing with if the atomic mass of the molecules increase.

We can write equation (2.26) another form with divided by $2\pi c$;

$$\bar{\nu} = \frac{1}{2\pi c} \sqrt{\frac{k}{\mu}} \quad (2.27)$$

Vibrational mode numbers and types depends on the feature of any molecule, as a general rule; linear molecules have $3N-5$ different vibrational modes and non-linear molecules have $3N-6$ different vibrational modes [162], where N is the total atom number in any molecule.

On the other hand, dipole moments can be change during the atomic displacement and only some vibrational modes absorb infrared radiation because absorption needs net dipole moment for each mode. Absorption frequencies from vibrational mode occurs a specific pattern for the identification of the molecules species. These absorption frequencies are plotted for transmittance intensity as x-axis and wavenumber “ cm^{-1} ” as y-axis. One of the most common and standard method for the stone analysis study is the infrared analysis [163-166].

In addition, there are some varieties as sub-methods in infrared spectroscopy which can provide several benefits. Information about the identity of the components of sample can be obtained by infrared spectroscopy. Also, it allows analyzing in a short time, and the current generation of Fourier transform infrared (FT-IR) spectrometers provides data of extremely high signal-to-noise ratio. Figure 2.24 shows basic principles of a Fourier transform infrared spectrometer.

Potassium bromide (KBr) pellet and attenuated total reflection (ATR) techniques seems to be most popular methods for sample preparation in the FT-IR. In KBr pellet technique, a handmade sample disc which includes both specimen and dried KBr powder is prepared. But, that disk can be formed only under the temperature and high pressure. KBr technique gives opportunity especially for Far-IR region studies.

However, ATR is a contact sampling method that involves an optical crystal with a high refractive index and excellent IR transmitting properties. Also, ATR is one of the most popular sampling techniques used by FT-IR Spectroscopy because it is quick, non-destructive and requires no sample preparation. Although easier sample preparation is the main advantage of ATR.

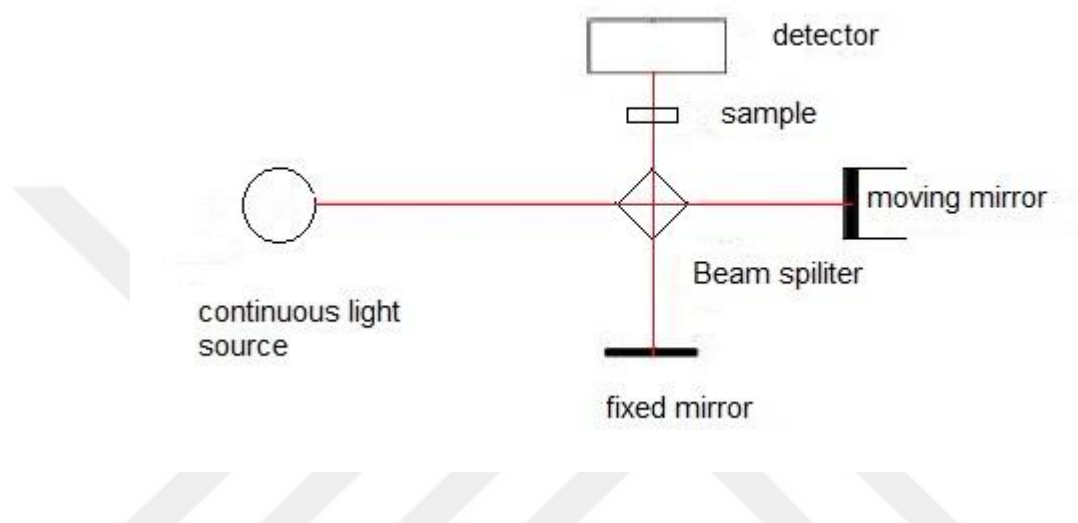


Figure 2.24: Fourier transform infrared spectrometer setup. Mirrors, light source, beam splitter, sample holder and detector are illustrated.

2.2.3.4 X-Ray Diffraction

X-ray diffraction (XRD) is very important experimental technique and utilized for identification of the atomic and molecular structure of materials, however these materials must be in crystal form [167]. Atoms are located regular 3-D positions in crystal materials, and there arise as only some specific structures [168]. These structures called as unit cells. In this regard, X-ray diffraction pattern can be used as a fingerprint for identification of each crystal structure. XRD has been use as basic method for various researches [169].

Several materials such as, metals, minerals, salts and several organic molecules can be investigated with this efficient technique. Each crystal structure has a characteristic diffraction pattern. Unknown sample's identity can be found by comparing with spectral pattern with reference.

Elastic scattering can be occurred after X-rays hit the atoms which are located in crystal structure [170]. In this scattering process generally x-rays cancel or support each other,

they called as destructive and constructive interference, respectively. However only some specific angles for each crystal can be reflected by the x-ray with constructively. Thus, specific angles (constructive reflections) can be utilized in XRD technique. A schematic diagram of constructive interference is shown in Figure 2.25, also equation (2.28) describes the Bragg's law phenomena;

$$n\lambda = 2d(\text{hkl}) \sin(\theta) \quad (2.28)$$

In this equation λ is the wavelength of X-ray, n is an integer, d is the distance between layers of the atomic lattice, and θ is the angle between the scattered x-ray and the atomic layer. Also, this formula can be used for calculation for some parameters of crystal structure [171].

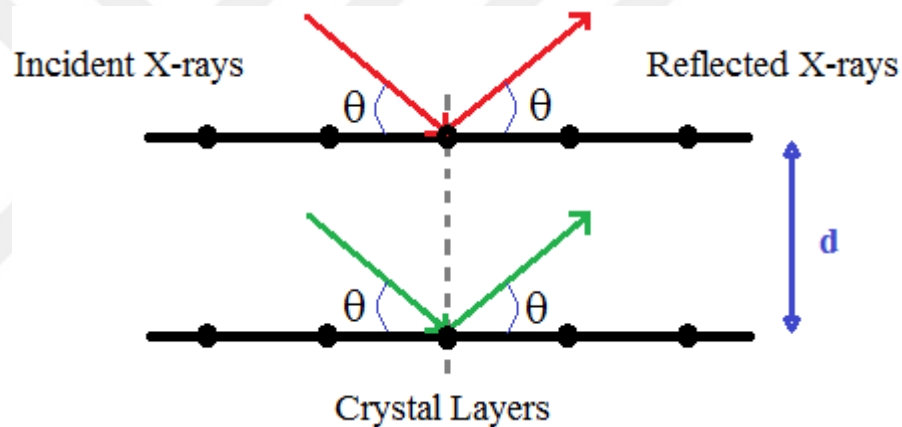


Figure 2.25: Coherent X-ray diffraction from crystal lattice. Red and green photons are reflected different layers of the crystal. But reflection angles are equal.

XRD instrument works with a goniometer which utilized for changing position of the sample holder. The goniometer turns as degree by degree and x-rays are scattered from crystal surfaces of sample depends of the atomic layers. Also detector of the system records both intensity and angle positions of diffracted X-rays simultaneously [172]. A schematic diagram of XRD instrument is shown in Figure 2.26.

Thus the characteristic diffraction pattern of the crystal can be determined. This pattern can be effected from the structure of the unit cell. Additionally intensity and angle position of the recorded patterns are depends on the number of the crystal planes and molecular structure, these scattering intensities and different angles are related to lattice parameters [173].

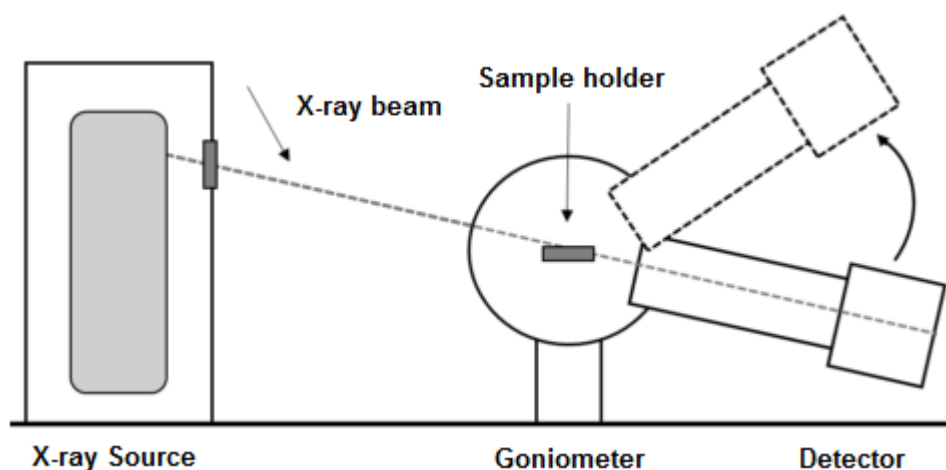


Figure 2.26: X-ray instrument diagram with source, sample holder, goniometer and detector parts.

2.2.3.5 Thermogravimetric Analysis

Thermogravimetric analysis (TGA) technique is one of the thermal analysis method which used to characterize a large variety of materials [174, 175]. Thermogravimetric analysis, determines weight loss of the samples as a function of temperature [176-178]. The technique can determine compositional properties of several compounds according to their organic and inorganic context. TGA needs minimum technical requirements to analyze the dehydration [179].

In this sense, the technique can measure weight changes on the sample, after cooled or heated [180]. Samples may gain or loss their mass due to the decomposition, oxidation, or dehydration reactions [181]. Thus, inorganic and organic components can be separated physically.

In TGA experiments the quantity and rate of change in the sample mass determined with the function of temperature or time in a stable atmosphere [182]. TGA technique is frequently used as an experimental method, for specifying thermal change of solids. In decomposition, the mass of reactants vaporizes and turns to gaseous and usually a residue of char.

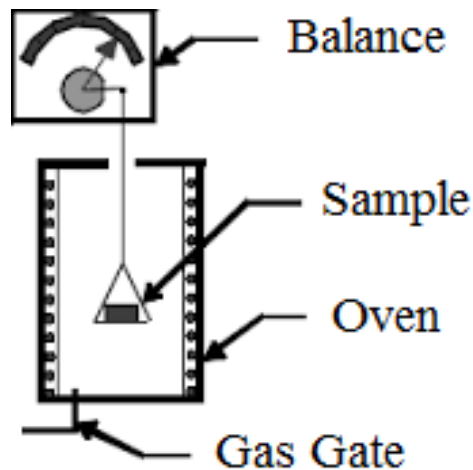


Figure 2.27: Thermogravimetric analysis setup. A balance utilizes for understanding mass changes during the heating process.

The schematic diagram of the TGA system is shown in Figure 2.27. Generally, TGA setup consists of microbalance oven, waste gas system and a computer for the control unit [183]. The sample is heated with constant rate while the difference of the mass is measured. A mass loss refers that some gases take place from the sample holder and a mass gain indicates sample and oxygen from the air can cause reaction.

In a typically TGA curve, the mass (m) is plotted on the y-axis and temperature (T) or time (t) is plotted on the x-axis [170]. TGA especially utilizes for the study of polymeric materials, in addition Thermogravimetric Analysis (TGA) had been commonly used for the urinary calculi characterization since 1970s [170].

2.2.3.6 Scanning Electron Microscopy

Scanning electron microscope (SEM) is an imaging method in which an electron beam interacts with sample surface. SEM involves a vacuum chamber and uses an electron generator in order to produce images of a sample. And also gives information about the composition and topography by scanning surface with a focused beam of electrons. Scanning Electron Microscopy technique has shown fine structure of several types of samples [184]. Generally, electrons are accelerated from tungsten electron generator and after then they hit the specimen surface.

A schematic diagram of an electron microscope is shown in Figure 2.18. Three different types of interactions occur between the electrons and specimen.

These interaction products are; secondary electrons, backscattered electrons, and photons which produce from characteristic X-rays. Consequently, three different output must be detected by different types of detectors,

Secondary electrons are low energetic, and appear after initial electron beam meets of the sample surface. Initial electrons from the generator take place of some electrons from the specimen surface. These relocate electrons are recorded from a specific detector. So, they are called as secondary electrons and, relevant detector can be collect signals from the specimen surface and converts to topography image [168].

On the other side, after initial electrons crash the specimen surface, they can remove back with elastic scattering, and they are labeled as backscattered electrons. Furthermore, their energies influences by the specimen density. Related detector embeds for recording signals from backscattering electrons which collect information about structure of specimen in SEM instruments [168].

Characteristic X-rays; are occurred when the initial electrons take off an inner shell electron from atoms of the specimen. After that another electron from outer shell of the atom fills this lower energetic orbital, and so characteristic X-rays can be emitted for according to the energy differences between inner and outer shell of any atom. This energy is very specific for each type of atom. Hence, in scanning electron microscopes, characteristic X-rays are used to determine elemental composition of the specimen.

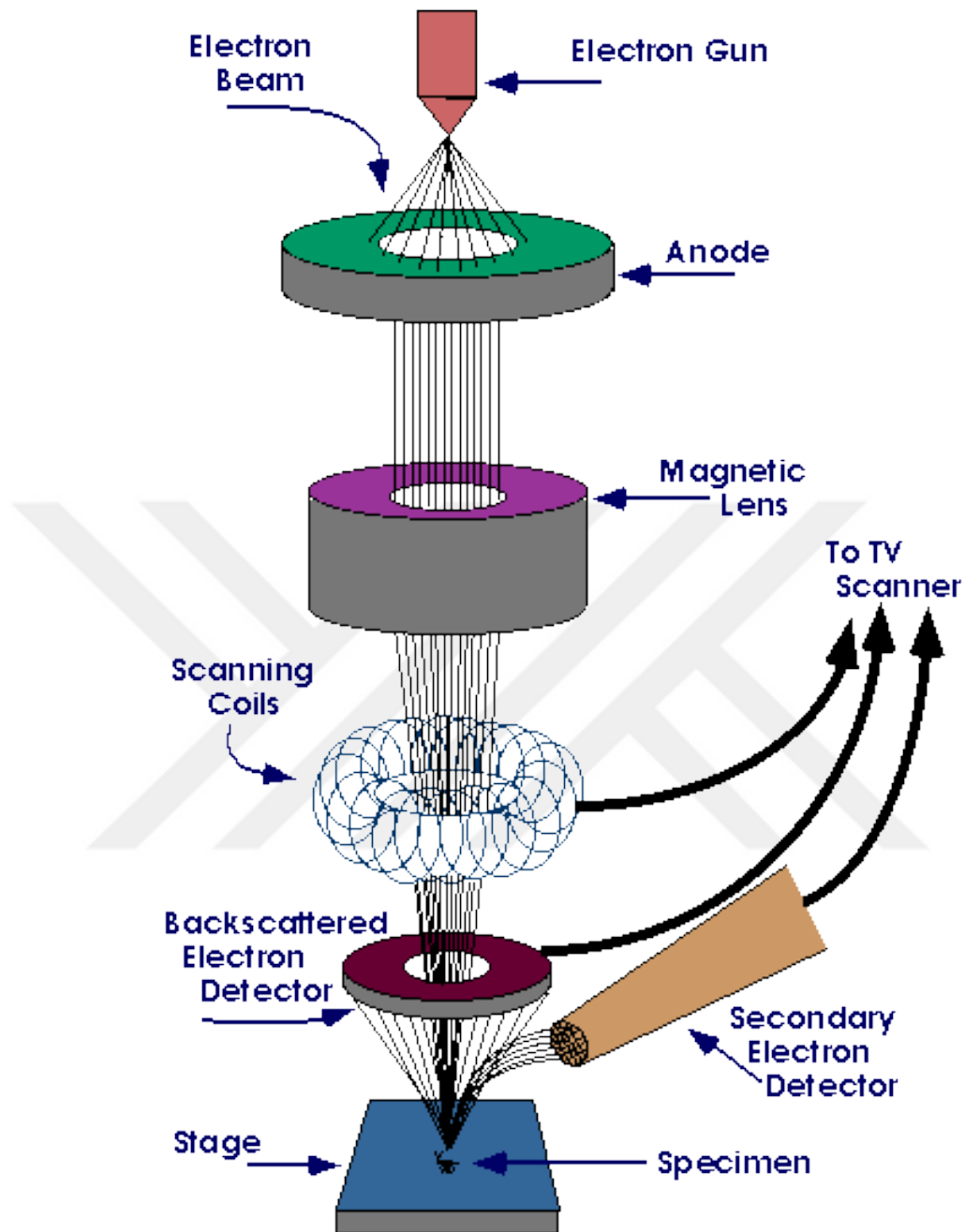


Figure 2.28: Scanning electron microscopy instrument diagram. Sample holder, condensers, lens and coils are illustrated.

Figure 2.29 illustrates this transfer phenomenon between orbitals. In other respects, Energy-Dispersive X-Ray Spectroscopy (EDX) is a useful tool for mineralogical researches [168]. It can be utilized for the elemental analysis by using characteristic X-rays. Generally, SEM and EDX are combined with the same instrument. Every atom has different characteristics X-rays, and energies of these photons can be used for determining

element contents for any specimens. Shape of the crystals can easily be determined by this technique [185].

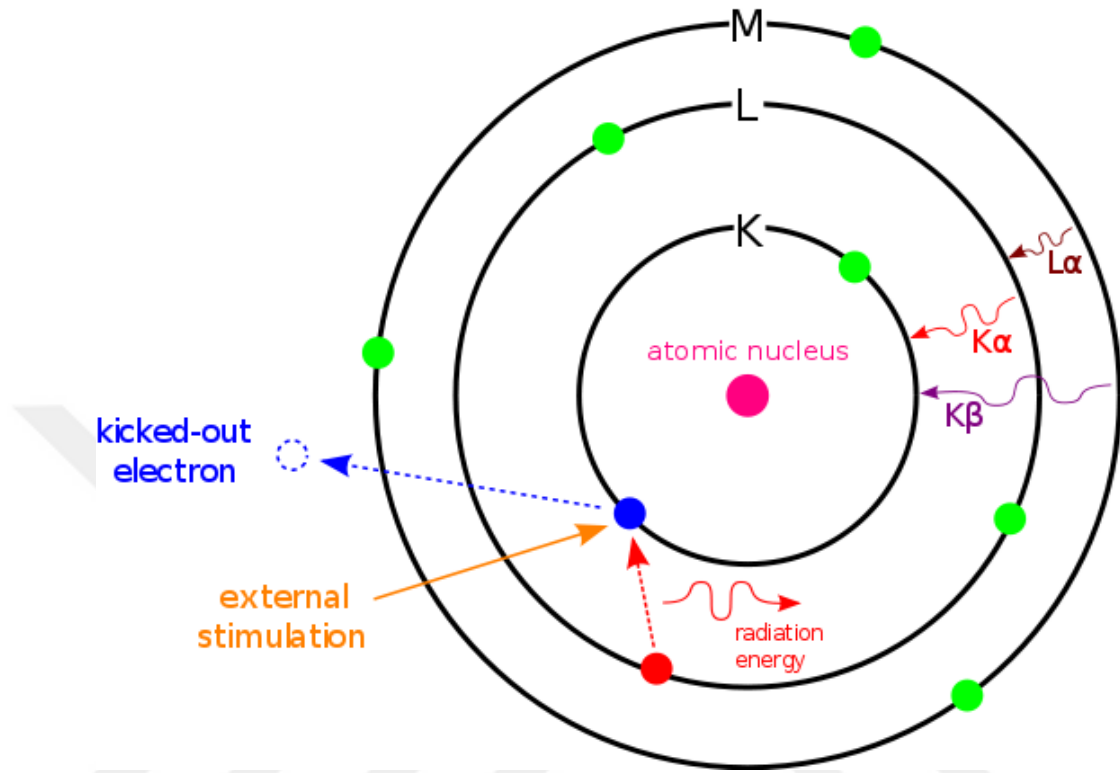


Figure 2.29: Emission of a characteristic X-rays from an atom after interaction with initial (external) and inner shell electron. Blue dot represents secondary electron and characteristic radiation emits after filling this orbital blank.

3. RESULTS

3.1 CHARACTERIZATION OF RENAL STONES

Human Renal stones were selected from Istanbul, Turkey and they were washed with deionized water in order to refine debris like mucous and blood. Samples were mixed ground in a mortar in order to make it fine powder.

The crystalline structures of the well powdered urinary stones were recorded by XRD using a Rigaku D/Max-III C spectrometer with Cu K α radiation, 1.5406 Å wavelength x-ray was used for taking diffraction pattern in the 2θ in range of 20°–70°.

The mid-region (4000 - 400 cm⁻¹) room temperature FT-IR spectra was recorded on Bruker Alpha Series Spectrometer with attenuated total reflectance (ATR) technique. In this technique the fine powder form of renal stones were directly placed into the sample holder without any other process.

FT-Raman spectra of the fine powder stones were recorded on Thermo Nicolet 6700 spectrometer at the room temperature and the region of (4000-400 cm⁻¹) and with using 1024 nm laser.

Morphologies of the stones were imagined by SEM on a JEOL JSM 7001F scanning electron microscope. The elemental compositions of stones were identified by SEM-EDX.

Perkin Elmer STA 6000 analyzer was detected the thermal stabilities of samples in TGA. Fine powder samples were heated from 30°C to 750 °C at a heating rate of 10 °C/min under N₂ atmosphere.

3.1.1 X-Ray Analysis

According to XRD phase analysis, identified compositions, chemical formulas, ICDD numbers and crystallite sizes of each sample are given in Table 3.1.

Table 3.1: Composition, formulas, international card numbers and average crystallite size of each sample.

Sample	D (nm)	Comp.	Formula	ICDD No
A1	10.87	Apatite	$\text{Ca}_5\text{P}_3\text{O}_{13}\text{H}_{1.3}\text{C}_{0.1}$	#99-100-3635
A2	44.17	Whewellite	$\text{Ca}_2\text{C}_4\text{O}_{10}\text{H}_{2.57}$	#99-100-0774
	13.07	Apatite	$\text{Ca}_5\text{P}_3\text{O}_{13}\text{H}_{1.3}\text{C}_{0.1}$	#99-100-3635
A3	52.00	Whewellite	$\text{Ca}_2\text{C}_4\text{O}_{10}\text{H}_{2.57}$	#99-100-0774
A4	37.37	Whewellite	$\text{Ca}_2\text{C}_4\text{O}_{10}\text{H}_{2.57}$	#99-100-0774
A5	53.03	Whewellite	$\text{Ca}_2\text{C}_4\text{O}_{10}\text{H}_{2.57}$	#99-100-0774
A6	59.12	Whewellite	$\text{Ca}_2\text{C}_4\text{O}_{10}\text{H}_{2.57}$	#99-100-0774
A7	43.77	Whewellite	$\text{Ca}_2\text{C}_4\text{O}_{10}\text{H}_{2.57}$	#99-100-0774

XRD powder patterns of sample A1 to A7 are presented in Figure 3.1 respectively.

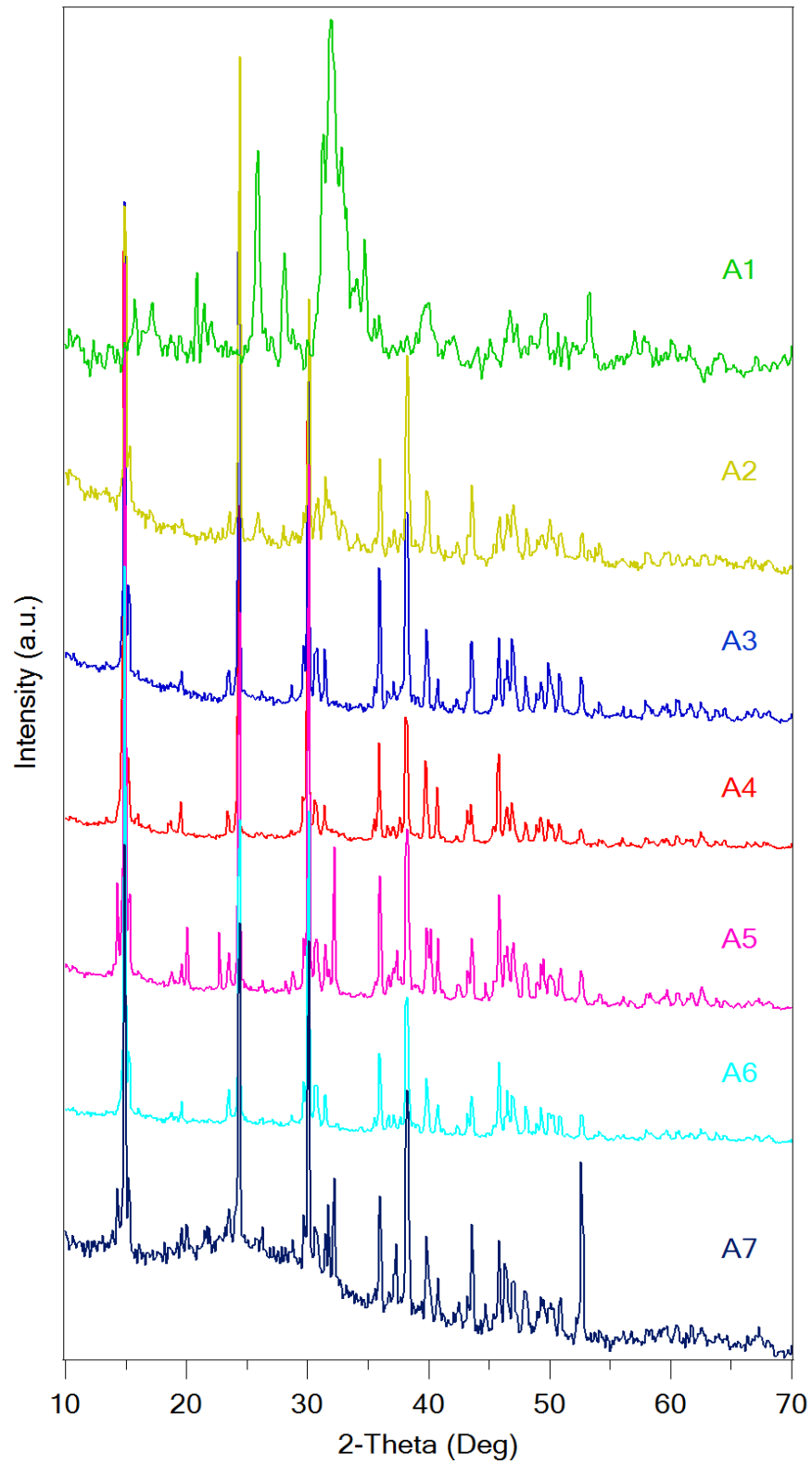


Figure 3.1: XRD powder patterns of sample A1 to A7. A1 and A2 have different XRD pattern then others.

3.1.2 FT-IR and FT-Raman Analysis

FT-IR spectra of samples A1 to A7 are presented in Figure 3.2.

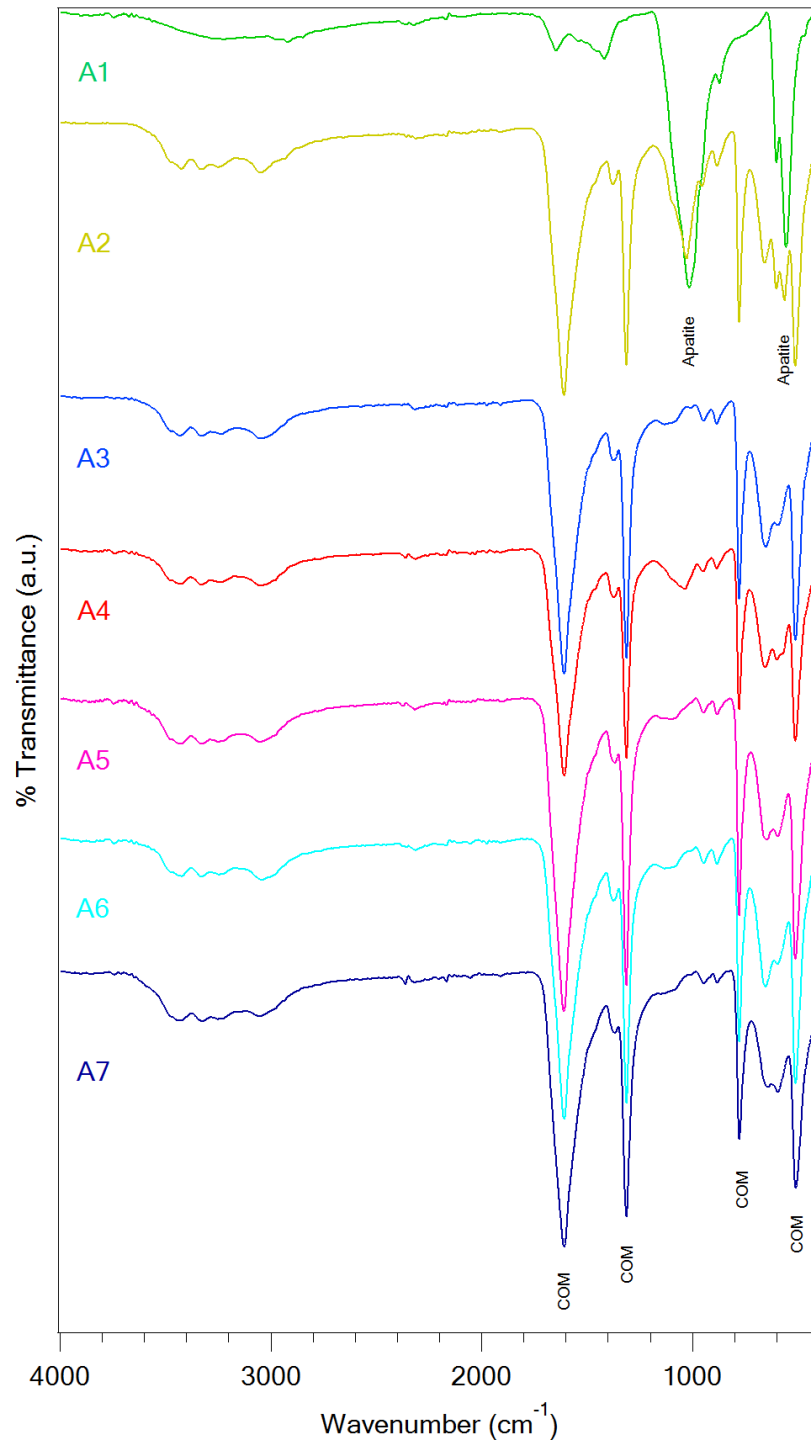


Figure 3.2: FT-IR spectra of samples A1 to A7. A1 and A2 have different pattern then others.

FT-Raman spectra of samples A1 to A7 are presented in Figure 3.3.

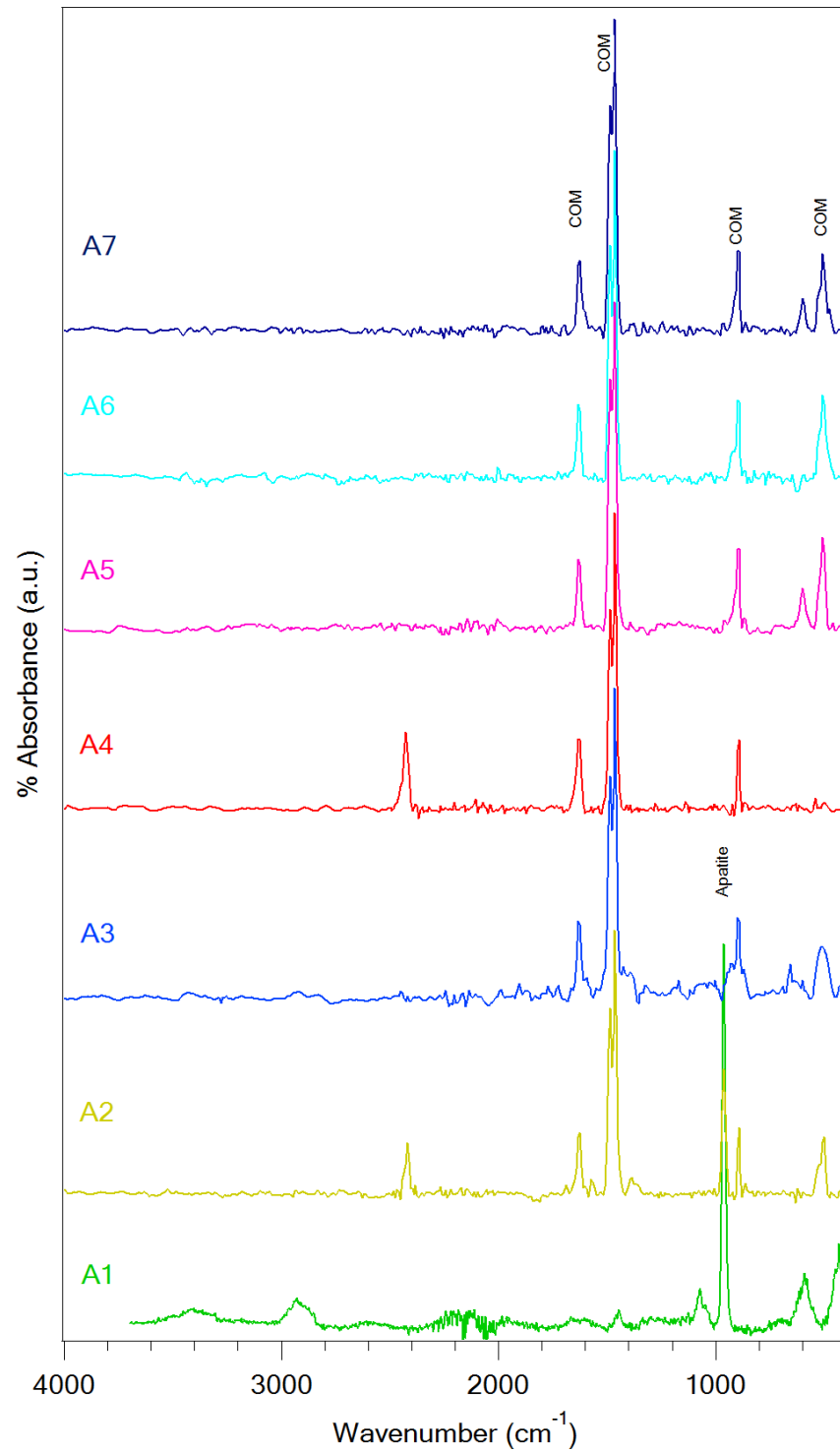


Figure 3.3: FT-Raman spectra of samples A1 to A7. A1 and A2 have different pattern then others.

The detailed FT-IR and FT-Raman spectral analyses are listed in Table 3.2 and Table 3.3.

Table 3.2: FT-IR frequencies (cm^{-1}), tentative assignments and compound names of the samples.

A1	A2	A3	A4	A5	A6	A7	Tentative Assignments	Comp.
-	511	511	511	511	511	511	O-C-O in plane bending	COM
555	563	-	-	-	-	-	PO_4^{3-} bending	Apatite
601	601	-	-	-	-	-	PO_4^{3-} bending	Apatite
-	660	657	657	657	657	657	Out of plane O-H bending	COM
-	778	778	778	778	778	778	C-C stretching	COM
871	871	-	-	-	-	-	Vibration of CO_3	Apatite
-	885	885	885	885	885	885	C-C stretching	COM
-	949	949	949	949	949	949	C-O stretching	COM
1020	1026	-	-	-	-	-	P-O stretching	Apatite
-	1312	1313	1313	1313	1313	1313	Vibration of C-O	COM
-	1374	1374	1374	1374	1374	1374	CO_3^{2-}	COM
-	1610	1609	1609	1609	1609	1609	Vibration of C=O	COM
1645	-	-	-	-	-	-	O-H deformation	Apatite
-	3041	3045	3047	3043	3040	-	O-H stretching	COM
-	3331	3330	3326	3321	3320	-	O-H stretching	COM
-	3421	3427	3435	3440	3420	3420	O-H stretching	COM

Table 3.3: FT-Raman frequencies (cm^{-1}), tentative assignments and compound names of the samples.

A1	A2	A3	A4	A5	A6	A7	Tentative Assignments	Comp.
429	-	-	-	-	-	-	Phosphate bands	Apatite
-	500	507	-	507	507	507	O-C-O in-plane bending	COM
-	892	892	893	893	893	893	C-C stretching	COM
962	962	-	-	-	-	-	P-O stretching	Apatite
1072	-	-	-	-	-	-	P-O stretching	Apatite
-	1463	1463	1463	1463	1463	1463	Vibration of C=O	COM
-	1486	1487	1486	1486	1486	1486	Vibration of C=O	COM
-	1625	1633	1633	1633	1633	1625	C-O asymmetric stretching	COM

3.1.3 Thermogravimetric Analysis

The total weight losses for all samples are summarized in Table 3.4.

Table 3.4: The total weight losses (parts of inorganic and organic content) for the samples.

Sample	% Inorganic content	% Organic content
A1	85	15
A2	45	55
A3	38	62
A4	35	65
A5	36	64
A6	37	63
A7	30	70

Thermogravimetric analysis was used for determining organic contents of the renal stone samples. The TGA thermograms of sample A1 to A7 are given in Figure 3.4, respectively.

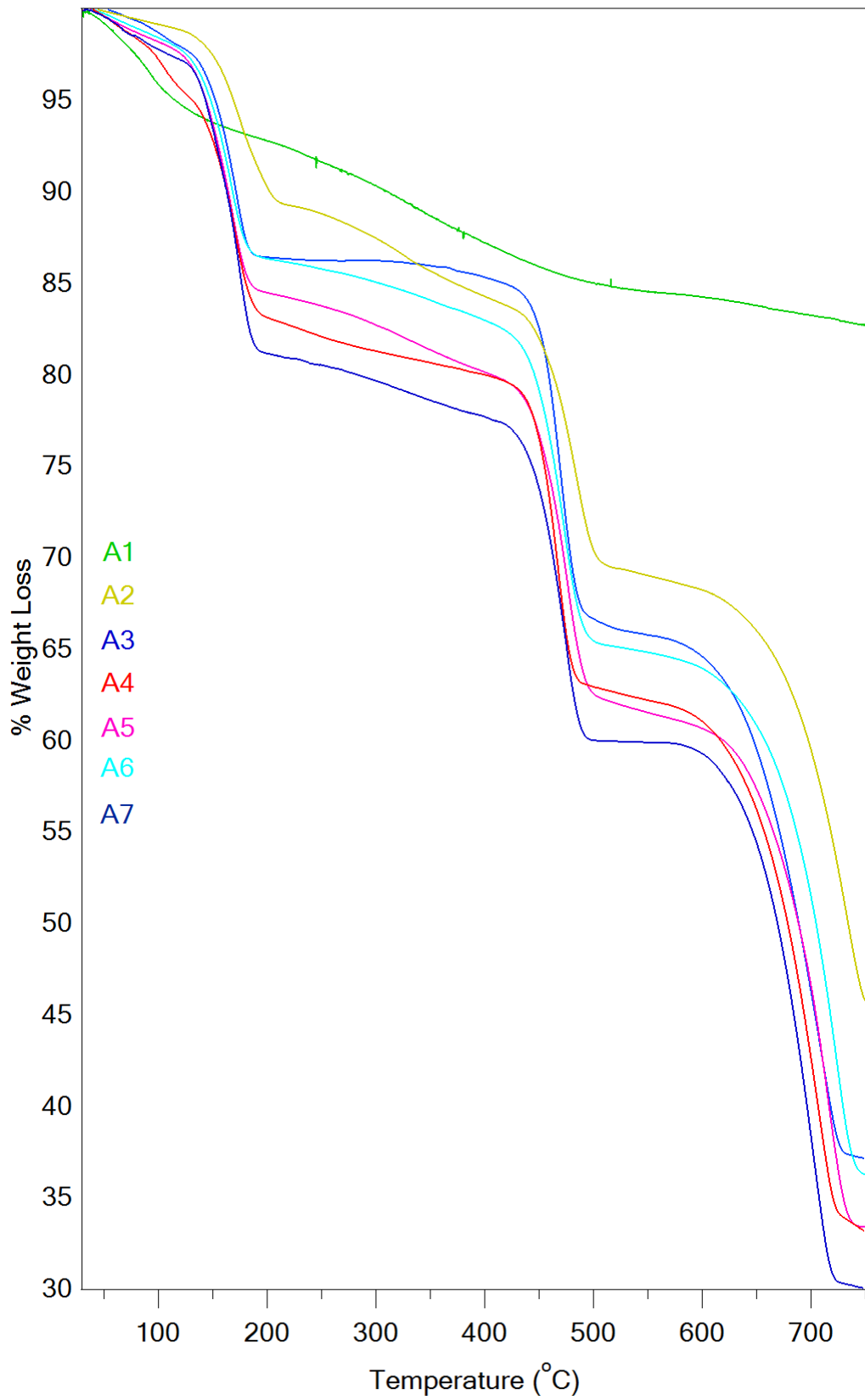


Figure 3.4: TGA thermograms of sample A1 to A7. A1 and A2 have different pattern then others.

The SEM micrographs and EDX spectra of samples A1 to A7 were presented in Figure 3.5, respectively.

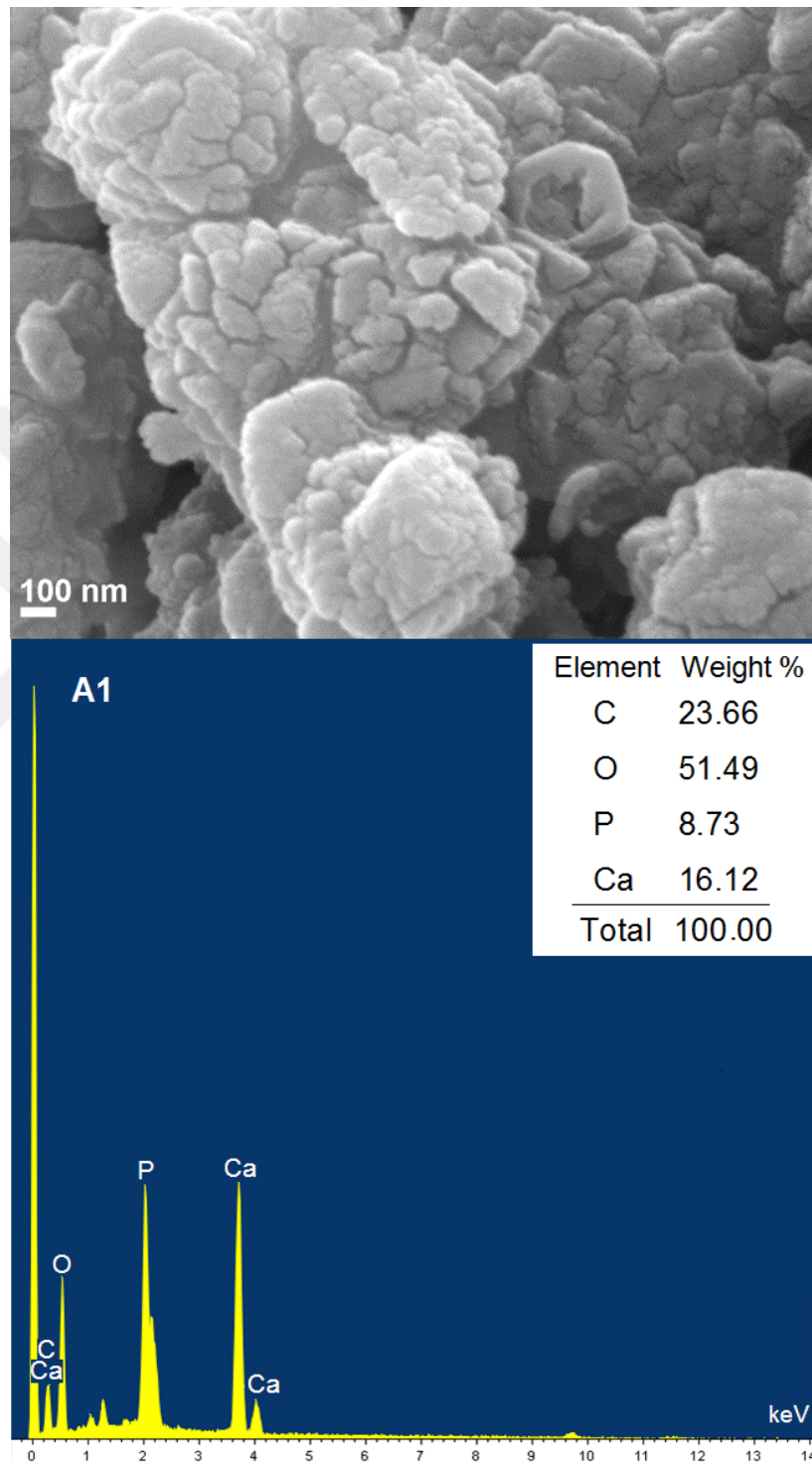


Figure 3.5: The SEM micrographs and EDX spectra of A1 to A7.

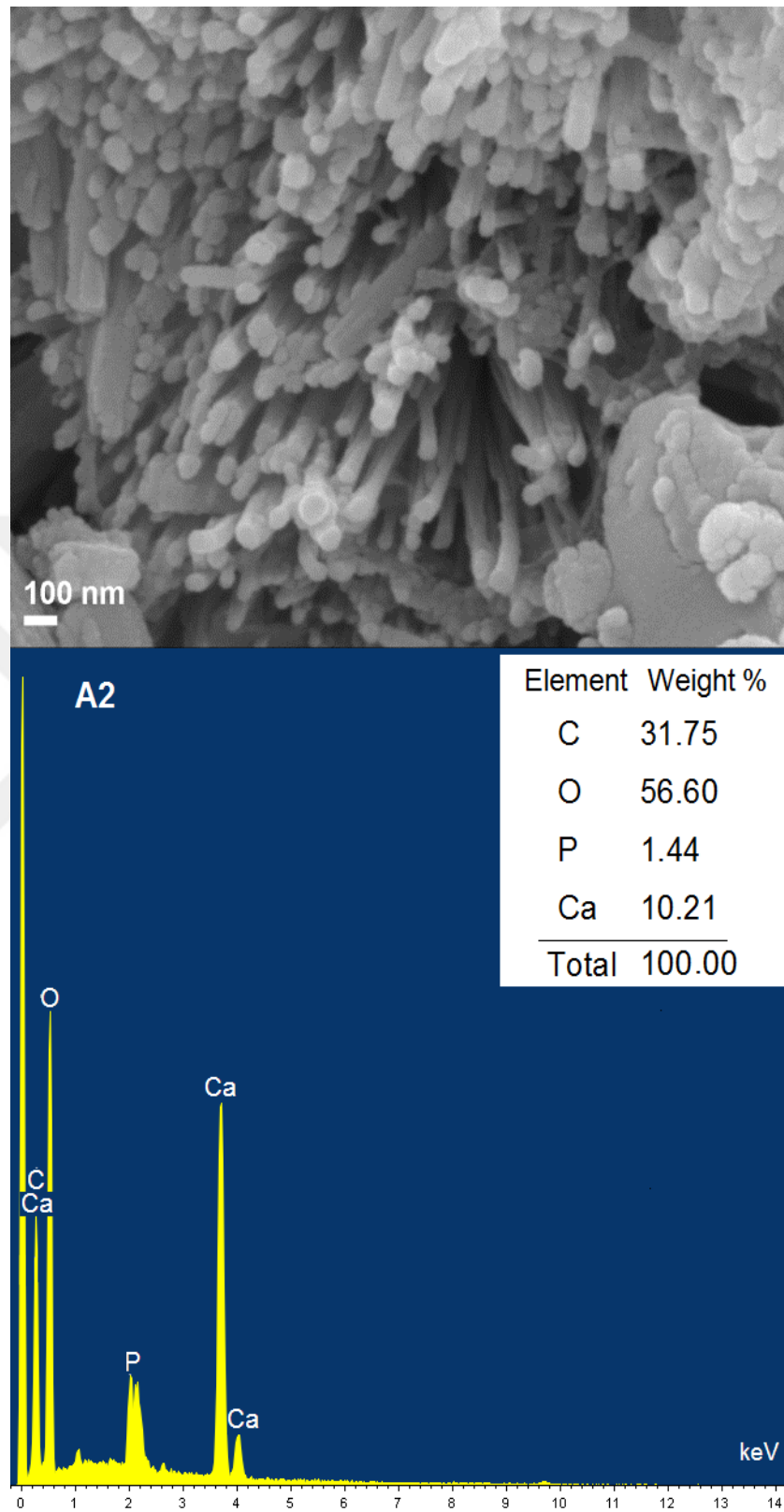


Figure 3.5 (continued):

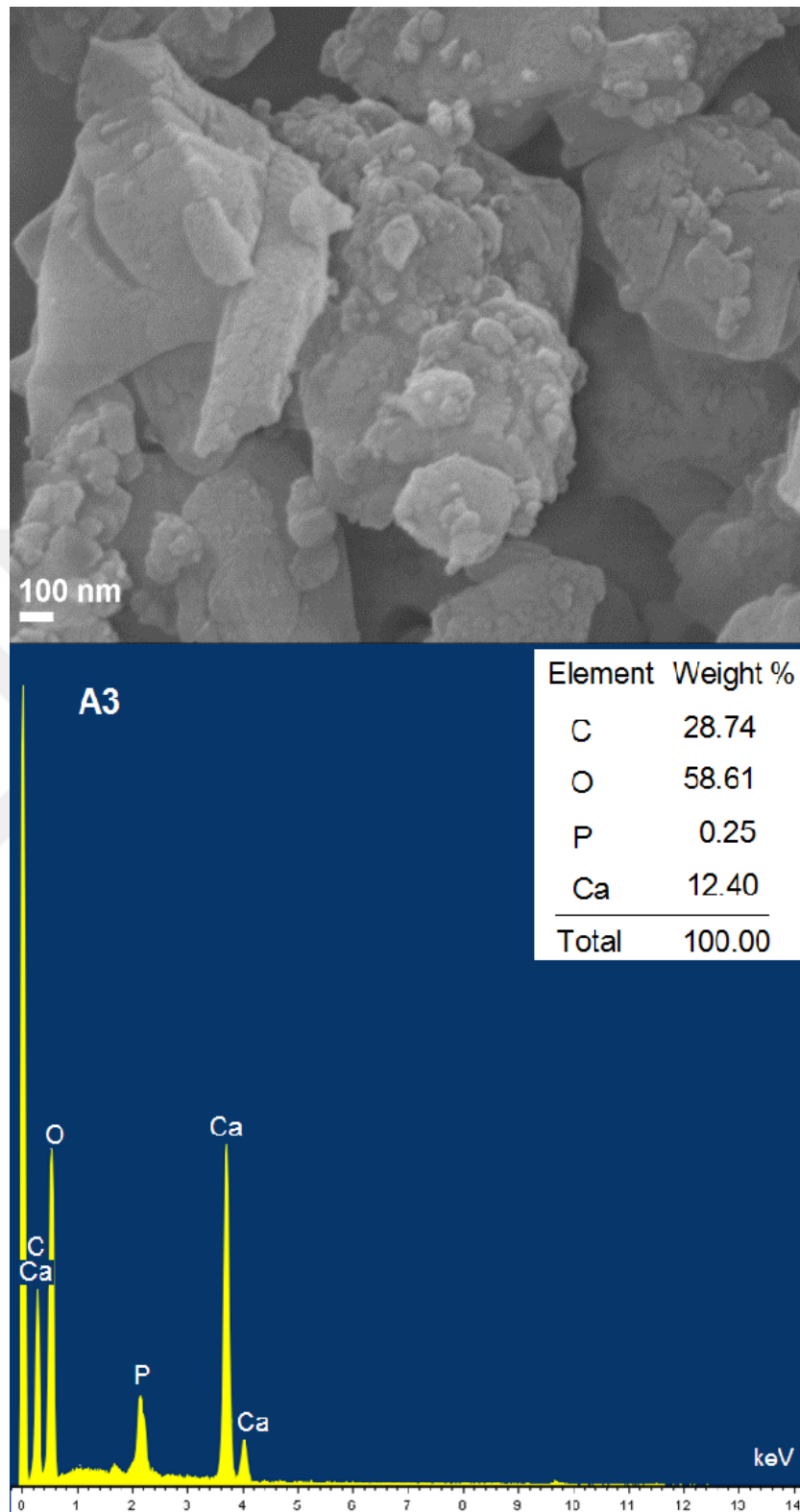


Figure 3.5 (continued):

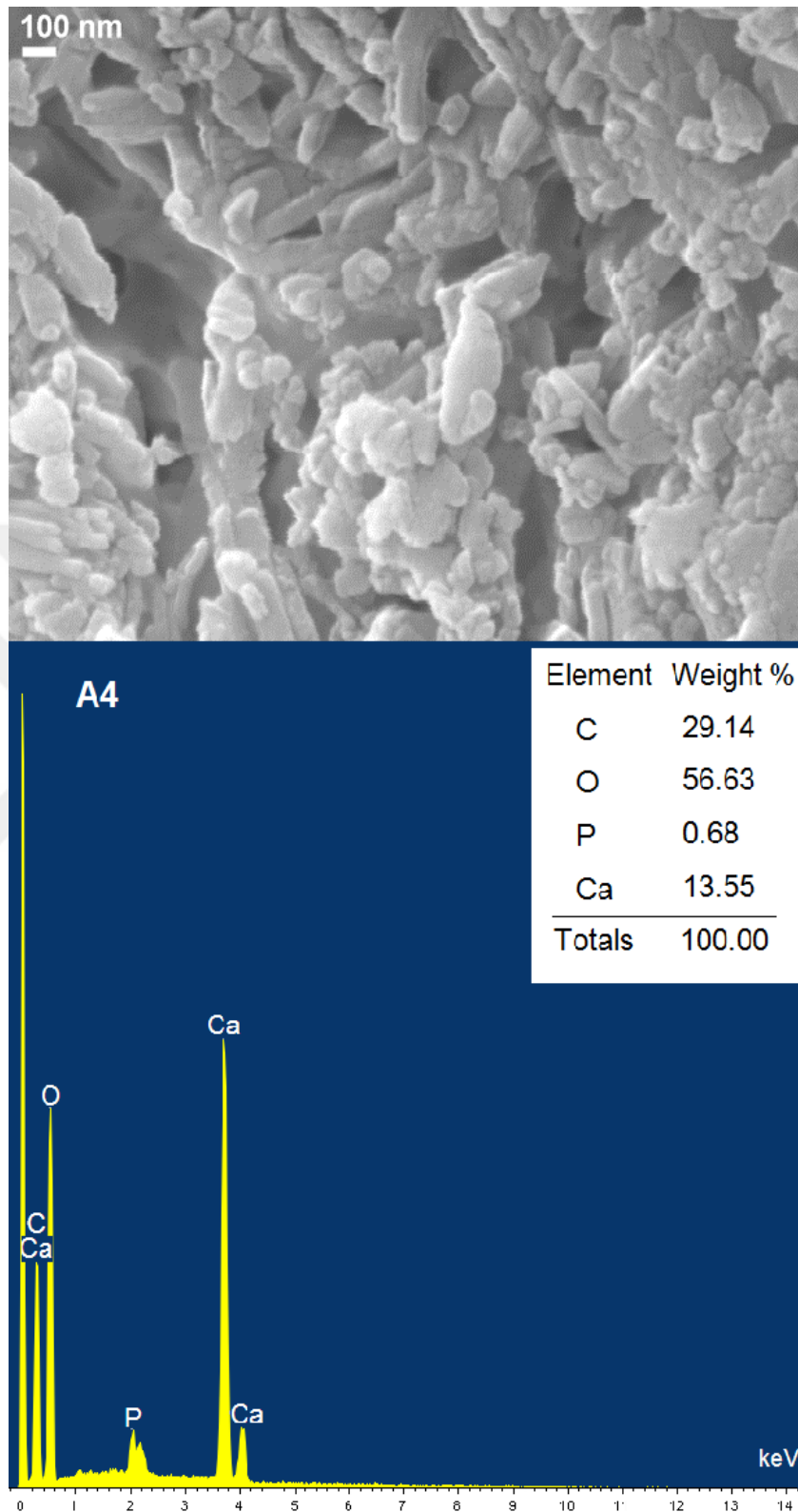


Figure 3.5 (continued):

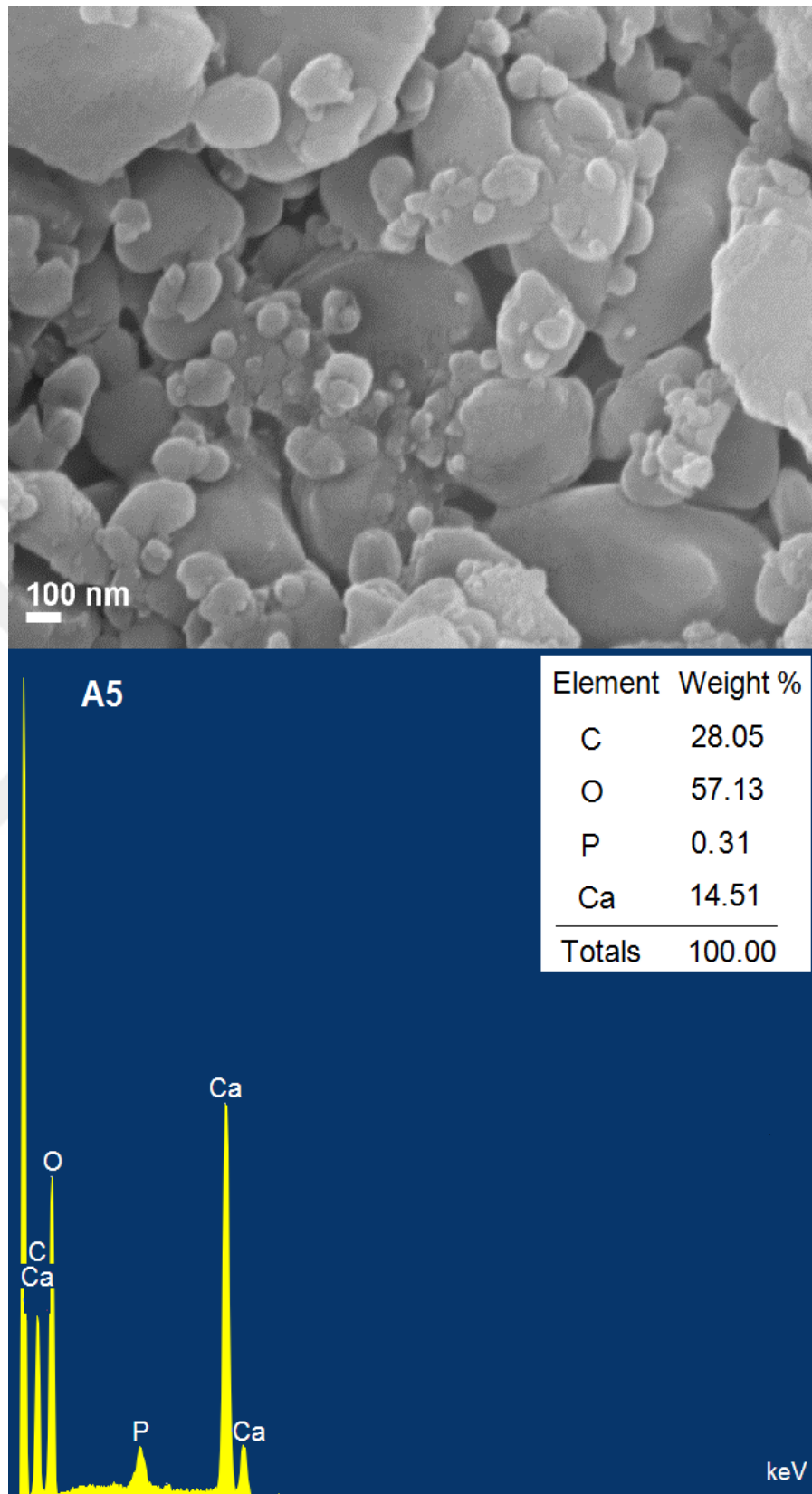


Figure 3.5 (continued):

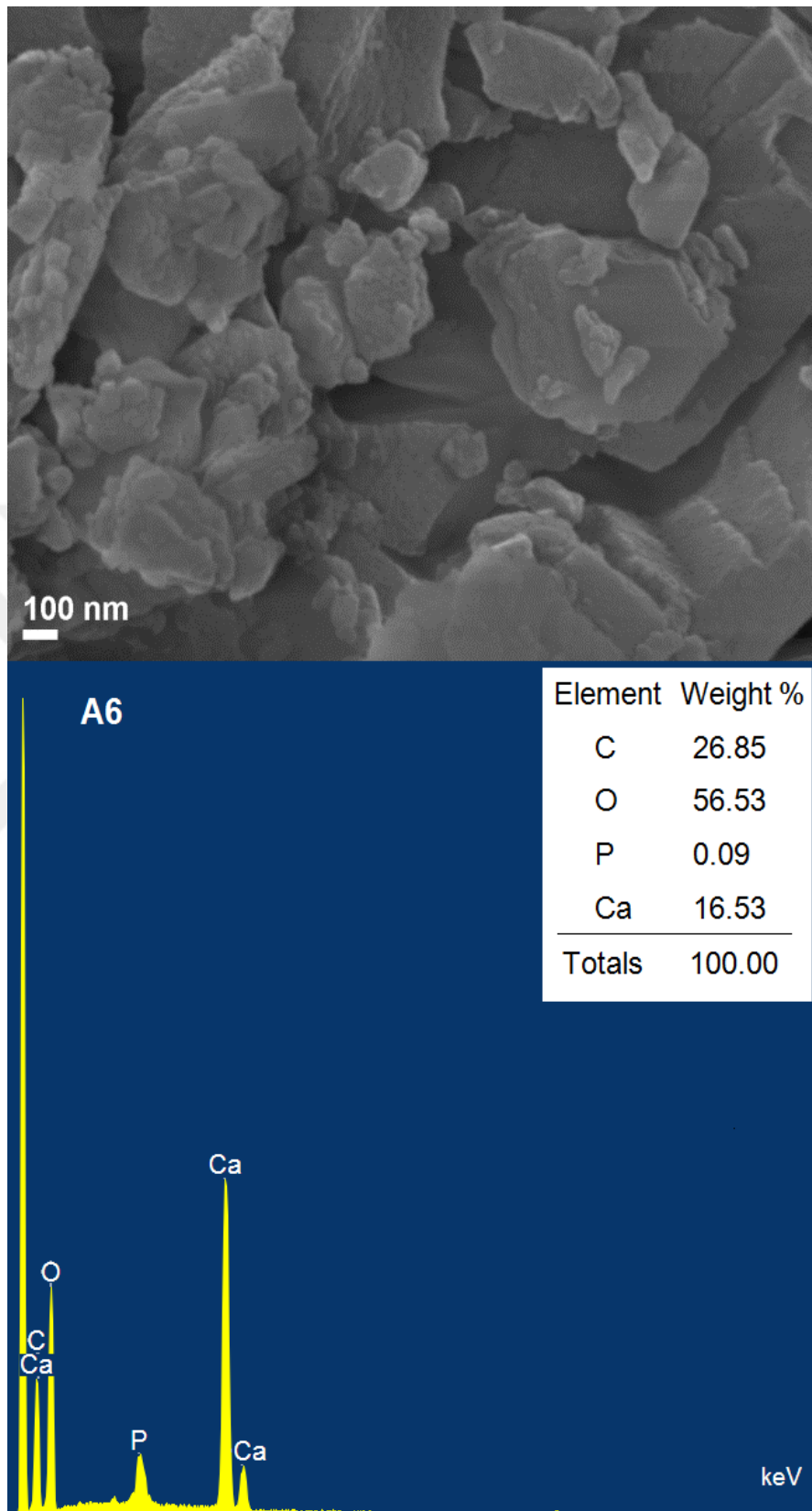


Figure 3.5 (continued):

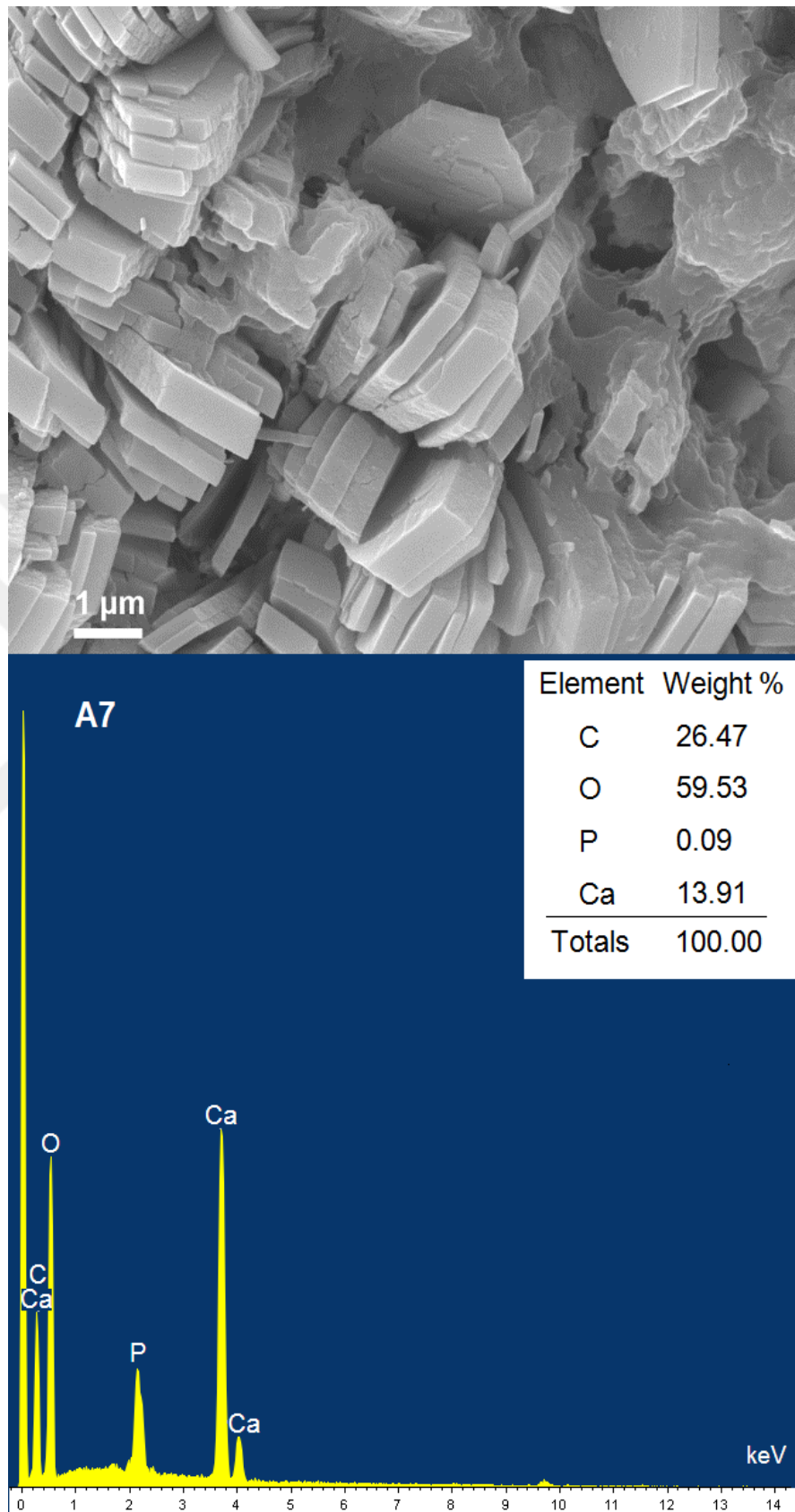


Figure 3.5 (continued):

3.2 FLUORESCENCE REDUCTION IN RAMAN SPECTROSCOPY WITH CHEMICAL BLEACHING ON RENAL STONES

Before starting the experiment, two different renal stone samples divided into two parts like as cross-section form with using a diamond saw. They are labelled as Sample 1 and Sample 2. A part from each of them is kept as control group and other ones are utilized for understanding the effects of chemical bleaching. Calcium phosphate (Apatite) and Calcium oxalate monohydrate (COM) are determined as compounds by FT-IR spectrometer for Sample 1 and Sample 2, respectively. Features of these compounds have been expressed in previous chapter extensively.

The chemical bleaching process is started by with the interaction between 30 % hydrogen peroxide solution and renal stone samples, and the process is finished after by using acetone for the cleaning of pollutes such as fats, proteins and other residual biological particles. During the experiment each renal stone samples exposed with 30 minutes, 2 hours and 24 hours chemical bleaching procedure, and their micro-Raman spectroscopic measurements have been done. Figure 2.2 shows bleached and non-bleached (before and after of the chemical interaction process with hydrogen peroxide) parts of the Sample1 and Sample 2, respectively.

The mid-region ($4000 - 400 \text{ cm}^{-1}$) room temperature FT-IR spectra was recorded on Bruker Alpha Series Spectrometer with attenuated total reflectance (ATR) technique. Following the bleaching protocol, samples were measured with micro-Raman spectrometer in the range $200-3500 \text{ cm}^{-1}$ at the room temperature. Study is performed via Thermo Scientific Dispersive Raman (DXR) spectrometer which equipped with an optical spatial resolution of the $\times 10$ magnification optical microscope. 532 nm green excitation laser source which gives high fluorescence background for many compounds were used.

In addition, ideal laser power were determined by trying different values on the same point of the sample. Laser power was changed but other properties hold in constant conditions for selecting the most proper parameters. Although different laser powers between 0.5 to 7 mW were tried for determining ideal conditions (fluorescence / Raman

intensity ratio) for each types of specimens, 5 mW were determined as the ideal power and measurements were done with this value.

Rayleigh scattering photons have been eliminated with an edge filter, where located on the spectrometer. The spectral resolution was around 2 cm^{-1} and aperture was $25\text{ }\mu\text{m}$ slit, also grating was 900 lines / mm. Finally, non-bleaching parts of the samples have been measured with FT-Raman spectrometer for understanding any spectral Raman shift could exist.



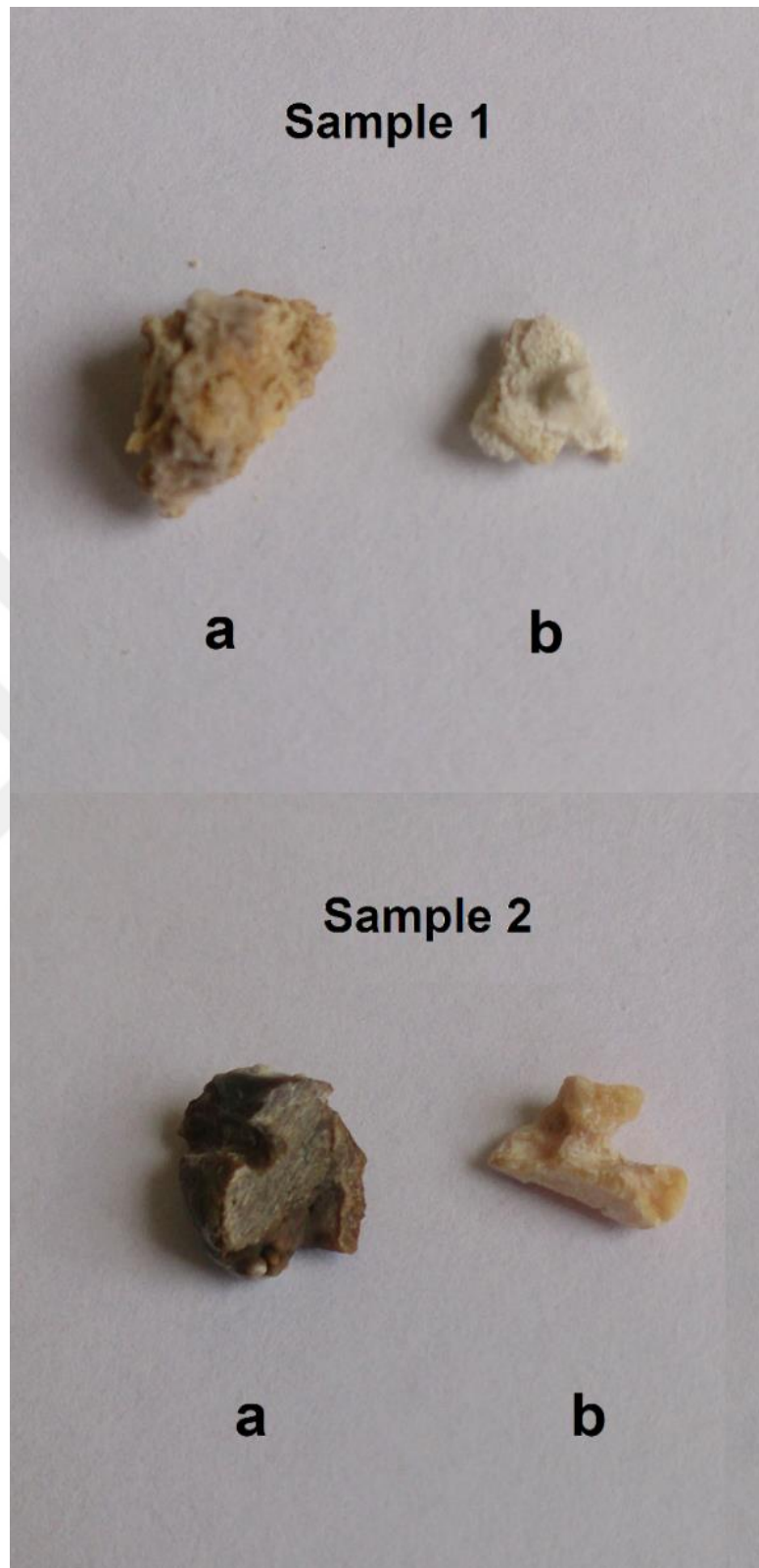


Figure 3.6: Bleached and non-bleached (before and after of the chemical interaction process with hydrogen peroxide) parts of the Sample 1 and Sample 2, respectively.

3.2.1 FT-IR Spectra

In order to ensure the characterization of the kidney stone specimens, stones were subjected to FT-IR spectroscopic analysis. Figure 3.6 gives FT-IR spectrum of both samples.

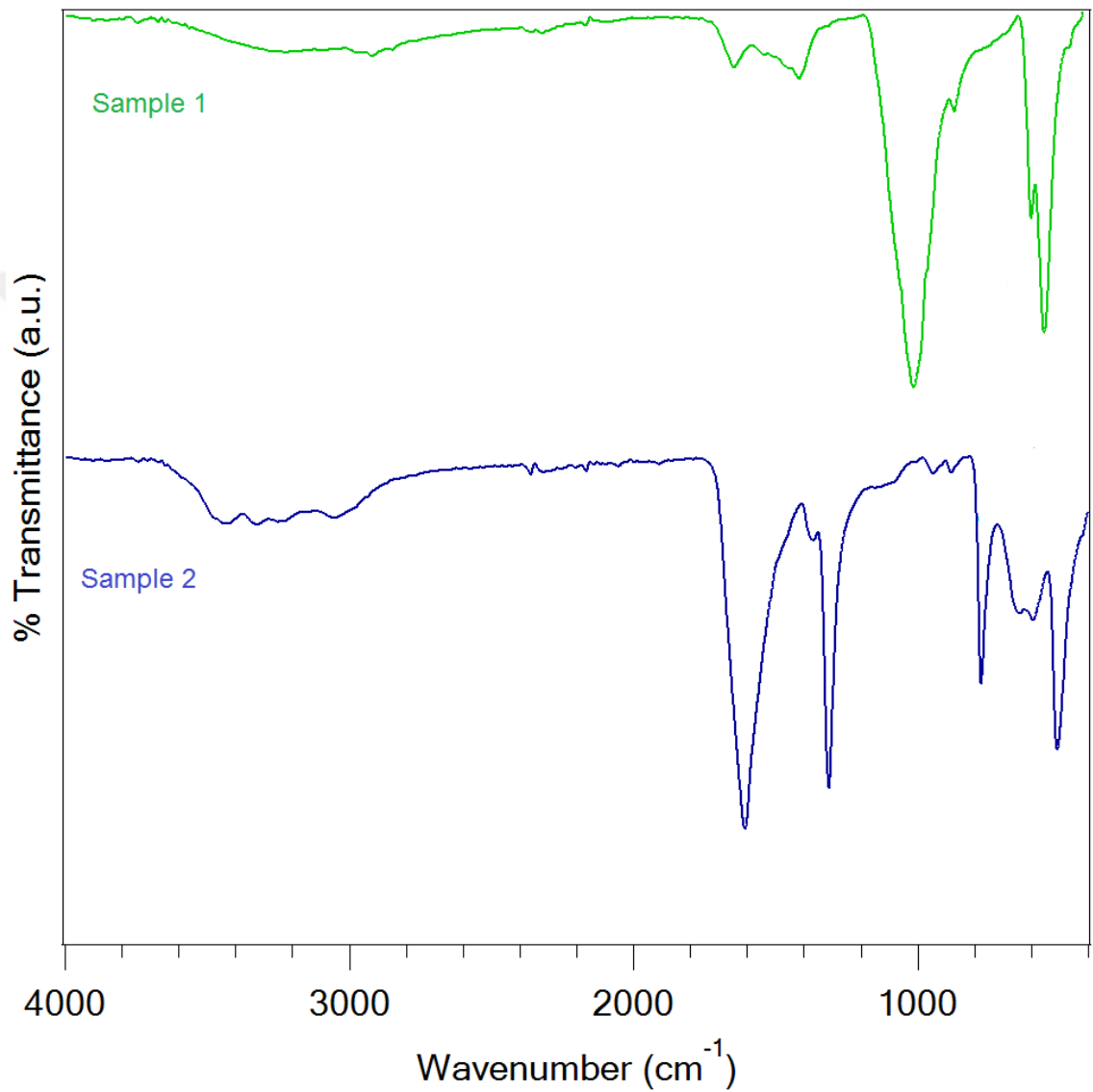


Figure 3.7: FT-IR spectra of Sample 1 and Sample 2, for determining the composition of stone types (before the chemical bleaching process).

FT-IR frequencies of the non-bleaching part of the Sample 1 and Sample 2 are listed in Table 3.5.

Table 3.5: FT-IR frequencies (cm^{-1}), tentative assignments and compound names of the Sample 1 and Sample 2 (before the bleaching process).

S1	S2	Tentative Assignments	Comp.
-	511	O-C-O in plane bending	COM
555	-	PO_4^{-3} bending	Apatite
601	-	PO_4^{-3} bending	Apatite
-	657	Out of plane O-H bending	COM
-	778	C-C stretching	COM
871	-	Vibration of CO_3	Apatite
-	885	C-C stretching	COM
-	949	C-O stretching	COM
1020	-	P-O stretching	Apatite
-	1313	Vibration of C-O	COM
-	1374	CO_3^{-2}	COM
-	1609	Vibration of C=O	COM
1645	-	O-H deformation	Apatite

3.2.2 Dispersive-Raman Spectra

Also, Figure 3.7 shows the changes of the fluorescence intensity which depends on the bleaching process time for Sample 1.

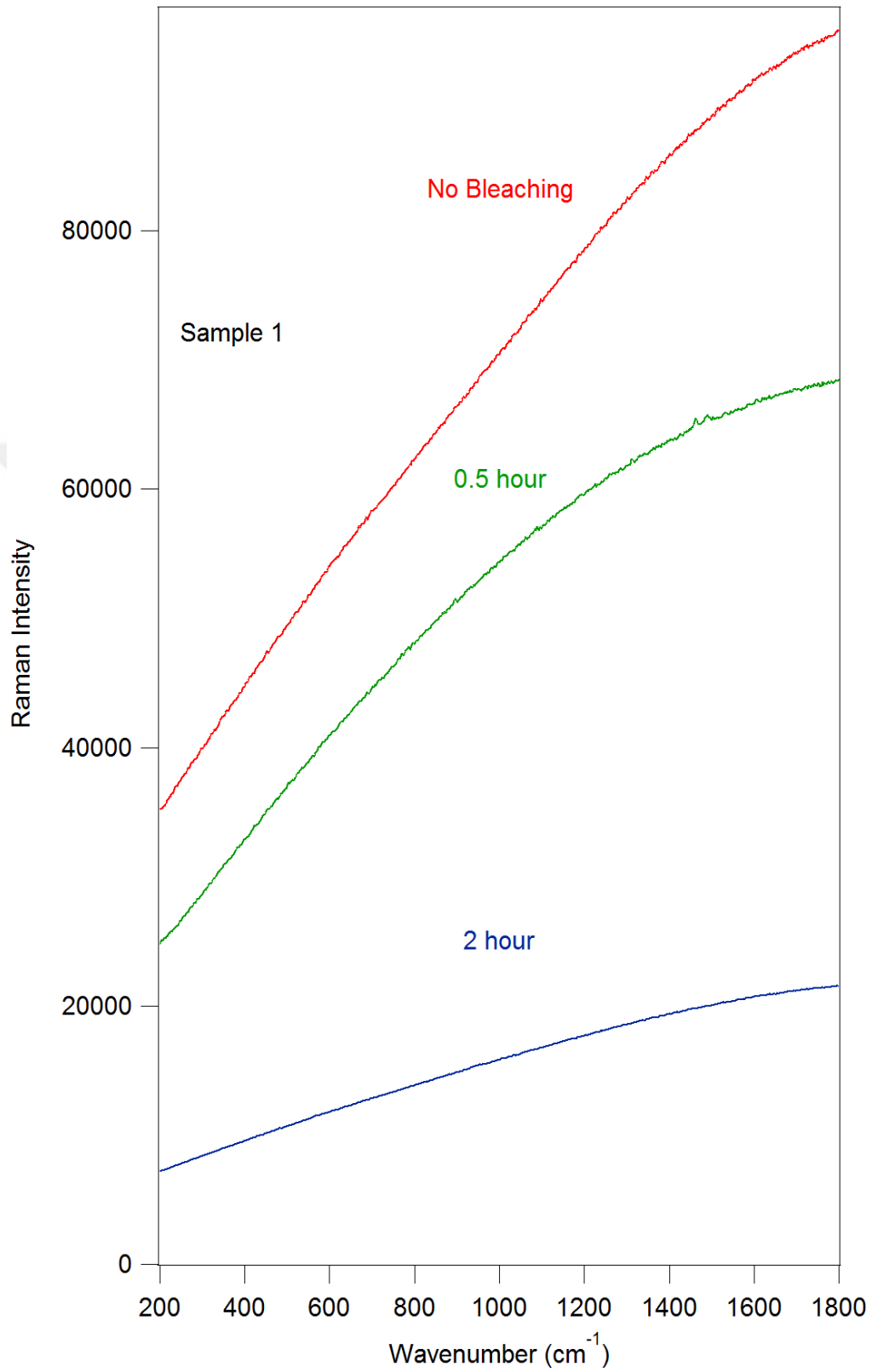


Figure 3.8: Changes of the Raman intensity which depends on the bleaching process time for Sample 1, Fluorescence background had been reduced for half-hour and two-hour bleached samples with same procedure, though it has not sufficient to obtain clear results.

Figure 3.8 shows the changes of the fluorescence intensity which depends on the bleaching process time for Sample 2.

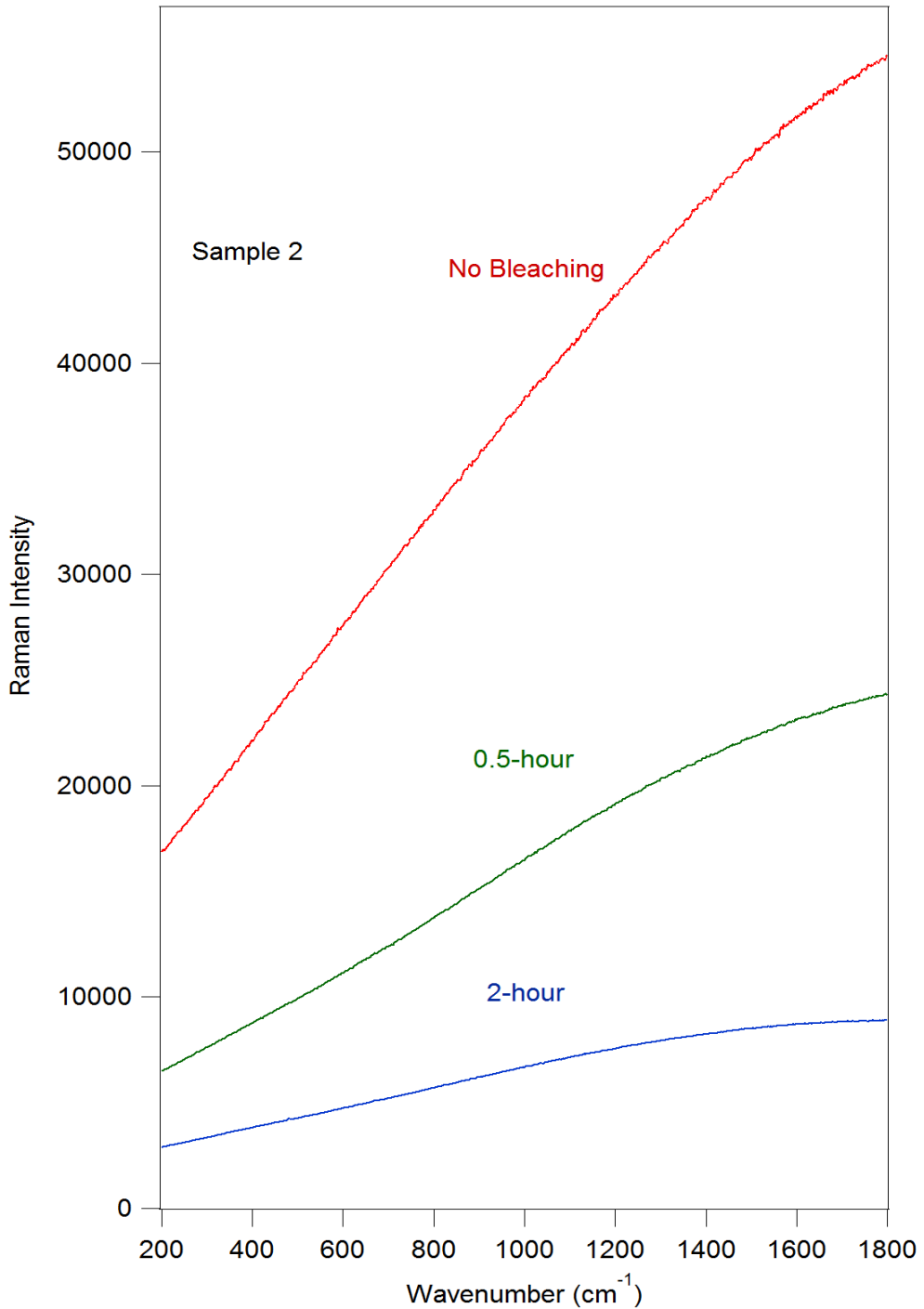


Figure 3.9: Changes of the Raman intensity which depends on the bleaching process time for Sample 2, Fluorescence background had been reduced for half-hour and two-hour bleached samples with same procedure, though it has not sufficient to obtain clear results.

The background fluorescence is reduced at reasonable levels and Raman spectrum of both samples could be recorded. Figure 3.9 and Figure 3.10 show dispersive Raman spectra of Sample 1 and Sample 2 after end of the bleaching process, respectively.

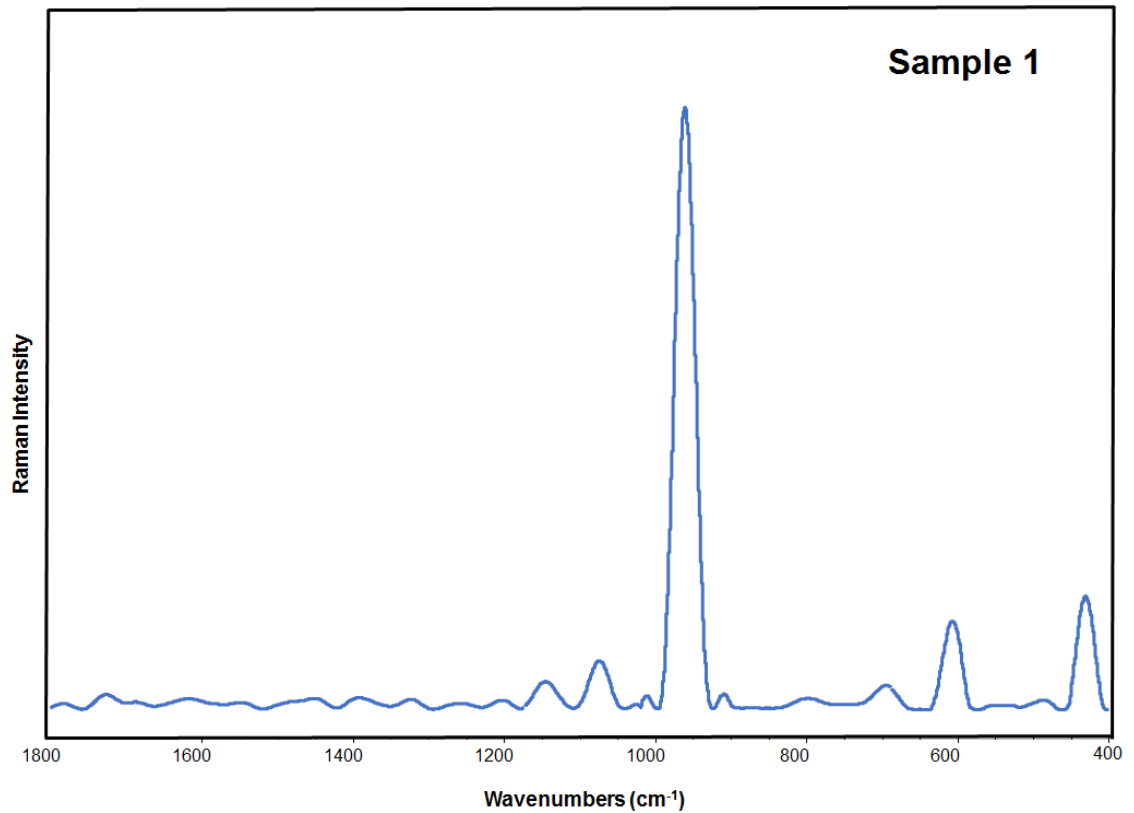


Figure 3.10: Dispersive Raman spectrum of the Sample 1, after the hydrogen peroxide based bleaching process (24 hour) for reduce fluorescence background.

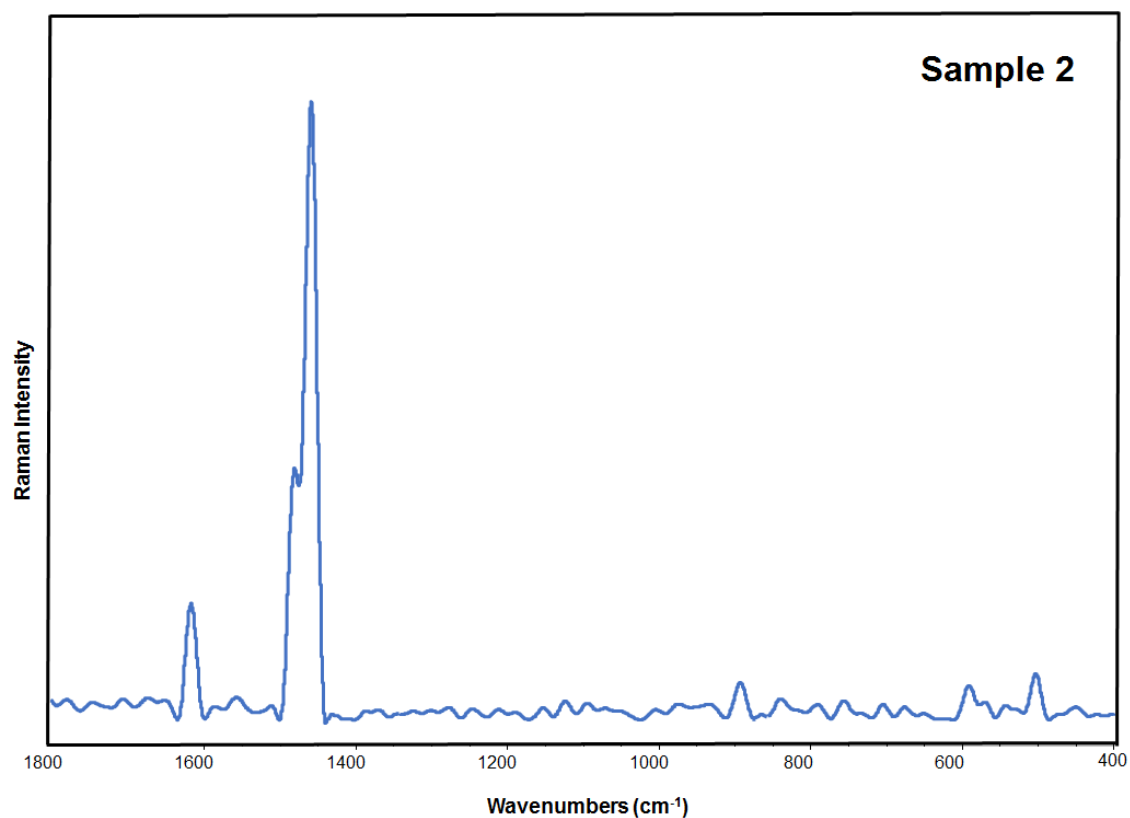


Figure 3.11: Dispersive Raman spectrum of the Sample 2, after the hydrogen peroxide based bleaching process (24 hour) for reduce fluorescence background.

3.2.3 FT-Raman Spectra

The FT-Raman spectra of Sample 1 and Sample 2 are given in Figure 3.11 and Figure 3.12, respectively.

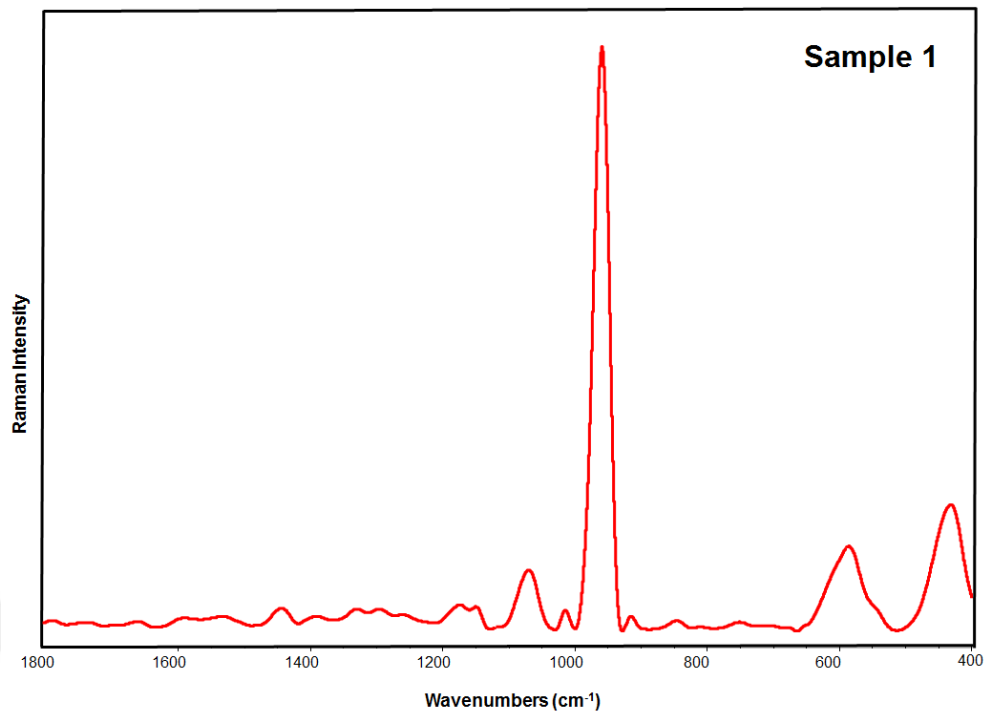


Figure 3.12: FT-Raman spectrum of Sample 1 with 1024 nm laser wavelength (before bleaching).

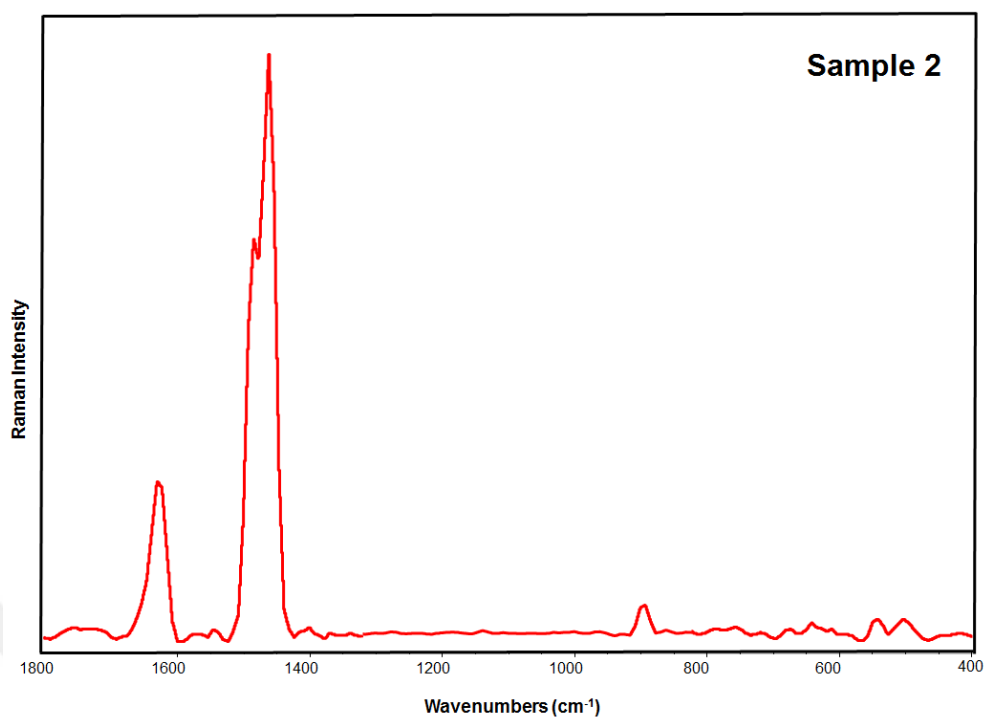


Figure 3.13: FT-Raman spectrum of Sample 2 with 1024 nm laser wavelength (before bleaching).

3.2.4 Comparison of the Raman Spectra

Raman spectral results of the Sample 1 and Sample 2 (before and after 24 h bleaching process) are given in Table 3.6.

Table 3.6: Raman frequencies and compound names of the Sample 1 and Sample 2 before and after bleaching.

Sample	Raman Frequencies (cm ⁻¹)		Comp.
	Before bleaching	After bleaching	
S1	962	962	Apatite
S2	1462	1463	COM

Also, Figure 3.13 and Figure 3.14 give comparison of Raman spectra for both Sample, respectively.

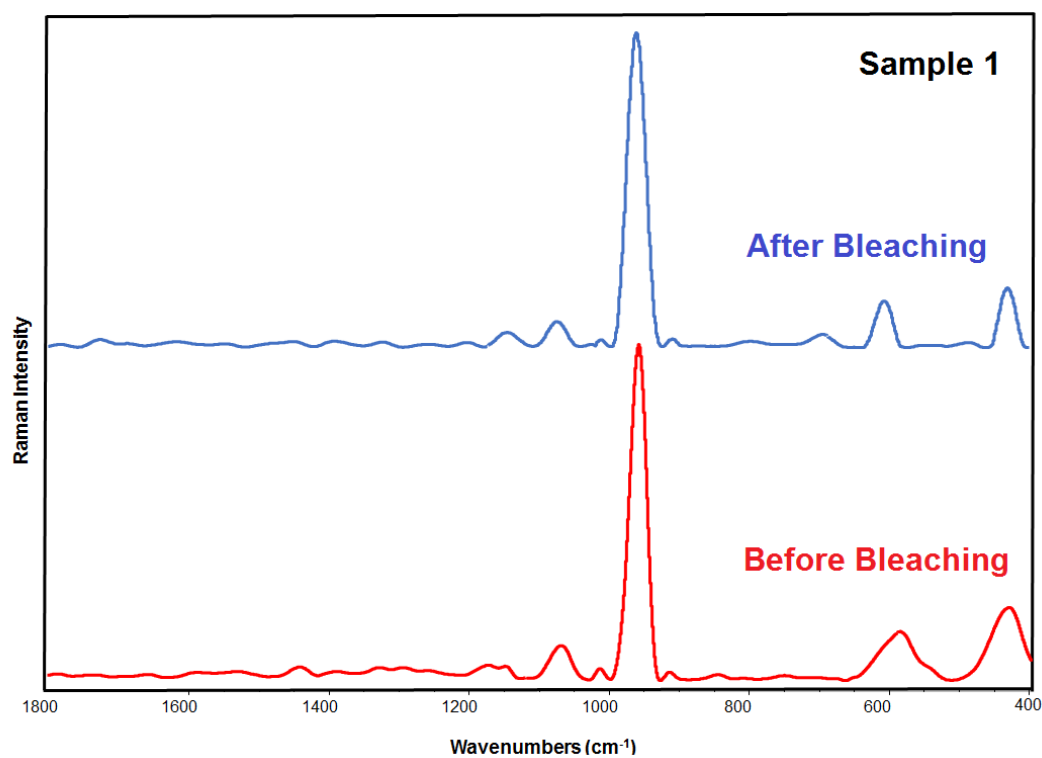


Figure 3.14: Sample 1 before (FT-Raman) and after (Dispersive Raman) bleaching spectra.

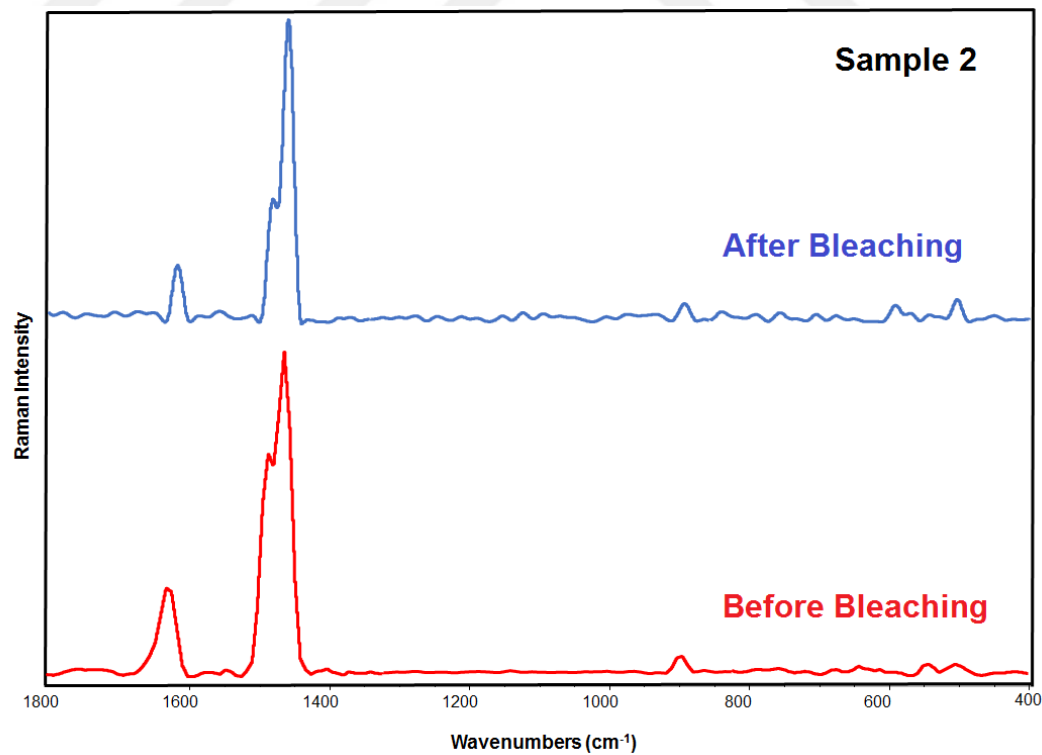


Figure 3.15: Sample 2 before (FT-Raman) and after (Dispersive Raman) bleaching spectra.

3.3 MICRO-RAMAN SPECTROSCOPIC INVESTIGATIONS ON URINE CRYSTALS

Urine sample was collected directly from a urinary stone patient in Medicana Hospital / Istanbul. Sample preparing started with centrifugation process, before that the sample was divided into many parts around 2 ml. Two of them were kept on un-centrifuged case, and other parts were centrifuged at 10^3 rpm for 10 minutes for remove from cells and debris. The sample is examined by a confocal microscope after the centrifuged process for determination of urinary crystal existence. Figure 2.3 shows confocal microscope images of the urine sample. Lastly, centrifuged urine sample was dropped on a lamella directly and that was dried under the room temperature conditions.

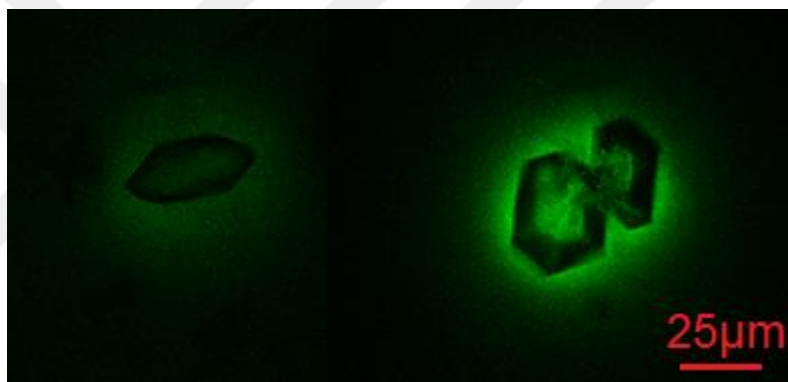


Figure 3.16: Confocal microscope images from urine sediment after centrifuge process for understanding the crystal existence.

Prepared urine sediments were investigated under the dispersive Raman microscope in the range $200\text{--}3500\text{ cm}^{-1}$ at the room temperature. Measurement process was needed only a drop of urine sediment. Study was performed by Thermo Scientific Dispersive Raman spectrometer (DXR) which equipped with an optical spatial resolution of the $\times 100$ magnification microscope (objective). The experimental preparation processes are illustrated in Figure 2.4 basically.

In addition to this, the wavelength of the excitation laser was 532 nm. Different laser powers were used between 0.5 to 5 mW, however optimum laser power designated to 3 mW when we consider the fluorescence and background problem. Because intensities of both fluorescence and Raman have increase and decrease simultaneously. 532 nm Rayleigh scattering photons were eliminated with an edge filter. The spectral estimating

resolution ($2.7 - 4.2 \text{ cm}^{-1}$), aperture $25 \text{ }\mu\text{m}$, grating 900 lines / mm. Polynomial baseline correction were applied.

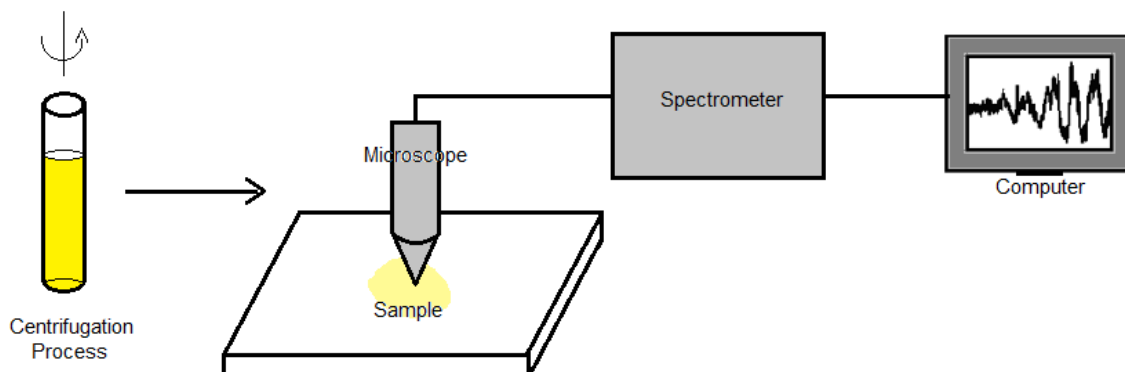


Figure 3.17: Schematic diagram of the micro-Raman spectroscopy system, which utilized for the observation of both spectral data and microscopic images from urine samples simultaneously.

3.3.1 Micro-Raman Spectra

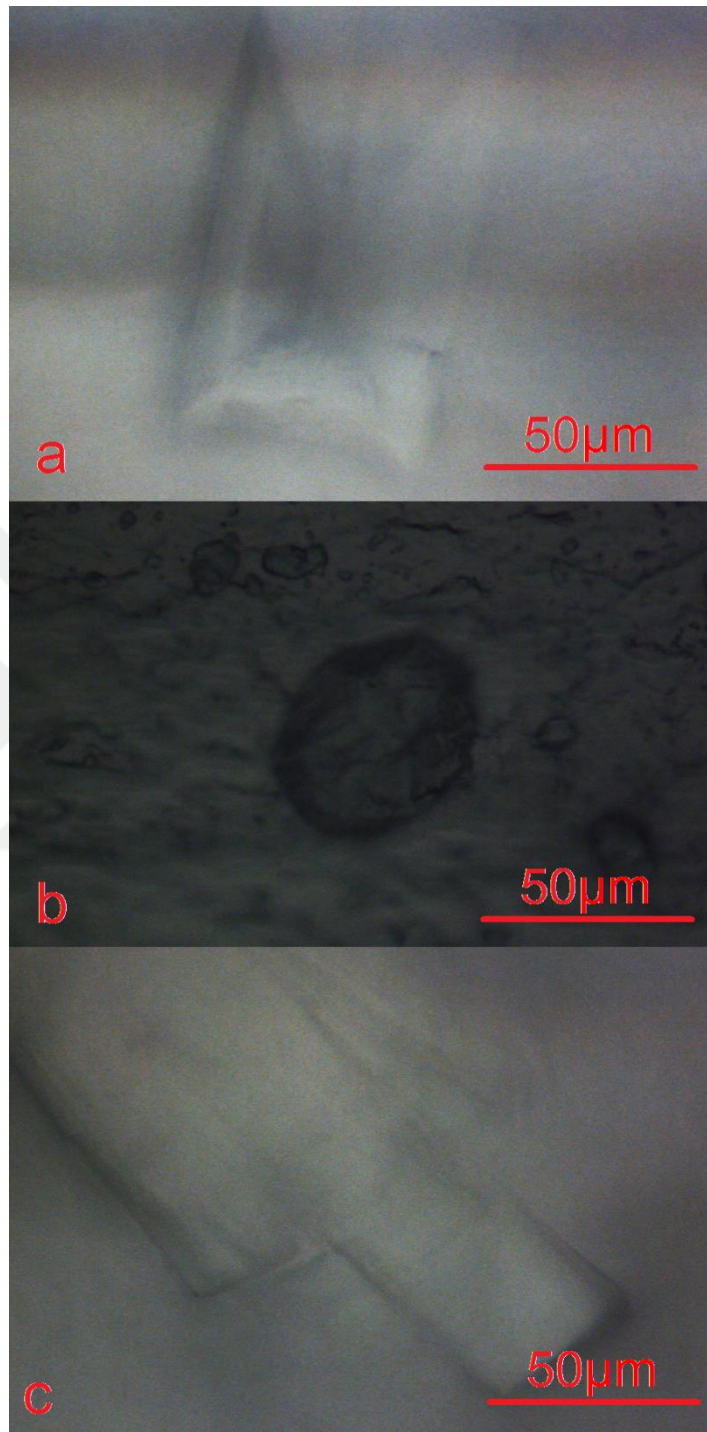


Figure 3.18: Images of Struvite (a), Uric acid (b), and Urea (c), crystals under the $\times 100$ objective Raman Microscope.

Raman bands of investigated urine crystals are shown in Table 3.7.

Table 3.7: The most intense Raman frequencies and assignments of investigated urine crystals with $\times 100$ Raman microscope.

Crystal Type	Raman Bands (cm^{-1})	Tentative Assignments
Struvite	987	PO_4 symmetric stretching
	943	PO_4 symmetric stretching
	564	Bending vibration
	426	Bending vibration
Uric Acid	1233	Ring vibrations
	1044	Ring vibrations
	993	Ring vibrations
	785	N-H out of plane bending and in plane bending
	624	Breathing vibrations
Urea	1006	C-N symmetric stretching
	529	-

Figure 3.16 shows the micro-Raman spectrum of struvite.

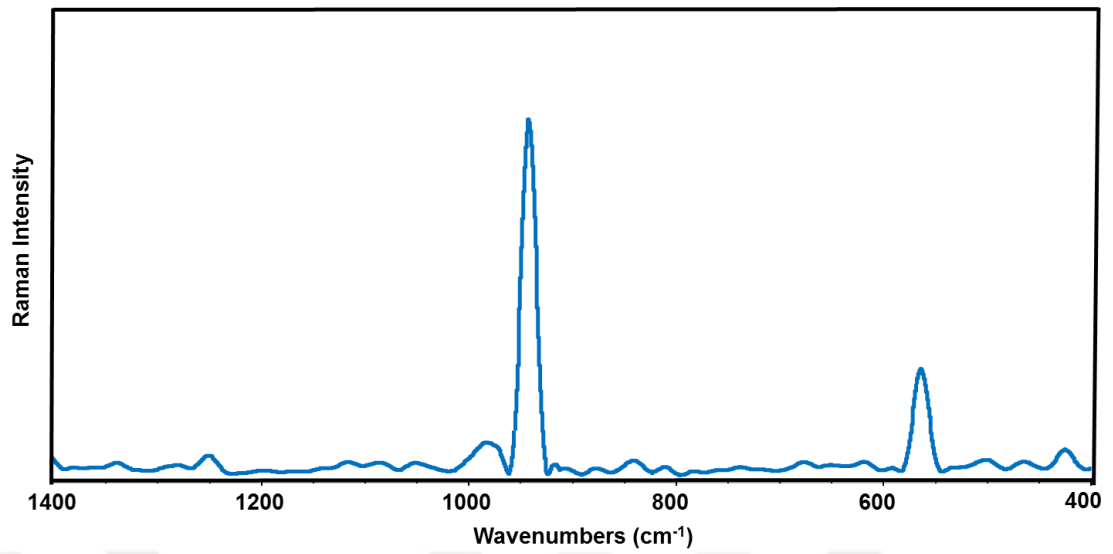


Figure 3.19: micro-Raman spectrum of Struvite crystal, it is observed with $\times 100$ Raman microscope.

Figure 3.17 shows the micro-Raman spectrum of Uric acid.

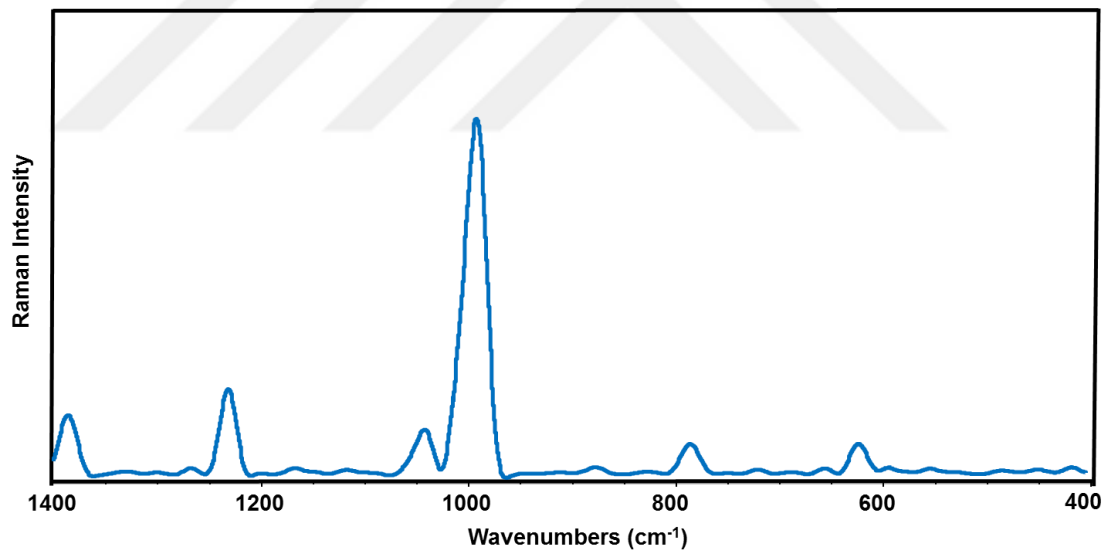


Figure 3.20: micro-Raman spectrum of Uric acid crystal, it is observed with $\times 100$ Raman microscope.

Figure 3.18 shows the micro-Raman spectrum of Urea.

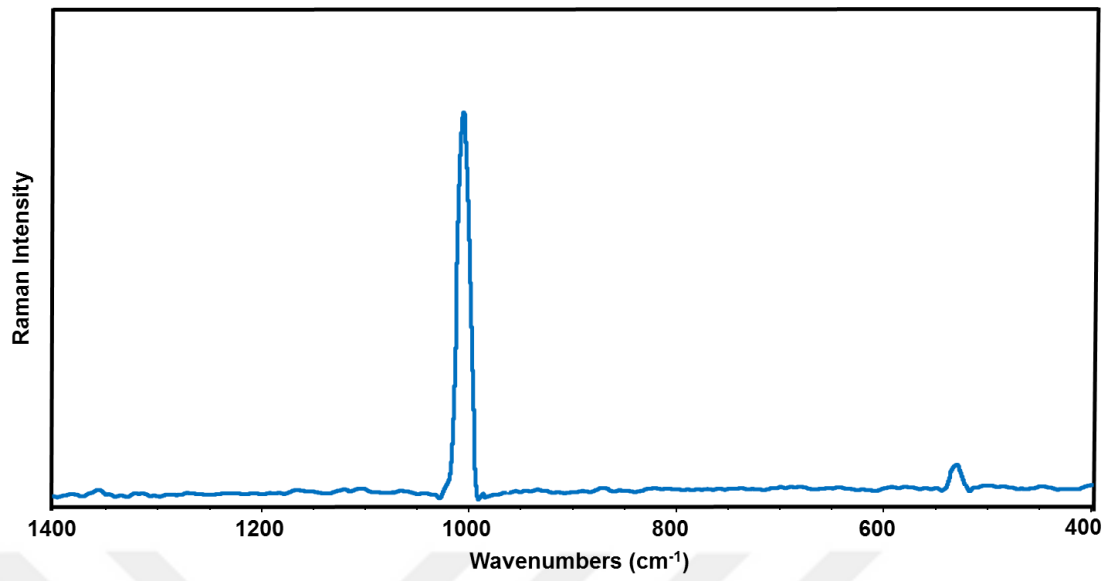


Figure 3.21: micro-Raman spectrum of Urea crystal, it is observed with $\times 100$ Raman microscope.

4. DISCUSSION

4.1 CHARACTERIZATION STUDIES ON RENAL STONES

4.1.1 X-Ray Analysis

XRD powder patterns of sample A1 to A7 are presented in Figure 3.1 respectively. According to XRD phase analysis, identified compositions of each sample are given in Table 3.1. According to these analyses, samples from A3 to A7 have the same composition of Calcium oxalate monohydrate ($\text{Ca}_2\text{C}_4\text{O}_{10}\text{H}_{2.57}$, COM), and its number in the international centre for diffraction data (ICDD) is (#99-100-0774). Among these 7 urinary samples, A1 and A2 have different composition. Sample A1 has apatite composition ($\text{Ca}_5\text{P}_3\text{O}_{13}\text{H}_{1.3}\text{C}_{0.1}$) also apatite's ICDD number is (#99-100-3635) and sample A2 was found to be a mixture of ($\text{Ca}_2\text{C}_4\text{O}_{10}\text{H}_{2.57}$, COM) and apatite ($\text{Ca}_5\text{P}_3\text{O}_{13}\text{H}_{1.3}\text{C}_{0.1}$). The XRD powder pattern of sample A2 revealed that the prominent peak (intensity ~80 %) is due to COM along with minor peaks of apatite.

These results also confirmed by FT-IR FT-Raman and EDX analyses. The average crystallite size (D) was calculated from the diffraction line-width of XRD pattern (calculated for the most intense peak in XRD powder pattern), based on Scherrer's relation (4.1);

$$D, \text{ thickness} = 0.9 \lambda / (\beta \cos\theta) \quad (4.1)$$

Where, β is the full width at half maximum (FWHM) of the most intense peak, λ is the wavelength of the X-ray radiation, and θ is the angle for the most intense XRD peak. Minimum average crystallite size is 10.87 nm belonging to A1 (apatite), and maximum average crystallite size is 59.12 nm for the sample A6 (COM).

As we understand from these results, average crystallite size is around 10 nm for apatite stones and 50 nm for COM stones. Calculated average crystallite sizes are summarized in Table 3.1.

4.1.2 FT-IR and FT-Raman Analysis

FT-IR and FT-Raman spectra of samples A1 to A7 are presented in Figure 3.2 and Figure 3.3 respectively. The detailed FT-IR and FT-Raman spectral analyses are also listed in Table 3.2 and Table 3.3.

In the FT-IR spectra (Figure 2.2), band at 511 cm^{-1} indicates that the presence of O-C-O in plane bending vibration of COM [74]. Phosphates involving PO_4^{3-} ion remark that bending and stretching vibrations arise in the frequencies region between $300\text{-}600\text{ cm}^{-1}$ and $900\text{-}1200\text{ cm}^{-1}$ respectively [186, 187]. In this study PO_4^{3-} bending vibration has characteristic bands observed at 555 , 563 and 601 cm^{-1} , these peaks remark Calcium phosphate (apatite). Spectra occur weak peak at 871 cm^{-1} in calcium phosphate type crystals that belong to the CO_3 ion [188].

The peaks at 665 cm^{-1} and 779 cm^{-1} are corresponding to O-H out of plane bending and C-C stretching respectively [189]. These absorption peaks are recorded around 657 cm^{-1} and 778 cm^{-1} . The peaks due to 885 cm^{-1} correspond to C-C stretching of COM [190]. Also, the weak absorption bands around 953 cm^{-1} and 945 cm^{-1} indicate that the C-O stretching vibration [191, 192]. In this study the C-O stretching peak is observed at 949 cm^{-1} . The weak and shoulder peaks at 1370 cm^{-1} refer to CO_3^{2-} stretching [192]. In our spectra it is observed at 1374 cm^{-1} . Intense band at 1319 cm^{-1} belongs to the C-O stretching [193].

That band is found at 1312 and 1313 cm^{-1} . Strong absorption peak around 1040 cm^{-1} refers to P-O stretching of calcium phosphate [190]. Broad and intense band around 1615 cm^{-1} sings to vibration of C=O for calcium oxalate monohydrate [190]. This peak is observed at 1609 cm^{-1} . Weak absorption band around 1645 cm^{-1} refer to the O-H deformation for the apatite [190]. The entity of calcium oxalate monohydrate molecules in renal stones are identified by extensive symmetric and asymmetric O-H stretching bands between 3047 and 3477 cm^{-1} [189].

For FT-Raman spectra, the weak band appears at 505 cm^{-1} is due to O-C-O in plane bending of calcium oxalate monohydrate [194]. In our study this band is recorded at 505 cm^{-1} . Peaks at 896 cm^{-1} and at 1631 cm^{-1} are signed as C-C stretching and C-O asymmetric stretching of COM, respectively [195].

In this study, these bands are observed around 892 cm^{-1} and at 1633 cm^{-1} . P–O stretching mode of calcium phosphates or apatite shows as strong band at the 959 cm^{-1} [196]. And additionally, strong peak between 1000 and 1100 cm^{-1} refers to the bending vibration of PO_4^{3-} [195]. In this work, bending vibration of the band PO_4^{3-} indicated at 962 cm^{-1} and 1072 cm^{-1} respectively. Calcium oxalate monohydrate (COM) and Calcium oxalate dehydrate (COD) have nearly same band positions, however COM arise with C=O vibration at 1488 cm^{-1} [197, 198]. This band is recorded at 1486 cm^{-1} .

4.1.3 Thermogravimetric Analysis

Thermogravimetric analysis was used for determining organic and inorganic contents of the renal stone samples. The TG thermograms of sample A1 to A7 are given in Figure 3.4, respectively. Sample A2 to A7 show almost same thermal behavior. They consist of five distinct stages of weight loss, given in Figure 3.4. The endothermic weight loss occurring up to $\sim 150\text{ }^\circ\text{C}$, which corresponds to the evaporation of water molecules present in the sample. The weight loss up to $450\text{ }^\circ\text{C}$ is due to the decomposition of organic components in the sample.

The weight loss between $450\text{ }^\circ\text{C}$ and $550\text{ }^\circ\text{C}$ is due to the conversion of anhydrous calcium oxalate into calcium carbonate with a release of carbon oxide {Figure 3.4 (green)} [199, 200]. The major respective weight loss observed between 550 and $750\text{ }^\circ\text{C}$ is due to the conversion of anhydrous calcium oxalate into calcium carbonate and the decomposition of calcium carbonate to calcium oxide. The total weight losses for all samples are summarized in Table 3.4.

4.1.4 SEM and EDX Analysis

Scanning electron microscope (SEM) is used to investigate the surface morphology and compositions of the urinary stones. It can be utilized in order to collect more information about crystalline structures of the renal stones, so SEM analysis can be used for corroborating X-ray diffraction analysis.

Also SEM is coupled with Energy dispersive X-ray spectroscopy (EDX) which could make possible to get both qualitative and quantitative results about the elemental composition of urinary stones. The SEM micrographs and EDX spectra of samples A1 to A7 have been presented in Figure 3.5, respectively. In SEM micrographs; A1 has almost

same morphology of apatite. A2 has prismatic rod type crystals. A4 shows the monodisperse and uniform flower-like microstructures. A5 shows the spherulitic crystals of Calcium oxalate monohydrate. A3, A6 and A7 show the typical plate-like morphology [201].

EDX analysis for the samples of A1 to A7 have detected carbon (C), oxygen (O), calcium (Ca), and phosphorus (P) elements as major components. Oxygen's ratio between 51 to 59 % for all samples, carbon shows distribution between 23 to 29 %. Additionally calcium has a rate around 10 % to 16 %. However phosphorus used as distinctive element for these samples, because only A1 and A2 has sufficient amount of phosphorus around 8.7 % and 2 %, respectively. And the phosphorus ratio is under 1 % for A3 to A7. Because we know that A1 contains only COM, A2 has both COM and apatite, but A3 to A7 have not contain any phosphate type structure (such as apatite).

As we know from previous methods such as XRD, FT-IR or FT-Raman A1 and A2 already contain phosphate in the form of apatite. Each sample confirmed the chemical formula derived from mentioned methods and they are good agreement with related sample.

4.2 FLUORESCENCE REDUCTION IN RAMAN SPECTROSCOPY WITH CHEMICAL BLEACHING ON RENAL STONES

4.2.1 FT-IR Spectra of Samples

In order to ensure the characterization of the kidney stone specimens, they were subjected by FT-IR spectroscopy. Figure 3.6 gives FT-IR spectrum of both samples. Sample 1 arise as Calcium phosphate (apatite) stone. Bending and stretching vibrations of apatite are observed in the region of 300-600 cm^{-1} and 900-1200 cm^{-1} for (PO_4^{3-}) ions respectively [186, 187]. Accordingly, in this study, PO_4^{3-} bending vibration was recorded around 555, 601 cm^{-1} . Also, a weak peak at 871 cm^{-1} occurred for CO_3 vibration of apatite [188]. Strong absorption peak around 1040 cm^{-1} refers to P-O stretching, and weak absorption band around 1645 cm^{-1} refer to the O-H deformation [190]. These peaks are observed at 1020 and 1645 cm^{-1} , respectively.

Besides that, Sample 2 is determined as Calcium oxalate monohydrate (COM) stone. The peak at 511 cm^{-1} remarks that the presence of O-C-O in plane bending vibration in this types of structures [74]. Also, bands at 779 cm^{-1} and 665 cm^{-1} are corresponding to C-C stretching and O-H out of plane bending for COM, respectively [189]. These bands are observed at 778 cm^{-1} and 657 cm^{-1} . The bands around 885 cm^{-1} corresponds to C-C stretching of COM [190].

Weak peak around 953 cm^{-1} or 945 cm^{-1} indicate that the C-O stretching [191, 192]. In this work the C-O stretching peak is recorded at 949 cm^{-1} . The weak and shoulder band around 1370 cm^{-1} refers to CO_3^{2-} stretching [192]. It is found at 1374 cm^{-1} for Sample 2. Intense peak at 1319 cm^{-1} arises as C-O stretching [193]. That band is found at 1313 cm^{-1} . And finally, broad and intense band around 1615 cm^{-1} indicate that vibration of C=O [190]. This peak observed around 1609 cm^{-1} in this spectrum.

4.2.2 Chemical Bleaching Process

In this point, similar bleaching procedure of mentioned papers were applied on renal stones but, fluorescence background reduction have not achieved. It was noticed that none of the procedures which have been given in the literature are not fully applicable to kidney stones. For example, 360 minutes bleaching procedure were applied some of the papers for other bio-minerals but this level have not enough for eliminate the fluorescence background in renal stones. Finally, I have determined the most appropriate bleaching procedure after the application of different approaches.

In this procedure, I have tried to extend the chemical bleaching time (24 hours detergent approach) and as a result of this we observed decreases in the background fluorescence intensity. I have noted that hydrogen peroxide has serious impact on the appearance of the samples. It affected surface of the sample egregiously. However acetone have not shown significant effect on the sample color or spectroscopic results. It was more useful to utilize acetone for only cleaning the surface after the end of the hydrogen peroxide bleaching procedure.

It should be emphasized that, different points on the sample surface have to be measured in order to record a good spectrum since the urinary stones have heterogenic structure. They are composites, made up from inorganic and an organic matrix phase such as lipids

and proteins [202, 203]. Besides, to ensure homogeneity, powder form of the samples were prepared in a mortar, then they were subjected to chemical bleaching with hydrogen peroxide in a tube around six hours. However, contrary to expectations the fluorescent background had increased.

As a result, we can say that the most useful way to chemical bleaching of renal stones is, taking a cross-section surface with diamond saw and measuring several different points from that surface.

Figure 3.7 and Figure 3.8 show the changes of the fluorescence intensity which depends on the bleaching process time for Sample 1 and Sample 2, respectively. Since there is too much fluorescence intensity in the non-bleached part of the samples, it is impossible to get any spectroscopic meaning from them. First, only half hour and followed by two hour bleaching procedures are applied for both samples. Cross-section surfaces of the samples are affected by both hydrogen peroxide and acetone, however the background fluorescence is not sufficiently reduced for determining any Raman bands.

4.2.3 Dispersive Raman Spectra

Then, the chemical bleaching time have extended to 24 hour for both Sample 1 and Sample 2. Thus, the background fluorescence was reduced at reasonable levels and Raman spectrum of both samples could be recorded. Figure 3.9 and 3.10 show dispersive Raman spectra of Sample 1 and Sample 2 after end of the 24 hour bleaching process. Fluorescence reduction had been achieved for both of them with 24 hour procedure. The most intense and characteristic Raman peaks were determined for the samples obviously. The most intense peak has located at 962 cm^{-1} for Sample 1, and this peak is assigned as P-O stretching of apatite mineral [204]. Additionally, an intense peak is appeared after same process for Sample 2 at 1462 cm^{-1} . This peak is very prevalent for calcium oxalate monohydrate, and assigned to the vibration of C=O [20].

We can understand from the results that, 24 hour bleaching procedure has achieved enough fluorescence reduction for both Sample 1 and Sample 2. Although mineral / matrix ratio had changed for both sample, there are not any noticeable frequency shifts in Raman spectra. Hence, I can say that this method is not suitable for quantitative studies

for kidney stones. However that method is very proper for qualitative characterization measurements.

4.2.4 FT-Raman Spectra

For comparison of the results, and in order to understand is there any contamination, I have investigated non-bleaching part of the samples with FT-Raman spectrometer, with 1024 nm excitation laser source. Also same vibrational frequencies are detected under with different spectrometers and laser wavelengths. The FT-Raman spectra of Sample 1 and Sample 2 are given in Figure 3.11 and Figure 3.12, respectively.

The most characteristic (finger print) Raman frequencies of Sample 1 (Apatite) was measured at 962 cm^{-1} and Sample 2 (Calcium oxalate monohydrate) was measured at 1463 cm^{-1} , respectively. FT-Raman results also demonstrated the accuracy of chemical bleaching method.

4.2.5 Comparison of Raman Spectra

Figure 3.13 and Figure 3.14 show the comparison of the Raman spectral results for both Samples. We can obviously understand from these results, there is not any contamination at end of the chemical bleaching process. Because 1024 nm FT-Raman spectra of both Sample have similar Raman peaks when considering with the 532 nm Dispersive Raman spectra results. Some of the intensities are changed by chemical bleaching agents but, there is not any frequency shift or impurity peak for each Sample 1 and Sample 2. The significant peak of Sample 1 and Sample 2 is around 962 cm^{-1} and 1462 cm^{-1} for both measurement, respectively.

4.3 MICRO RAMAN SPECTROSCOPIC INVESTIGATIONS ON URINE CRYSTALS

After centrifugation process, prepared samples were investigated with microscope which located in the micro-Raman spectrometer. I have noticed that, 10 min centrifuged parts of the urine involved higher number of crystals than others. So, I have concentrated on 10 min centrifuged samples especially. We also tried to investigate our sample with different optic lenses such as $\times 20$ and $\times 50$, however minimum fluorescence background

has been provided with only $\times 100$ objective. Further, $\times 100$ lens supplied optimum images in order to distinguish crystals and other particles. Raman bands of investigated urine crystals are shown in Table 3.7.

4.3.1 Struvite

Primarily observed crystal is magnesium ammonium phosphate hexahydrate ($\text{MgNH}_4\text{PO}_4 \times 6\text{H}_2\text{O}$), also Struvite is the mineralogical name of this compound. Generally, formation of that crystal is related with kidney infections [205]. Proteus bacterium lives in urinary system and produces a kind of enzyme it's called as "urease". This enzyme catalysis the hydrolysis of urea to ammonia [206]. Eventually urine pH is lifted, and induced formation of some ions, aggregation of these ions cause crystallization of struvite [207]. Figure 3.15 (a) shows that microscopic image of struvite crystal from urine sediment. It can clearly defined as from its well-known shape.

Micro-Raman spectrum of the struvite crystal can be assigned with the most intense peak of PO_4^{3-} vibration easily. Figure 3.16 shows the micro-Raman spectrum of struvite. Also we known that, struvite crystals have coffin like shapes and this information can be used for comparison the result. In this study, the shape of the crystal is in good agreement with our micro-Raman spectrum (Figure 3.15 (a)). Moreover observed micro-Raman spectrum in good agreement with de literature. According to the paper of Daudon et al., PO_4 group show a symmetric stretching mode at 944 cm^{-1} [208]. Likewise Stefov et al. [209] observed that band at 939 cm^{-1} .

In this measurement, phosphate symmetric stretching vibration mode was observed around 943 cm^{-1} . Also, the stretching and bending vibrations of the PO_4 tetrahedra were effected from temperature [207]. Additionally, Prywer J. et al., observed the symmetric bending vibrations at 425 cm^{-1} [207]. This peak was recorded at 426 cm^{-1} in our spectrum. According to the Prywer J. et al., 988 cm^{-1} are stretching vibrations of PO_4 tetrahedra.

In our study stretching vibrations of PO_4 tetrahedra was observed at 987 cm^{-1} . Bending vibration for struvite is appeared around 565 cm^{-1} [207, 210]. In this study that band is observed around 564 cm^{-1} .

4.3.2 Uric Acid

Uric acid ($C_5H_4N_4O_3$) is the second examined crystal and which is an outcome of purine metabolism in the urine. Some studies mentioned that the uric acid concentrations can be related with renal diseases [211]. The sodium salt of uric acid has a poor solubility in water and crystals are aggregated at levels greater than 6.4 mg/dl [212]. Uric acid crystal has shown in Figure 3.15 (b).

Figure 3.17 shows the micro-Raman spectrum of Uric acid. We can't make any predictions from Figure 3.15 (b), because shape of the imagined crystal is irregular. However, the peaks at 627, 784, and 999 cm^{-1} are assigned to the ring vibrations [213]. The band at 627 cm^{-1} corresponds to ring breathing vibration [213]. In our spectrum this frequency observed at 624 cm^{-1} . Also the peak at 785 cm^{-1} is assigned to N-H out of plane bending and in plane bending vibrations [214]. Similarly, this ring vibration is recorded at 785 cm^{-1} in this measurement.

Additionally the most intense and characteristic frequency is detected at 993 cm^{-1} in our study. 900-300 cm^{-1} region have several vibration modes including ring vibration, bending vibration, and C-O, C-C, C-N, N-C-C stretching modes [213]. These peaks are measured at 1044 cm^{-1} and 1233 cm^{-1} in our study.

4.3.3 Urea

Urea ($CO(NH_2)_2$) is the last observed crystal of this study, and it has two amino groups. It appears after end of the urea cycle. The body excretes urea for avoid the effects of ammonia [215]. Urea is found in both blood and urine, and it is a widespread marker for lots of urinary troubles [216, 217]. Generally, this kinds of crystals are formed as prism shape, some regular shaped urea crystals are shown in Figure 3.15 (c).

Figure 3.18 shows the micro-Raman spectrum of Urea. Generally, urea crystals appear as prismatic shapes. Figure 3.12 (c) shows microscopic image of regular shaped urea crystal. Presences of urea molecules are referred by characteristic Raman peaks at 527 and 1006 cm^{-1} [218, 219]. The most intense peak for urea is located around 1006 cm^{-1} , that peak corresponds to C-N symmetric stretching [216]. In this research, similarly these frequencies are observed around 529 and 1006 cm^{-1} , respectively.

5. CONCLUSION AND RECOMMENDATIONS

In this thesis, X-ray Diffraction (XRD), Fourier Transform Infrared (FT-IR), Fourier Transform Raman (FT-Raman), Scanning Electron Microscopy (SEM) images, Energy-Dispersive X-ray Analysis (EDX) and Thermogravimetric Analysis (TGA) have been applied on human renal stones for characterization. Also, this thesis offers a solution for reducing background fluorescence problem for Raman spectroscopic measurements in renal stone samples. Finally, the thesis includes micro-Raman spectroscopic studies for observation of urine crystals directly from urine.

Renal stone analysis is very important because it influences correct diagnosis and treatment. Urolithiasis is most common urological sickness however stone formation mechanism is still not fully understood. The first part of the study includes classical kidney stone analysis. The urinary stone samples were observed with several experimental methods, and their chemical compositions have also been determined. The component of A1 is determined as apatite. A2 contains both calcium oxalate monohydrate and apatite, while samples A3 to A7 have composed of only calcium oxalate monohydrate. This study indicates that, both XRD and FT-IR/Raman techniques are powerful, sensitive, reliable and less time consuming for the classification of human urinary stones.

The surface morphologies and the compositions of the urinary stones were examined by using SEM coupled with EDX. A1 has almost the same morphology of apatite. A2 consists of prismatic rod type crystals. A4 shows the monodisperse and uniform flower-like microstructures. A5 contains the spherulitic crystals of COM. A6 and A7 show the typical plate-like morphology. EDX analysis of each sample confirmed the chemical formula derived from XRD powder pattern of related sample while the morphologies have different shapes. Thermal analysis results showed the characteristic peaks for dehydration and decomposition of calcium oxalate monohydrate and apatite up to 700 °C.

As a result, systematic and detailed study of the kidney stones was performed for several kidney stones which were collected from Istanbul-Turkey for the first time. These results can be useful for the researchers studying on kidney stones and related diseases. Besides, this investigation can be considered as a base study for taking a step on this topic and subsequent researches. In addition, second and third parts of the study were associated with each other.

Second part of the study is related with the background fluorescence problem in Raman spectroscopy for bio-mineralized tissues (renal stones). Several investigations try to reduce background fluorescence in Raman spectroscopy, because Raman spectrum involves more information about such molecules rather than the fluorescence signals. There are lots of papers related with fluorescence reduction for Raman spectroscopy of bone or teeth samples, however chemical bleaching studies for renal stones have not been investigated yet. This part of the thesis is the first study on this topic, hence the result has a great importance. Fluorescence problem plays significant role in Raman spectroscopic investigations especially while studying with lower laser wavelengths. Excitation laser wavelength is very important because, the probability of fluorescence emitting could be decreased with lower laser frequencies.

Accordingly, in order to keep away from the fluorescence, choosing the correct excitation laser wavelength is fundamental method, however this approach does not always offer a solution. Besides, several techniques such as experimental, computational, photo bleaching or chemical bleaching can be used in order to avoid fluorescence background from Raman spectra.

This part of the study shows that chemical bleaching method with hydrogen peroxide, causes reduction on fluorescence background for Raman spectroscopic investigations of renal stones. Samples were measured by dispersive Raman spectroscopy. 532 nm laser have been utilized as excitation source. Different laser powers between 0.5 to 7 mW have been tried for determining ideal conditions for both of the renal stone samples.

Experiments prove that 5 mW laser power should be used for optimum signal fluorescence ratio for each sample. Ideal chemical bleaching time is around 24 hours for two different types of renal stone sample. Fluorescence reduction had been achieved for

both of them after applying these approximation. The most intense peak was located at 962 cm^{-1} for Sample 1, and at 1462 cm^{-1} for Sample 2. These peaks are significant signs for apatite and calcium oxalate monohydrate of Sample 1 and 2 respectively. Since the samples of the studies have same components, results have a good agreement with FT-IR and FT-Raman spectra, and the results of the first part of the study. Thus, unsurprisingly results of the first and second part of the study are in compliance and support each other.

Also, in the previous (first) part, thermogravimetric analysis results of investigated samples show that stones have heterogenic structure, which means that they involve organic and inorganic materials. For this reason, in the second part; different points on the sample surface have to be measured in order to record a good spectrum. Because the samples of the both parts have same physical and chemical properties. This research emphasizes that stones must be cut in cross-section form before the bleaching process and surfaces should be measured at several different points after bleaching in order to obtain a good spectrum. Although mineral / matrix ratio had changed for both sample, there are not any noticeable frequency shifts in Raman spectra.

So, we can say that this method is not suitable for quantitative studies. Consequently, this study can be utilized as a bleaching procedure for the Raman spectrum of urinary stones. Hence, chemical bleaching is a useful way to decrease fluorescence for bio-minerals and it can be used an alternative method in place of the photo-bleaching.

Lastly, current urinary calculi analysis techniques need at least a visible size of sample in practice. However after using modern treatment techniques such as Extracorporeal Shock Wave Lithotripsy (ESWL), the residual stone fragments are too small for aggregation and characterization. Micro-Raman spectroscopy is very proper and prevalent technique for biological sample analysis and especially for mineralized tissues. Also that technique allows analysis of very small fractions of beyond classical approaches.

The third part of the study has revealed that micro-Raman spectroscopy is a favorable method for the identification of urine micro-crystals. In prevalent investigations; sufficient amounts of renal stone samples can easily be characterized with common techniques; however characterization would be difficult when stones formed as sand-like (powder) particles or sub-visible crystals. But, after applying modern treatment

techniques, residual stone fragments are generally too small for considering collection and analysis. In this sense, the third part of the study gives great results for collecting information from these small stone particles unlike from current researches. Also, only a few investigations have tried to identify invisible stone fragments or urine crystals from directly urine yet. Especially urea crystal had been measured with this kind of method for the first time with this thesis.

Prelusively, the urine sample was dropped on a lamella directly after centrifugation and samples were dried, after that urine sediments have measured under the dispersive micro-Raman microscope. Measurement process only needs a drop of urine sediment. Although several centrifugation process have been tried for determining the ideal centrifugation time and conditions, 10 min centrifuged parts of the urine involve higher number of crystals than others. 532 nm green laser source have been used in this investigations without too much fluorescence background problem.

Furthermore, optimum microscope lens has determined as $\times 100$ objective, from considering both images and spectra. In this study, the crystals of magnesium ammonium phosphate hexahydrate (Struvite), uric acid and urea have directly determined from the urine sample. The microscopic images of crystals have in good agreement with micro-Raman analysis of the results. The spectra of crystals have some marker characteristic peaks for understanding the crystal types. The most characteristic peaks were determined as, 943 cm^{-1} for Struvite, 993 cm^{-1} for Uric acid and 1006 cm^{-1} for Urea.

As a result, the micro-Raman spectroscopy technique can be used effectively for the detection of urine crystals. Further, this method seems very practical, especially for clinical applications because, sample preparation needs only a few minutes and it has quite simple results. And, perhaps, this technique may be utilized for the prediction of urinary stone type in the future, or it can be used as early diagnostic tool for renal stone growth.

REFERENCES

- [1]. Lopez, M., Hoppe, B., 2010, History, epidemiology and regional diversities of urolithiasis *Pediatr. Nephrol.*, 25, 49–59.
- [2]. Jing, Z., Guo, Z. W., Ning, J., Jia, W. Y., Yan, G., Fang, Y., 2010, Analysis of urinary calculi composition by infrared spectroscopy: a prospective study of 625 patients in eastern China, *Urol. Res.*, 38, 111-115..
- [3]. Kim, H. H., Jo, M. K., Kwak, C., Park, S. K., Yoo, K.Y., Kang, D., Lee, C., 2002, Prevalence and epidemiologic characteristics of urolithiasis in Seoul-Korea, *Urology*, 59, 517-521.
- [4]. Lee, Y. H., Huang, W. C., Tsai, J. Y., Lu, C. M., Chen, W. C., Lee, M. H., Hsu, H. S., Huang, J. K., Chang, L. S., 2002, Epidemiological studies on the prevalence of upper urinary calculi in Taiwan, *Urol. Int.*, 68, 172-177.
- [5]. Hesse, A., Brandle, E., Wilbert, D., Kohrmann, K. U., Alken, P., 2003, Study on the prevalence and incidence of urolithiasis in Germany comparing the years 1979 vs. 2000, *Eur. Urol.*, 44, 709-713.
- [6]. Stamatelou, K. K., Francis, M. E., Jones, C. A., Nyberg, L. M., Curhan, G. C., 2003, Time trends in reported prevalence of kidney stones in the United States: 1976-1994, *Kidney Int.*, 1817-1823.
- [7]. Chou, Y. H., Li, C. C., Wu, W. J., Juan, Y. S., Huang, S. P., Lee, Y. C., Liu, C. C., Li, W. M., Huang, C. H., Chang, A. W., 2007, Clinical study of uric acid urolithiasis, *J. Med. Sci.*, 23, 298-301..
- [8]. Blanco, F., López, M. M., Serranti, S., Bonifazi, G., Havel, J., Valiente, M., 2012, Hyperspectral imaging based method for fast characterization of kidney stone types, *J. Biomedical Optics*, 17, 1-12.
- [9]. Elmacı, A. M., Ece, A., Akın, F., 2014, Pediatric urolithiasis: metabolic risk factors and follow-up results in a Turkish region with endemic stone disease, *Urolithiasis*, 42, 421-426.
- [10]. Miller, N. L., Evan, A. P., Lingeman, J. E., 2007, Pathogenesis of renal calculi, *Urol. Clin. North Am.*, 34, 295-313.
- [11]. Curhan, G. C., 2007, Epidemiology of stone disease, *Urol. Clin. North Am.*, 34, 287-293.
- [12]. Chauhan, C. K., 2011, *Growth and characterization of struvite and related crystals*, Thesis (PhD), Saurashtra University.

- [13]. Manciu, F. S., Govani, J. R., Durrer, W. G., Reza, L., Pinales, L. A., 2009, Inhibition of urinary calculi-a spectroscopic study, *Journal of Raman Spectroscopy*, 40, 861-865.
- [14]. Kasidas, G. P., Samuell, C. T., Weir T. B., 2004, Renal stone analysis: why and how?, *Ann. Clin. Biochem.*, 41, 91-97.
- [15]. Taylor, E. N., Curhan, G. C., 2006, Diet and fluid prescription in stone disease, *Kidney International*, 70, 835-839.
- [16]. Curham, G. C., 2011, Urinary tract stone disease, *Part I, Chapter 1*, Springer-Verlag, 3-8.
- [17]. Khalil, S. K. H., Azooz, M. A., 2007, Application of vibrational spectroscopy in identification of the composition of the urinary stones, *J. Applied Science Research*, 3, 387-391.
- [18]. Daudon, M., Protat, M. F., Reveillaud, R. J., Jaeschke-Boyer, H., 1983, Infrared spectrometry and Raman microprobe in the analysis of urinary calculi", *Kidney international*, 23, 842-850.
- [19]. Pucetaite, M., Velicka, M., Tamosaityte, S., Sablinskas V., 2014, Application of SERS spectroscopy for detection of trace components in urinary deposits, *Plasmonics in Biology and Medicine*, 8957, 1-8, 2014.
- [20]. Lawson, E. E., Barry, B. W., Williams, A. C., Edwards, H. G. M., 1997, Biomedical applications of raman spectroscopy, *Journal of Raman Spectroscopy*, 28, 111-117.
- [21]. Paluszkiwicz, C., Gałka, M., Kwiatek, W., Parczewski, A., Walas, S., 1997, Renal stone studies using vibrational spectroscopy and trace element analysis, *Biospectroscopy*, 3, 403-407.
- [22]. Kontoyannis, C. G., Bouropoulos, N. C., Koutsoukos, P. G., 1997, Use of Raman spectroscopy for the quantitative analysis of calcium oxalate hydrates: Application for the analysis of urinary stones, *Applied Spectroscopy*, 51, 64-67.
- [23]. Walsh, W. R, Guzelsu, N., 1994, Compressive properties of cortical bone: mineral-organic interfacial bonding. *Biomaterials*, 15, 37-145.
- [24]. Abjornson, C, De-Paula, C. A., Kotha, S. P., Johnson, L. A., Guzelsu, N., 1998, Changes in the mechanical and material properties of bone related to increasing molarities of sodium fluoride, *Trans of Annual Meeting of the Orthopaedic Research Society*, 23, 957.
- [25]. Chiu, Y.-C., Yang, H.-Y., Lu, S.-H., Chiang, H. K., 2010, Micro-Raman spectroscopy identification of urinary stone composition from ureteroscopic lithotripsy urine powder, *J. Raman Spectrosc.*, 41, 136-141.
- [26]. Daudon, M., Jungers, P., 2004, Clinical value of crystalluria and quantitative morphoconstitutional analysis of urinary calculi, *Nephron. Physiol.*, 98, 31-36.

- [27]. He, J.-Y., Deng, S.-P., Ouyang, J.-M., 2010, Morphology, particle size distribution, aggregation, and crystal phase of nanocrystallites in the urine of healthy persons and lithogenic patients, *IEEE Trans. Nanobioscience.* 9, 156-163.
- [28]. Sahubert, G., 2006, Stone analysis, *Urol. Res.*, 34, 146-150.
- [29]. Sahubert, G., 2011, Urinary tract stone disease, *Part I, Chapter 29*, Springer-Verlag, 341-354.
- [30]. Elmacı, A. M., Ece, A., Akın, F., 2014, Pediatric urolithiasis: metabolic risk factors and follow-up results in a Turkish region with endemic stone disease, *Urolithiasis*, 42, 421-426.
- [31]. Sheng, X., Ward, M. D., Wesson, J. A., 2005, Crystal surface adhesion explains the pathological activity of calcium oxalate hydrates in kidney stone formation, *Journal of American Society Nephrology*, 16, 1904-1908.
- [32]. Dao, N. Q., Daudon, M., 1997, *Infrared and Raman Spectra of Calculi*, Elsevier, Paris, France.
- [33]. Gremlich, H. U., Yan, B., 2001, *Infrared and Raman spectroscopy of biological Materials*, Marcel Dekker Inc., New York
- [34]. Walton, R. C., Kavanagh, J. P., Heywood, B. R., Rao, P. N., 2005, Calcium oxalates grown in human urine under different batch conditions, *J. Cryst. Growth.*, 284, 517-529.
- [35]. Carmona, P., Bellanato, J., Escolar, E., 1997, Infrared and Raman spectroscopy of urinary calculi, *Biospectroscopy*, 3, 331-346.
- [36]. Daudon, M., Donsimoni, R., Hennequin, C., Fellahi, S., Le, M. G., Paris, M., Troupe, S., Lacour, B., 2005, Sex and age related composition of 10617 calculi analyzed by infrared spectroscopy, *Urol Res*, 23, 319-326..
- [37]. Scholz, D., Schwille, P. O., Ulbrich, D., Bausch, W. M., Sigel, A., 1979, Composition of renal stones and their frequency in a stone clinic: relationship to parameters of mineral metabolism in serum and urine, *Urol Res*, 7, 161-170.
- [38]. Moradi-Bidhendi, N., Turner, I. G., 1995, Development of a new technique for the Hodgkinson, A., 1979, Composition of urinary tract calculi from some developing countries, *Urol Int*, 34, 26-35.
- [39]. Pak, C.Y., Poindexter, J. R., Adams, H. B., Pearle, M. S., 2003, Predictive value of kidney stone composition in the detection of metabolic abnormalities, *American J. Med.*, 115, 26-32.
- [40]. Otnes, B., 1983, Crystalline composition of urinary stones in Norwegian patients, *Scand J. Urol Nephrol*, 17, 85-92.

- [41]. Schubert, G., Brien, G., 1986, Composition and texture of calcium oxalate calculi in children”, *Int Urol Nephrol*, 18, 141-145.
- [42]. Ahlawat, R., Goel, M. C., Elhence, A., 1996, Upper urinary tract stone analysis using X- ray diffraction: results from a tertiary referral centre in northern India, *Natl Med J India*, 9, 10-12.
- [43]. Bouzidi, H., Brauwere, D., Daudon, M., 2011, Does urinary stone composition and morphology help for prediction of primary hyperparathyroidism?, *Nephrol Dial Transplant*, 26, 565-572.
- [44]. Bibilash, B. S., Vijay, A., Marickar, F. Y. M., 2010, Stone composition and metabolic status, *Urol Res*, 38, 211-213.
- [45]. Giannossi, M. L., Mongelli, G., Tateo, F., Summa, V., 2012, Mineralogical and morphological investigation of kidney stones of a Mediterranean region (Basilicata, Italy), *J. Xray Sci Technol*, 20, 175-186.
- [46]. Silva, S. F., Matos, D. C., Silva, S. L., Ede, D. F., Campos, H. H., Silva, C. A., 2010, Chemical and morphological analysis of kidney stones: a double-blind comparative study, *Acta Cir Bras*, 25, 444-448..
- [47]. Schubert, G., 1996, 70.000 Urinary stone analyses - analytical and metaphylactic aspects, Pak CYC, Resnick MI, Preminger GM, eds. *Urolithiasis*, Dallas: Millet the Printer, 452–453.
- [48]. Mandel, N. S., Mandel, G. S., 1989, Urinary tract stone disease in the United States veteran population, geographical analysis of variations in composition, *Journal of Urol.*, 142, 1516-1521.
- [49]. Ansari, M. S., Gupta, N. P., Hemal, A. K., Dogra, P. N., Seth, A., Aron, M., Singh, T. P., 2005, Spectrum of stone composition: structural analysis of 1050 upper urinary tract calculi from northern India, *Int J. Urol*, 12, 12-16.
- [50]. Khan, A. S., Rai, M. E., Gandapur, G., Pervaiz, A., Shah, A. H., Hussain, A. A., Siddiq, M., 2004, Epidemiological risk factors and composition of urinary stones in Riyadh Saudi Arabia, *J. Ayub Med Coll Abbottabad*, 16, 56-58.
- [51]. Kerr, A., Laing, M., 1992, Mineralogical studies of human urinary calculi from Natal, *Environ Geochem Health*, 14, 19-25.
- [52]. Walker, V., Stansbridge, E. M., Griffin, D. G., 2013, Demography and biochemistry of 2800 patients from a renal stones clinic, *Annals of Clinical Biochemistry*, 50, 127-139.
- [53]. Prien, E. L., Prien, E. L., 1968, Composition and structure of urinary stone, *The American journal of medicine*, 45, 654-672.

- [54]. Daudon, M., Bader, C. A., Jungers, P., 1993, Urinary calculi: review of classification methods and correlations with etiology, *Scanning Microsc.*, 7, 1081-1104.
- [55]. Evan, A., 2010, Physiopathology and etiology of stone formation in the kidney and the urinary tract, *Pediatric Nephrology*, 5, 831-841.
- [56]. Daudon, M., Jungers, P., 2004, Clinical value of crystalluria and quantitative morphoconstitutional analysis of urinary calculi, *Nephron Physiology*, 98, 31-36.
- [57]. Daudon, M., Jungers, P., 2004, Drug-induced renal calculi, *Drugs*, 64, 245-275.
- [58]. Anderson, J. C., 2007, *Quantitative and qualitative investigations into urinary calculi using infrared microspectroscopy*, Thesis (PhD), Miami University Oxford.
- [59]. Gulley-Stahl, H., 2010, *An Investigation into quantitative ATR-FT-IR imaging and Raman microspectroscopy of small mineral inclusions in kidney biopsies*, Thesis (PhD), Miami University.
- [60]. Meng, M. V., 2007, *Urinary Stone Disease-The practical guide to medical and surgical management*, Humana Press Inc., Totowa.
- [61]. Tommaso, D. D., Hernandez, S. E. R., Du, Z., Leeuw, N. H., 2012, Density functional theory and interatomic potential study of structural, mechanical and surface properties of calcium oxalate materials, *RSC Advances*, 2, 4664-4674.
- [62]. Molview Co., *Molecular images*, www.molview.org, [2017].
- [63]. Tazzoli, V., Domeneghetti, C., 1980, The crystal structures of whewellite and weddellite: re-examination and comparison, *American Mineralogist*, 65, 327-334.
- [64]. Lonsdale, K., 1968, Epitaxy as a growth factor in urinary calculi and gallstones, *Nature*, 217, 56-58.
- [65]. Zhang, D., Qi, L., Ma, J., Cheng, H., 2002, Morphological control of calcium oxalate dihydrate by a double-hydrophilic block copolymer, *Chemistry Materials*, 14, 2450-2457.
- [66]. Osborn, J. F., 1980, The materials science of calcium phosphate ceramics, *Biomaterials*, 1, 108-111.
- [67]. Dihel, C., 2012, Coherent scatter computed tomography for core composition analysis of intact kidney stones-prospective clinical evaluation, The School of Graduate and Postdoctoral Studies The University of Western Ontario London, Canada.
- [68]. Parmar, M. S., 2004, Kidney stones, *British Medical Journal*, 328, 1420-1424.

- [69]. Alkhraisat, M. H., Rueda, C., Cabarcos, E. L., 2011, Strontium ions substitution in brushite crystals: The role of strontium chloride, *Journal of Functional Biomaterials.*, 2, 31-38.
- [70]. Ringertz, H., 1996, The molecular and crystal structure of uric acid, *Acta Cryst.*, 20, 397-403.
- [71]. Sutor, D. J., 1975, Constituents of urinary calculi containing struvite, *British Journal of Urology International*, 47, 585-587.
- [72]. Whitaker, A, Jeffery, J. W., 1970, The Crystal Structure of Struvite, $MgNH_4PO_4 \cdot 6H_2O$, *Acta Cryst.*, 26, 1429-1440.
- [73]. Fogazzi, G. B., Cameron, J. S., Ritz, E., et al., 1994, The history of urinary microscopy to the end of the 19th century, *American Journal of Nephrol.* 14, 452-457.
- [74]. Fogazzi, G. B., 1996, Nephrology Dialysis Transplantation Crystalluria: a neglected aspect of urinary sediment analysis, *Nephrol. Dial. Transplant.*, 11, 379-387.
- [75]. Bird, G., 1844, Urinary deposits their diagnostic value, pathology and therapeutical indications, Churchill, London.
- [76]. Tyson J., 1880, A guide to the examination of urine for the use of physicians and students, 3rd edn., Lindsay and Blakiston, Philadelphia.
- [77]. Robertson, W. G., Peacock, M., B. E. C., 1969, Nordin, Calcium crystalluria in recurrent renal stone formers, *Lancet*, 294, 21-24.
- [78]. Hallson, P. C., Rose, G. A., 1978, A new urinary test for stone activity, *Br. J. Urol.*, 50, 442-448.
- [79]. Daudon, M., Hennequin, C., Boujelben, G., Lacour, B., Jungers, P., 2005, Serial crystalluria determination and the risk of recurrence in calcium stone formers, *Kidney Int.*, 67, 1934-1943.
- [80]. Daudon, M., Jungers, P., 2004, Clinical value of crystalluria and quantitative morphoconstitutional analysis of urinary calculi, *Nephron. Physiol.*, 98, 31-36.
- [81]. Nene, S., 2013, *Diffusionless transition in tricosane and reversible inhibition of calcium oxalate monohydrate*, Thesis (PhD), The University of Western Ontario.
- [82]. Deng, H. J. Y., Ouyang, S. P., Ming, J., 2010, Morphology, particle size distribution, aggregation, and crystal phase of nanocrystallites in the urine of healthy persons and lithogenic patients, *IEEE Transactions on Nanobioscience*, 9, 156-163.

- [83]. Wesson, J. A., Ganne, V., Beshensky, A. M., Kleinman, J. G., 2005, Regulation by macromolecules of calcium oxalate crystal aggregation in stone formers, *Urol. Res.*, 33, 206-212.
- [84]. Winkens, R. A., Wielders, J. P., Degenaar, C. P., Van Hoof, J. P., 1988, Calcium oxalate crystalluria, a curiosity or a diagnostic aid?., *J. Clin. Chem. Clin. Biochem.*, 26, 653-654.
- [85]. Robert, M., Boullaran, A. M., Delbos, O., et al., 1998, Study of calcium oxalate crystalluria on renal and vesical urines in stone formers and normal subjects. *Urol. Int.*, 60, 41-46.
- [86]. Frochot, V., Daudon, M., 2016, Clinical value of crystalluria and quantitative morphoconstitutional analysis of urinary calculi, *International Journal of Surgery*, 36, 624-632.
- [87]. Gui, B. S., Huang, Z. J., Xu, X. J., Li, M. R., He, J. Y., Ouyang, J. M., 2010, Measurement of urine crystallites and its influencing factors by nanoparticle size analyzer, *J. Nanosci. Nanotechnol.*, 10, 5232-5241.
- [88]. Deng, F., Ouyang, J. M., 2006, Comparative investigations of ultrafine crystals in urine of healthy human and lithogenic patients, *Materials Science and Engineering C*, 26, 688-69.
- [89]. Cao, L. C., Jonassen, J., Honeyman, T. W., Scheid, C., 2001, Oxalate-induced redistribution of phosphatidylserine in renal epithelial cells: implications for kidney stone disease, *Amer. J. Nephrol.*, 21, 69-77.
- [90]. Ouyang, J. M., Xia, Z. Y., Zhang, G. N., Chen, H. Q., 2012, Nanocrystallites in urine and their relationship with the formation of kidney Stones, *Rev. Inorg. Chem.*, 32, 101-110.
- [91]. Shirane, Y., Kagawa, S., 1993, Scanning electron microscopic study of the effect of citrate and pyrophosphate on calcium oxalate crystal morphology, *J. Urol.*, 150, 1980-1983.
- [92]. Cao, L. C., Boeve, E. R., Schroder, F. H., Robertson, W. G., Ketelaars, G. A., Bruijn, W. C., 1992, The effect of two new semi-synthetic glycosaminoglycans (G871, G872) on the zeta potential of calcium oxalate crystals and on growth and agglomeration, *J. Urol.*, 147, 1643-1646.
- [93]. Nikkila, M. T., 1989, Urinary glycosaminoglycan excretion in normal and stone-forming subjects: significant disturbance in recurrent stone formers, *Urol. Int.*, 44, 157-159.
- [94]. Schwille, P. O., Schmiedl, A., Herrmann, U., Fan, J., Gottlieb, D., Manoharan, M., Wipplinger, J., 1999, Magnesium, citrate, magnesium citrate and magnesium-alkali citrate as modulators of calcium oxalate crystallization in urine, *Urol. Res.*, 27, 117-126.

- [95]. Ombra, M. N., Casula, S., Biino, G., Maestrale, G., Cardia, F., Melis, P., Pirastu, M., 2003, Urinary glycosaminoglycans as risk factors for uric acid nephrolithiasis: case control study in a Sardinian genetic isolate, *Urology*, 62, 416-420.
- [96]. Poon, N., Gohel, M. D. I., 2012, Urinary glycosaminoglycans and glycoproteins in a calcium oxalate crystallization system, *Carbohydr. Res.*, 347, 64-68.
- [97]. Ye, Z. Q., Deng, Y. L., Dong, C., 2003, Laboratory examination for urolithiasis, in *Calculi of Urinary System*, 1st edn., The People's Medical Publishing House, Beijing, 297.
- [98]. Hess, B., 2002, Nutritional aspects of stone disease, *Endocrin. Metab. Clin.*, 31, 1017-1030.
- [99]. Duan, C., Xia, Z., Zhang, G., Gui, B., Xue, J., Ouyang, J., 2013, Changes in urinary nanocrystallites in calcium oxalate stone formers before and after potassium citrate intake, *International Journal of Nanomedicine*, 8, 909-918.
- [100]. Pucetaite, M., Hendrixson, V., Zelvy, A., Jankevicius, F., Tyla, R., Ceponkus, J., Sablinskas, V., 2013, Application of infrared spectroscopic imaging in specular reflection mode for determination of distribution of chemical components in urinary stones, *Journal of Molecular Structure*, 1031, 38-42.
- [101]. Kocademir, M., Baykal, A., Kumru, M., Tahmaz, M. L., 2016, Structural characterization and vibrational studies of human urinary stones from Istanbul, Turkey, *Spectrochim. Acta A*, 160, 1-7.
- [102]. Karabacak, O. R., Dilli, A., Saltas, H., Yalçınkaya, F., Yörükoğlu, A., Sertçelik, M. N., 2013, Stone compositions in Turkey: An analysis according to gender and region, *Urology*, 82, 532-538.
- [103]. Mushtaq, S., Siddiqui, A. A., Naqvi, Z. A., Rattani, A., Talati, J., Palmberg, C., Shafqat, J., 2007, Identification of myeloperoxidase, α -defensin and calgranulin in calcium oxalate renal stones, *Clinica Chimica Acta*, 384, 41-47.
- [104]. Mandell, N. S., Mandell, I. C., Mandel, A. M. K., 2017, Accurate stone analysis: the impact on disease diagnosis and treatment, *Urolithiasis*, 45, 3-9.
- [105]. Knauf, F., Preisig, A., 2011, Drosophila: a fruitful model for calcium oxalate nephrolithiasis?, *Kidney Int.*, 80, 327-329.
- [106]. Daudon, M., Hennequin, C., Boujelben, G., Lacour, B., Jungers, P., Serial crystalluria determination and the risk of recurrence in calcium stone formers, *Kidney Int.*, 67, 1934-1943.
- [107]. Daudon, M., Cohen-Solal F., Barbey, F., Gagnadoux, M., Knebelmann, B., Jungers, P., 2003, Cystine crystal volumedetermination: a useful tool in the management of cystinuric patients, *Urol. Res.*, 31, 207-211.

- [108]. Zhu, W. Y., Xu, M., Wang, F. X., Ouyang, J. M., 2014, Comparative analysis of compositions between calcium phosphate calculi and urinary crystallites in the stone-formers, *Advanced Materials Research*, 881-883, 457-460.
- [109]. Zhang, G. N., Xia, Z. Y., Ouyang, J. M., Kuan, L., 2013, Study on nano and micro crystallites in urines of uric acid stone patients, *Advanced Materials Research*, 655-657, 1927-1930.
- [110]. Dyer, R., Nordin, B. E. C., 1967, Urinary crystals and their relation to stone formation, *Nature*, 215, 751-752.
- [111]. Dieppe, P., Swan A., 1999, Identification of crystals in synovial fluid, *Ann. Rheum. Dis.*, 58, 261-263.
- [112]. Moradi-Bidhendi, N., Turner, I. G., 1995, Development of a new technique for the extraction of crystals from synovial fluids, *Material Science Mater. Med.*, 6, 51-55.
- [113]. Gordon, C., Swan, A., Dieppe, P., 1989, Detection of crystals in synovial fluids by light microscopy: sensitivity and reliability, *Annals of Rheumatic Diseases*, 48, 737-742.
- [114]. Narhi, L. O., Schmit, J., Bechtold-Peters, K., Sharma, D., 2012, Classification of protein aggregates, *J. Pharm. Sci.* 101,493-498.
- [115]. Fogazzi, G. B., Passerini, P., Ponticelli, C., Ritz, E., 1993, *The Urinary Sediment, An Integrated View*, Masson, Milano.
- [116]. Kong, K., Kendall, C., Stone, N., Notingher, I., 2015, Raman spectroscopy for medical diagnostics - From in-vitro biofluid assays to in-vivo cancer detection, *Advanced Drug Delivery Reviews*, 89, 121-134.
- [117]. Sun, X. Y., J. Ouyang, M., Liu, A. J., Ding, Y. M., Gan, Q. Z., 2015, Preparation, characterization, and in vitro cytotoxicity of COM and COD crystals with various sizes, *Materials Science and Engineering C*, 57, 147-156.
- [118]. Angoni, K., Popp, J., Kiefer, W., 1998, A vibrational spectroscopy study of urinary sand, *Spectroscopy Letters*, 31, 1771-1782.
- [119]. Skrabal, P. M., 2012, *Spectroscopy: an interdisciplinary integral description of spectroscopy from UV to NMR*, vdf Hochschulverlag AG, Zürich.
- [120]. Morris, C. G., 1992, *Academic press dictionary of science and technology*, Academic press, San Diego, Usa..
- [121]. Pérez-Juste, I., Faza, O. N., 2015, *Structure Elucidation in Organic Chemistry: The Search for the Right Tools*, Maria-Magdalena, C., Chapter 1, 1st ed., Wiley, Weinheim Germany.
- [122]. Barrow, G. M., 1962, *Introduction to Molecular Spectroscopy*, McGraw-Hill, New York.

- [123]. Banwell, C. N., 1994, *Fundamentals of Molecular Spectroscopy*, 4th ed., McGraw-Hill, London.
- [124]. Jensen, P., Bunker, P. R., 2000, *Computational Molecular Spectroscopy*, John Wiley & Sons, Ltd, Chichester.
- [125]. Laane, J., 2009, *Frontiers of Molecular Spectroscopy*, 1st ed., Elsevier, Amsterdam.
- [126]. Atkins, P., Paula, J., 2010, *Atkins' Physical Chemistry*, 9th ed., Oxford University Press, Oregon, Usa.
- [127]. Vankov. A., 2005, On de Broglie Wave Nature, *Annales de la Fondation Louis de Broglie*, 30, 15-34.
- [128]. Maria-Magdalena, C., Bravo, J., 2015, *Structure Elucidation in Organic Chemistry: The Search for the Right Tools*, Wiley, Weinheim, Germany.
- [129]. Atkins, P. W., 2011, *Molecular Quantum Mechanics*, 5th ed., Oxford University Press, Oxford, England.
- [130]. Engel, T., 2013, *Quantum Chemistry and Spectroscopy*, 3rd ed., Pearson, Boston, Usa.
- [131]. Smith, E., Dent, G., 2005, *Modern Raman spectroscopy a practical approach*, John Wiley&Sons Ltd. West Sussex.
- [132]. Raman V.C., 1928, A new radiation, *Indian J. Phys*, 2, 387-398.
- [133]. Mahadevan, J. A., Richards, K. R., 1997, 19th International Conference, Chicago, pp. 2722-2728.
- [134]. Movasaghi, Z., Rehman, S., Rehman, I. U., 2007, Raman spectroscopy of biological tissues, *Apply. Spectroscopy Reviews*, 42, 493-541.
- [135]. Mazet, V., Carteret, C., Brie, D., Idier, J., Humbert, B., 2005, Background removal from spectra by designing and minimising a non-quadratic cost function, *Chemometrics and Intelligent Laboratory Systems*, 76, 121-133.
- [136]. Shreve, A. P., Cherepy, N. J., Mathies, R. A., 1992, Effective rejection of fluorescence interference in Raman spectroscopy using a shifted excitation difference technique, *Applied spectroscopy*, 46, 707-711.
- [137]. Yang, S., Li B., Slipchenko, M. N., Akkus, A., Singer, N. G., Yeni, Y. N., Akkus, O., 2013, Laser wavelength dependence of background fluorescence in Raman spectroscopic analysis of synovialfluid from symptomatic joints, *J. Raman Spectrosc.*, 44, 1089-1095.

- [138]. Min, Y. K., Yamamoto, T., Kohda, E., Ito, T., Hamaguchi, H., 2005, 1064 nm near-infrared multichannel Raman spectroscopy of fresh human lung tissues, *J. Raman Spectrosc.*, 36, 73-75.
- [139]. Sauer, M., Hofkens, J., Enderlein, J., 2011, Basic Principles of Fluorescence Spectroscopy, in Handbook of Fluorescence Spectroscopy and Imaging: From Single Molecules to Ensembles, Wiley-VCH Verlag GmbH & Co. KGaA, Weinheim, Germany. doi: 10.1002/9783527633500.ch1.
- [140]. Dong, Wei, Shuo, Chen & Quan, Liu, 2015, Review of Fluorescence Suppression Techniques in Raman Spectroscopy, *Applied Spectroscopy Reviews*, 50 (5), 387-406, DOI: 10.1080/05704928.2014.999936
- [141]. Chen, T. C., Shea, D. A., Morris, M. D., 2002, Effect of hydrogen peroxide bleaching on bone mineral/matrix ratio, *Applied spectroscopy*, 56, 1035-1037.
- [142]. Ferraro, J. R., Nakamoto, K., Brown, C. W., 2003, Introductory Raman Spectroscopy, 2nd ed., Academic Press, Elsevier Science, San Diego.
- [143]. Košářová, V., Hradil, D., Němec, I., Bezdička, P., Kanický, V., 2013, Microanalysis of clay-based pigments in painted artworks by the means of Raman spectroscopy, *Journal of Raman spectroscopy*, 44 (11), 1570-1577.
- [144]. Cadusch, P. J., Hlaing, M. M., Wade, S. A., McArthur, S. L., Stoddart, P. R., 2013, Improved methods for fluorescence background subtraction from Raman spectra, *J. Raman Spectrosc.*, 44, 1587-1595.
- [145]. Schulze, G., Jirasek, A., Yu, M. M. L., Lim, A., Turner, R. F. B., Blades, M. W., 2005, Investigation of selected baseline removal techniques as candidates for automated implementation, *Applied spectroscopy*, 59, 545-574.
- [146]. Sheppard, N., Chalmers, J. M., Griffiths, 2002, P. R. (Eds.), Handbook of Vibrational Spectroscopy, Vol. 1, John Wiley and Sons, Chichester, 1-32.
- [147]. Golcuk, K., Mandair, G. S., Callender, A. F., Sahar, N., Kohn, D. H., Morris, M. D., 2006, Is photobleaching necessary for Raman imaging of bone tissue using a green laser?, *Biochimica et biophysica acta*, 1758, 868-873.
- [148]. Butler, H. J., Ashton, L., Bird, B., Cinque, G., Curtis, K., Dorney, J., Esmonde, W. K., Fullwood, N. J., Gardner, B., Hirsch, P. L. M., Walsh, M. J., Ainslie, M. R. M., Stone, N., Martin, F. L., 2016, Using Raman spectroscopy to characterize biological materials, *Nature Protocol*, 11, 664-687.
- [149]. Penel, G., Leroy, G., Bre, E., 1998, New preparation method of bone samples for Raman microspectrometry, *Applied spectroscopy*, 52, 312-313, 1998.
- [150]. Vargas-Koudriavtsev, T., Durán-Sedó R., Sáenz-Bonilla, P., Bonilla-Mora, V., Guevara-Bertsch, M., Jiménez-Corrales, R. A., Herrera-Sancho, O. A., 2015, Effect of tooth-bleaching agents on phosphate concentration in dental enamel by means of Raman spectroscopy, *Revista Odontológica Mexicana*, 19, 228-235.

- [151]. Unal, M., Akkus, O., 2015, Raman spectral classification of mineral and collagen-bound water's associations to elastic and post yield mechanical properties of cortical bone, *Bone*, 81, 315-326.
- [152]. Mandair, G. S., Morris, M. D., 2015, Contributions of Raman spectroscopy to the understanding of bone strength, *Bonekey Reports*, 4, 1-8.
- [153]. Shea, D. A., Morris, M. D., 2002, Bone Tissue Fluorescence Reduction for Visible Laser Raman Spectroscopy, *Appl. Spectrosc.*, 56, 182-186.
- [154]. Silveira, J. M., Longelin, S., Mataa, A. D., Carvalho, M. L., 2012, Identification of oxygen in dental enamel following tooth bleaching using confocal micro Raman spectroscopy, *J. Raman Spectrosc.*, 43, 1089-1093.
- [155]. Konstantinos, C., 2016, *Growth, structure and mechanical properties of phosphate based bio-composites studied by ex situ and in situ Raman Spectroscopy*, Thesis (PhD), University of York.
- [156]. Ritza, M., Vaculíková, L., Kupková, J., Plevová, Nová, L. B., 2016, Different level of fluorescence in Raman spectra of montmorillonites, *Vibrational Spectroscopy*, 84, 7-15.
- [157]. Freeman, J. J., Wopenka, B., Silva, M. J., Pasteris, J. D., 2001, Raman Spectroscopic Detection of Changes in Bioapatite in Mouse Femora as a Function of Age and In Vitro Fluoride Treatment, *Calcif Tissue Int*, 68, 156-162.
- [158]. Morris, M. D., Mandair, G. S., 2011, Raman Assessment of Bone Quality, *Clinical Orthopaedics and Related Research.*, 469 (8) 2160-2169, doi:10.1007/s11999-010-1692-y.
- [159]. Griffiths, P. R., Haseth, J. A., 2007, *Fourier transform infrared spectroscopy*, 2th Edition, John Wiley & Sons Inc.: Hoboken.
- [160]. Colthup, N. B., Daly, L. H., Wiberley, S. E., 1990, *Introduction to Infrared and Raman spectroscopy*, 3rd Edition, Academic Press Limited: London.
- [161]. Atkins, P., Jones, L., 2008, *Chemical principles the quest for insight*, 4th ed., W.H Freeman and Company.
- [162]. McQuarrie, D., Simon, J., 1999, *Molecular thermodynamics*, University Science Books.
- [163]. Rebenthich, G., Berg, W., Pirlich, W., Omán D., 1988, Assessment and maintenance of the quality of urolith analyses in a comparison of methods. 4th International ring test to check quality, *Int Urol Nephrol*, 20, 35-45.
- [164]. Hesse, A., Kruse, R., Geilenkeuser, W. J., 2005, Quality control in urinary stone analysis results of 44 ring trials (1980 -2001)., *Clinical Chemistry and Laboratory Medicine*, 43, 298.

- [165]. Álvarez, J. L. G., Martínez, M. J. T., Fernández, M. A., 2012, Development of a method for the quantitative analysis of urinary stones, formed by a mixture of two components, using infrared spectroscopy, *Clinical Biochemistry*, 45, 582-587.
- [166]. Kravdal, G., Helgo, D., Moe, M. K., 2015, Infrared spectroscopy is the gold standard for kidney stone analysis, *Tidsskrift for Den norske legeförening*, 4, 313-314.
- [167]. Sutor D. J., Scheidt S., 1968, Identification standards for human urinary calculus components, using crystallographic methods, *Br. J. Urol.* 40, 22-28.
- [168]. Al-Atar, U., 2000, *Materials characterization of calcium oxalate monohydrate kidney stones*, Thesis (PhD), Simon Fraser University.
- [169]. Verezhak, M., 2006, *Growth, structure and mechanical properties of phosphate based bio-composites studied by ex situ and in situ Raman Spectroscopy*, Thesis (PhD), Grenoble Alpes University.
- [170]. Laurita-Plankis, G., 2014, *Investigation of the structural influence on the properties of functional inorganic oxides*, Thesis (PhD), Oregon State University.
- [171]. Jenkins, R., 1999, *X-Ray fluorescence spectrometry*, In: *X-Ray fluorescence spectrometry*, John Wiley & Sons, Inc., 2nd ed., Canada.
- [172]. Rigaku, 2006, X-Ray Diffractometer Miniflex II Instruction Manual, Manual No: ME14966A02.
- [173]. West, A. R., 2014, *Solid state chemistry and its applications*, 2nd ed., Wiley, UK.
- [174]. Szumera, M., 2012, Charakterystyka wybranych metod termicznych. Cz. 1, Laboratoria, Aparatura, *Badania*, 6, 28-34.
- [175]. Schultze, D., 1974, *Termiczna analiza różnicowa*, PWN, Warszawa, Poland.
- [176]. Crelling, J. C., Hippo, E. J., Woerner, B. A., West, D. P., 1992, Combustion characteristics of selected whole coals and macerals, *Fuel*, 71, 151-158.
- [177]. Chen, Y., Mori, S., Pan, 1996, W., Studying the mechanisms of ignition of coal particles by TG-DTA, *Thermochim. Acta*, 275, 149-158.
- [178]. Tognotti, L., Malotti, A., Petarca, L., Zanelli, S., 1985, Measurement of ignition temperature of coal particles using a thermogravimetric technique *Combust. Sci. Technol.*, 44, 15-28.
- [179]. Melgar, A., Pérez, J. F., Borge, D., 2008, Kynetic Study of the Biomass Devolatilization Process in Particles Sizes between 2-19 mm by Means of Thermogravimetric Analysis, *Dyna*, 123-131.

- [180]. Carrasco, F, Pagès, P, Gámez, P. J, Santana, O. O., Maspoch, M. L., 2010, Processing of poly(lactic acid): Characterization of chemical structure, thermal stability and mechanical properties, *Polymer Degradation and Stability*, 95, 116-125.
- [181]. Kiran, B., 2009, *Investigation of the effect of urine proteins on calcium oxalate crystallization*, Thesis (MS), Marmara University.
- [182]. Skoog, D. A., Holler, F. J., Crouch, S. R., 2007, Principles of Instrumental Analysis. Belmont, CA: Thomson Brooks/Cole, 6th ed. Ch. 31, 894-897.
- [183]. Daniel, R., Baiardo, M., 2006, Advanced Materials Characterization by Thermal Analysis, Calorimetry and Rheology, TGA TA Instruments Guide, New Castle, England.
- [184]. Grases, F.; Costa-Bauzá, A.; Ramis, M.; Montesinos, V.; Conte, 2002, A. Simple classification of renal calculi closely related to their micromorphology and etiology, *Clinica Chimica Acta*, 322, 1-2, 29-36.
- [185]. Lucena, F., B., 2014, *Chemical speciation on urinary lithiasis*, Thesis (PhD), Universitat Autònoma de Barcelona.
- [186]. Selvaraju, R., Thirupathi, G., Raja, A., 2012, FT-IR spectral studies on certain human urinary stones in the patients of rural area, *Spectrochimica Acta Part A: Molecular and Biomolecular Spectroscopy*, 93, 260–265.
- [187]. Khaskheli, M. H., Sherazi, S. T. H., Ujan, H. M., Mahesar, S. A., 2012, Transmission FT-IR spectroscopic analysis of human kidney stones in the Hyderabad region of Pakistan, *Turk J Chem*, 36, 477–483.
- [188]. Carpentier, X., Daudon, M., Traxer, O., Jungers, P., Mazouyes, A., Matzen, G., Véron, E., Bazin, D., 2009, Relationships between carbonation rate of carbapatite and morphologic characteristics of calcium phosphate stones and etiology, *Urology*, 73, 968-975.
- [189]. Matsuzaki, S., Matsuzaki, K., Tanikawa, T., Masuda, A., Matsunaga, F., 1995, Sequential analysis of recurrent calcium calculi by infrared spectroscopy, *Int. J. Urol.*, 2, 235-237.
- [190]. Selvaraju, R., Raja, A., Thirupathi, G., 2015, FT-IR spectroscopic, thermal analysis of human urinary stones and their characterization, *Spectrochimica Acta Part A: Molecular and Biomolecular Spectroscopy*, 137, 1397-1402.
- [191]. Lee, Y. H., Huang, W. C., Tsai, J. Y., Huang, J. K., 1999, The efficacy of potassium citrate based medical prophylaxis for preventing upper urinary tract calculi: A midterm followup study, *J. Urol.*, 161, 1453–1457.
- [192]. Wilson, E. V., Bushirib, M. J., Vaidyan, V. K., 2010, Characterization and FT-IR spectral studies of human urinary stones from Southern India, *Spectrochimica Acta A*, 77, 442-445.

- [193]. Shing, H. T. H., Yang, S. L., Cheng, C. L., Cheng, W. T., 2011, Preliminary feasibility study of FT-IR microscopic mapping system for the rapid detection of the composited components of prostatic calculi, *Urol. Res.*, 39, 165-170.
- [194]. Girija, E. K., Kalkura, S. N., Sivaraman, P. B., Yokogawa, Y., 2007, Preliminary feasibility study of FT-IR microscopic mapping system for the rapid detection of the composited components of prostatic calculi, *Journal of Scientific and Industrial Research*, 66, 632-639.
- [195]. Selvaraju, R., Raja, A., Thiruppathi, G., 2013, Chemical composition and binary mixture of human urinary stones using FT-Raman spectroscopy method, *Spectrochimica Acta A: Molecular and Biomolecular Spectroscopy*, 114, 650-657.
- [196]. Aminzadeh, A., Shahabi, S., Walsh, L. J., 1999, Raman spectroscopic studies of CO₂ laser-irradiated human dental enamel, *Spectrochimica Acta Part A: Molecular and Biomolecular Spectroscopy*, 55, 1303-1308.
- [197]. Edwards, H. G. M., Farwell, D. W., Jenkins, R., Seaward, M. R. D., 1992, Vibrational Raman spectroscopic studies of calcium oxalate monohydrate and dihydrate in Lichen Encrustations on Renaissance Frescoes, *Journal of Raman Spectroscopy*, 23, 185-189.
- [198]. Frost, R. L., 2004, Raman spectroscopy of natural oxalates, *Anal. Chim. Acta*, 517, 207-214.
- [199]. Kohutova, A., Honcova, P., Podzemna, V., Bezdiccka, P., Vecernikova, E., Louda, M., Seidel, J., 2010, Thermal analysis of kidney stones and their characterization, *Journal of Thermal Analysis and Calorimetry*, 101, 695-699.
- [200]. Shamema, A. A., Arul, K. T., Kumar, R. S., Kalkura, S. N., 2015, Physicochemical analysis of urinary stones from Dharmapuri district, *Spectrochim. Acta A*, 134, 442-448.
- [201]. Huia, J., Lia, H., Zheng, X., Maa, H., Fan, D., Liu, H., Wang, Y., 2015, Control synthesis and self-assembly of calcium apatite at low temperatures, *Ceramics International*, 41, 6194-6202.
- [202]. Khan, S. R., Shevock, P. N., Hackett, R. L., 1988, Presence of lipids in urinary stones: Results of preliminary studies, *Calcified Tissue International*, 42, 91-96.
- [203]. Sandersius, S., Rez, P., 2007, Morphology of crystals in calcium oxalate monohydrate kidney stones, *Urol Res*, 35, 287-293.
- [204]. Tsuda, H., Materia, J. A., 1994, Orientational Micro-Raman spectroscopy on hydroxyapatite single crystals and human enamel crystallites, *Journal of Dental Research*, 73, 1703-1710.
- [205]. K.H. Bichler, E. Eipper, K. Naber, V. Braun, R. Zimmermann, S. Lahme, 2002, Urinary infection stones, *International Journal of Antimicrobial Agents*, 19, 488-498.

- [206]. McLean, R. J. C., Nickel, J. C., Cheng, K. J., Costerton, J. W., 1988, The ecology and pathogenicity of urease-producing bacteria in the urinary tract, *Crit. Rev. Microbiol.*, 16, 37-79.
- [207]. Prywer, J., Kasprowicz, D., Runka, T., 2016, Temperature-dependent μ -Raman investigation of struvite crystals, *Spectrochimica Acta Part A: Molecular and Biomolecular Spectroscopy*, 158, 18-23.
- [208]. Kodati, V. R., Tomasi, G. E., Turumin, J. L., Tu, A. T., 1991, Raman Spectroscopic identification of phosphate-type kidney stones, *Applied Spectroscopy*, 45, 581-583.
- [209]. Stefov, V., Cahil, A., Šoptrajanov, B., Najdoski, M., Spirovski, F., Engelen, B., Lutz, H. D., Koleva, V., 2009, Infrared and Raman spectra of magnesium ammonium phosphate hexahydrate (struvite) and its isomorphous analogues. VII: Spectra of protiated and partially deuterated hexagonal magnesium caesium phosphate hexahydrate, *Journal of Molecular Structure*, 924, 100-106.
- [210]. Frost, R. L., Weier, M. L., Martens, W. N., Henry, D. A., Mills, S. J., 2005, Raman spectroscopy of newberyite, hannayite and struvite, *Spectrochimica Acta*, 62, 181-188.
- [211]. Kang, D. H., Nakagawa, T., Feng, L., Watanabe, S., Han, L., Mazzali, M., Truong, L., Harris, R., Johnson, R. J., 2002, A role for uric acid in the progression of renal disease, *J. Am. Soc. Nephrol.*, 13, 2888-2897.
- [212]. Raphael, S., 1983, *Lynch's Medical Laboratory Technology*, 4th ed., W. B. Saunders, Philadelphia, Usa.
- [213]. Kodati, V. R., Tu, A. T., Turumin, J. L., 1990, Raman spectroscopic identification of uric-acid-type kidney stone, *Applied Spectroscopy*, 44, 1134-1136.
- [214]. Selvaraju, R., Raja, A., Thirupathi, G., 2013, Chemical composition and binary mixture of human urinary stones using FT-Raman spectroscopy method, *Spectrochimica Acta Part A: Molecular and Biomolecular Spectroscopy*, 114, 650-657.
- [215]. Keuleers, R., Desseyn, H. O., Rousseau, B., C. Alsenoy, V., 1999, Vibrational analysis of urea, *Journal of Physical Chemistry A*, 103, 4621-4630.
- [216]. Leordean, C., Canpean, V., Astilean, S., 2012, Surface-Enhanced Raman Scattering (SERS) Analysis of Urea Trace in Urine, Fingerprint, and Tear Samples, *Spectroscopy Letters*, 45, 550-555.
- [217]. Ahmad, S., I., 2010, *Studies some biophysical aspects of human renal excretory fluid*, Thesis (PhD), Jawaharlal Nehru Technological University.
- [218]. Saatkamp, C. J., Almeida, M. L., Bispo, J. A. M., Pinheiro, A. L. B., Fernandes, A. B., Silveira, L., 2016, Quantifying creatinine and urea in human urine through Raman spectroscopy aiming at diagnosis of kidney disease Quantifying creatinine

and urea in human urine diagnosis of kidney disease, *Journal of Biomedical Optics*, 21, 1-7.

- [219]. Premasiri, W. R., Clarke, R. H., Womble, M. E., 2001, Urine analysis by laser Raman spectroscopy, *Lasers in surgery and medicine*, 28, 330-334.



CURRICULUM VITAE

Personal Information	
Name Surname	Mustafa Kocademir
Place of Birth	Alanya
Date of Birth	January 1986
Nationality	<input checked="" type="checkbox"/> T.C. <input type="checkbox"/> Other:
Phone Number	0242 511 (24-68)
Email	mustafakocademir@gmail.com
Web Page	



Educational Information	
B. Sc.	
University	Ankara University
Faculty	Engineering
Department	Physics Engineering
Graduation Year	2010

M. Sc.	
University	Fatih University
Institute	The Graduate School of Sciences and Engineering
Department	Physics
Programme	Physics
Graduation Year	2013

Ph. D.	
University	Istanbul University
Institute	Institute of Graduate Studies in Science and Engineering
Department	Department of Physics
Programme	Physics Programme
Graduation Year	2017

Publications	
<p>[1]. Kumru, M., Altun, A., Kocademir, M., Küçük, V., Bardakçı, T., Şaşmaz, İ., 2016, Combined experimental and quantum chemical studies on spectroscopic (FT-IR, FT-Raman, UV-Vis, and NMR) and structural characteristics of quinoline-5-carboxaldehyde, <i>Journal of Molecular Structure</i>, 1125, 302–309.</p>	

- [2]. Kocademir, M., Baykal, A., Kumru, M., Tahmaz, M. L., 2016, Structural characterization and vibrational studies of human urinary stones from Istanbul, Turkey, *Spectrochimica Acta Part A: Molecular and Biomolecular Spectroscopy*, 160, 1–7.
- [3]. Kumru, M., Kucuk, V., Kocademir, M., Alfanda, H. M., Altun, A., Sari, L., 2015, Experimental and theoretical studies on IR, Raman, and UV–Vis spectra of quinoline-7-carboxaldehyde, *Spectrochimica Acta Part A: Molecular and Biomolecular Spectroscopy*, 134, 81–89.
- [4]. Kumru, M., Küçük, V., Kocademir, M., 2012, Determination of structural and vibrational properties of 6-Quinolinecarboxaldehyde using FT-IR, FT-Raman and Dispersive-Raman experimental techniques and theoretical HF and DFT (B3LYP) methods, *Spectrochimica Acta Part A: Molecular and Biomolecular Spectroscopy*, 96, 242–251.

Conference Proceedings

- [1]. Mustafa Kumru, Mustafa Kocademir, Tayyibe Bardakçı, “Combined experimental and theoretical studies on the vibrational and electronic spectra of 5-Quinolinecarboxaldehyde”, 70th International Symposium on Molecular Spectroscopy, Champaign-Urbana, Illinois-USA Jun, pp. 225, 2015.
- [2]. M. Kumru, M. Kocademir, H. M. Alfanda, “Experimental and Theoretical Studies on the Electronic Absorption Spectra of Quinoline Carboxaldehydes”, WI05, pp. 173, 16-20 June 2014, University of Illinois at Urbana-Champaign, IL 61801 USA
- [3]. Mustafa Kumru, Mustafa Kocademir, Levent Sari, “Determination of structural and vibrational properties of quinoline-7-carboxaldehyde using experimental FT-IR, FT-Ra and dispersive-Ra techniques and theoretical HF and DFT calculations”, O11, 15-20 Sept., 2013, I. International Turkish Congress on Molecular Spectroscopy (TURCMOS2013)” - Istanbul – Turkey
- [4]. Mustafa Kumru, M. Kocademir, Tayyibe Bardakçı, "Determination of structural and vibrational properties of 5-Quinolinecarboxaldehyde using experimental FT-IR, FT-Raman techniques and theoretical HF and DFT methods", 68th International Symposium on Molecular Spectroscopy, Columbus, Ohio / U.S.A, Jun. 2013.

Research Projects

- [1]. “Structural and Vibrational (Infrared and Raman) Spectroscopic Investigations of Renal Stones”, University Research Fund, May 2015 – May 2016, Researcher, Amount: 8000 TL.

- [2]. “Vibrational analysis and molecular structure determination of quinoline derivatives via FT-IR, FT-Ra and dispersive Ra techniques”, University Research Fund, Nov 2010-Jul 2012, Researcher, Amount: 15,000 TL.

Certificates

- [1]. Intern, NanoMagnetics Instruments Co., Ankara, Turkey, 2009.
- [2]. Winter School on “Physics and Chemistry of Solids: Theory and Experiment”, Bilkent University, Nov 6-13, 2011, Ankara, Turkey.

